Revised Load Rating Procedures for Deteriorated Prestressed Concrete Beams

Principal Investigator (s)
Alex Stripsky
Dr. Sergio Breña,
Dr. Jessica Boakye
Dr. Scott Civjan
Dr. Simos Gerasimidis

University of Massachusetts Amherst

Research and Technology Transfer Section
MassDOT Office of Transportation Planning

U.S. Department of Transportation
Federal Highway Administration

Technical Report Document Page

1. Report No. 23-047	2. Government Accession No. n/a	3. Recipient's Catalog No. n/a
4. Title and Subtitle Revised Load Rating Procedures for Deteriorated Prestressed Concrete Beams		5. Report Date August 2023
		6. Performing Organization Code 23-047
7. Author(s) Alex Stripsky, Sergio Breña, Jessica Boakye, Scott Civjan, and Simos Gerasimidis		8. Performing Organization Report No.
9. Performing Organization Name and Address University of Massachusetts Amherst UMass Transportation Center 130 Natural Resources Way Amherst, MA 01003		10. Work Unit No. (TRAIS) n/a
		11. Contract or Grant No. n/a
12. Sponsoring Agency Name and Address Massachusetts Department of Transportation Office of Transportation Planning Ten Park Plaza, Suite 4150, Boston, MA 02116		13. Type of Report and Period Covered Final Report - November 2023 (April 2021 - November 2023)
		14. Sponsoring Agency Code n/a
15. Supplementary Notes Project Champion - Richard Mulcahy, MassDOT		

16. Abstract

The first prestressed concrete bridge in the United States was built in the early 1950s. Since then, several typical sections have been developed for use in bridge construction including I-beams, deck slabs, box beams, double tees, and so forth. In bridges under aggressive environments, corrosion deterioration of prestressing strands and stirrups has occurred, creating challenges associated with determining the strength of deteriorated existing bridge sections. The MassDOT *LRFD Bridge Manual* includes provisions to estimate strength of corrosion deteriorated prestressed concrete box beams, allowing engineers to calculate the load rating of these types of bridges. The provisions are based on the observed condition of the bridge, particularly with regard to estimates of strand area reductions to estimate residual strength. In bridges with adjacent box beams or deck slabs, corroded reinforcement is difficult to identify because only the top and bottom surfaces of the superstructure elements are accessible. The goals of this research are to evaluate the existing strength calculation procedures and to provide recommendations on how to properly evaluate the reduction in strand area based on the observed condition of the bottom surface of the prestressed box or deck beams.

17. Key Word Prestressed concrete, deterioration, corrosion, flexural strength, load rating	18. Distribution Statement n/a		
19. Security Classif. (of this report) unclassified	20. Security Classif. (of this page) unclassified	21. No. of Pages 134	22. Price n/a

Form FOT F1700.7 (8-72) Reproduction of completed page authorized

This page left blank intentionally.

Revised Load Rating Procedures for Deteriorated Prestressed Concrete Beams

Final Report

Prepared By:

Alex Stripsky
Graduate Research Assistant

Sergio Breña, PhD
Principal Investigator

Jessica Boakye, PhD
Co-Principal Investigator

Scott Civjan, PhD
Co-Principal Investigator

Simos Gerasimidis, PhD
Co-Principal Investigator

University of Massachusetts Amherst
131 Natural Resources Way
Amherst, MA 01003

Prepared For:

Massachusetts Department of Transportation
Office of Transportation Planning
Ten Park Plaza, Suite 4150
Boston, MA 02116

November 2023

This page left blank intentionally.

Acknowledgments

Disclaimer

This page left blank intentionally.

Executive Summary

This study of Revised Load Rating Procedures for Deteriorated Prestressed Concrete Beams was undertaken as part of the Massachusetts Department of Transportation (MassDOT) Research Program. This program is funded with Federal Highway Administration (FHWA) State Planning and Research (SPR) funds. Through this program, applied research is conducted on topics of importance to the Commonwealth of Massachusetts transportation agencies.

This report summarizes a 27-month research project investigating the effects of corrosion-induced deterioration on the load-carrying capacity of prestressed concrete beams and any recommendations to the current load rating procedures described in the MassDOT *LRFD Bridge Manual (1)*. The study consisted of reviewing existing literature, reviewing inspection procedures and reports, testing out-of-service prestressed concrete beams with documentation of current condition, and quantitative analyses to determine the adequacy of current load rating procedures and recommended procedures.

For deterioration, the following deterioration metrics were used for load rating procedures: (1) longitudinal cracking, (2) concrete spalling, (3) exposed stirrups, and (4) exposed strands. Rust staining and differential deflection were originally considered to be added to the list of metrics. However, neither is a true indicator that there is corrosion-induced deterioration in the beams. Rust staining could be the result of rust from various components of the deck (i.e., railings) seeping through the beam through water runoff. Differential deflection could be from camber tolerances or differing losses of prestress from one beam to another, subsequently causing additional deflection if the losses are greater. Thus, neither metric was added to the list of deterioration metrics.

Six total specimens from two bridges were obtained for experimental testing. Each beam was documented with the amount of deterioration that each exhibited. Each beam was then tested in a 4-point bending configuration to achieve a maximum moment at midspan. Five of the six specimens failed in flexure, and one failed in shear. Of the five that had failed in flexure, three showed no signs of deterioration, with the results matching this finding, whereas the other two did show visible signs of deterioration, with the results matching this finding.

With the results from the deteriorated beams and the documented deterioration, a different procedure was proposed for calculating the capacity of the beams. This was compared with calculations using the current procedure.

Both the MassDOT *LRFD Bridge Manual (1)* procedures and that proposed in this report give capacity calculations lower than what was observed experimentally. The MassDOT *LRFD Bridge Manual* procedure gives a far more conservative capacity calculation than the procedure proposed herein. With this, this report recommends the proposed procedure to supersede the current procedure in the MassDOT *LRFD Bridge Manual*.

This page left blank intentionally.

Table of Contents

List of Tables

This page left blank intentionally.

List of Figures

List of Acronyms

Acronym	Expansion
AASHTO	American Association of State Highway and Transportation Officials
ACI	American Concrete Institute
ADT	Average Daily Traffic
ASTM	American Society for Testing and Materials
CDP	Concrete Damage Plasticity
FEM	Finite-Element Model
FHWA	Federal Highway Administration
FRC	Fiber-Reinforced Concrete
IMF	Induced Magnetic Field
INDOT	Indiana Department of Transportation
LRFD	Load and Resistance Factor Design
MassDOT	Massachusetts Department of Transportation
MFL	Magnetic Flux Leakage
NBI	National Bridge Inventory
NYSDOT	New York State Department of Transportation
ODOT	Ohio Department of Transportation
PC	Prestressed Concrete
PCI	Precast/Prestressed Concrete Institute
PennDOT	Pennsylvania Department of Transportation
UHPC	Ultrahigh Performance Concrete
UMass	University of Massachusetts Amherst

This page left blank intentionally.

1.0 Introduction

This study of Revised Load Rating Procedures for Deteriorated Prestressed Concrete Beams was undertaken as part of the Massachusetts Department of Transportation (MassDOT) Research Program. This program is funded with Federal Highway Administration (FHWA) State Planning and Research (SPR) funds. Through this program, applied research is conducted on topics of importance to the Commonwealth of Massachusetts transportation agencies.

1.1 Background

Construction of precast concrete bridges increased in the 1950s and continued to grow in popularity into the 1960s and 1970s, especially as a greater variety of precast prestressed concrete (PC) beam shapes started being produced. Some of the most commonly used beam shapes for bridge construction consisted of PC slabs, PC box beams, and PC beam bridges. Initially, bridges with PC slabs and PC box beams were constructed by placing beams adjacent to each other. This type of bridge is referred to as having butted or adjacent beam superstructure. More recently, the use of spread PC beam bridges has increased. Butted beam bridges are highly economical because they eliminate the formwork needed for deck construction. One of the drawbacks of this type of bridge, however, is that they are difficult to inspect and provide a natural pathway for chloride-laden water to seep between units because the sections are placed next to each other. Chloride-contaminated water may then make its way into the concrete section causing deterioration of the internal steel reinforcement. The deterioration of PC box beams and PC slabs predominantly occurs by corrosion of the internal reinforcement (strands, stirrups) leading to spalling, which may cause a reduction in flexural and shear strength of the units. Deterioration of these types of bridges is common in the northeast region due to the use of deicing chlorides for roadway treatment during winter months.

1.2 Objectives

This research is intended to identify and recommend a revised load rating procedure that incorporates strand deterioration through observed beam condition. This is done by noting what has been done in the past with other departments of transportation, reviewing other research, identifying common deterioration metrics by reviewing inspection reports, experimental testing of deteriorated beams, estimating capacity using a revised procedure and comparing it to the current procedure in the MassDOT *LRFD Bridge Manual (1)*.

This page left blank intentionally.

2.0 Literature Review

2.1 Prestressed Concrete Bridge Research
from Other States

2.1.1 Pennsylvania

On December 27, 2005, a fascia beam on the Lake View Drive Bridge carrying State Route 1014 over I-70 in Washington, Pennsylvania, failed under service loads without warning of impending failure *(2)*. The failure occurred near the midspan of the bridge (Figure 2.1). Forensic analysis revealed that 20 of the 60 prestressed strands in the fascia beam were severed, and 39 of 60 had some level of corrosion. Beams from that bridge were sent to Lehigh University to be studied to improve load rating procedures. The beam flexural capacities were tested to correlate observed damage and remaining capacity. The investigation attributed failure of the beam to several factors. Improper fabrication of the shear keys between adjacent PC box beams allowed chlorides to leak through between the beams and penetrate the concrete. These chlorides accelerated corrosion of the strands and stirrups, compromising the flexural strength and shear strength of the beam and the ability for load to be distributed to adjacent members by corroding post-tensioning strands. The cardboard void forms, much like cardboard used in household boxes, used during fabrication of the box beams shifted during construction, allowing for the dimensions of the void and dimensions of the beam to change, causing a reduction in the thickness of the flanges and webs. Too many vent holes allowed the chloride-laden water to penetrate the concrete more easily.

Investigators at Lehigh University provided extensive recommendations to the Pennsylvania Department of Transportation (PennDOT) for modified load rating procedures for this type of bridge. One of the key recommendations related to flexural strength calculation procedures— eliminating corroded strands exhibiting section loss and a reduction in areas of adjacent strands because of their likelihood of also exhibiting similar levels of corrosion. The recommendations include procedures to determine overall flexural capacity of deteriorated beams based on the field observations made. Section loss was estimated from visual observations and provided recommendations on the use of those revised strand section areas to determine moment strength.

Figure 2.1: Lake View Bridge collapse

The research team from Lehigh developed a new rating procedure for PC box-beam bridges. PennDOT adopted these procedures to specifically rate box-beam bridges, but these methods could possibly be extended to rating of purely PC slab bridges (not mentioned in the study). Recommendations for condition rating suggest the beam in the bridge with the lowest rating should be the rating for the entire bridge superstructure. This method is extremely conservative in the case of a bridge with deteriorated components because of the large strength and rating differences between nondeteriorated and deteriorated beams. Although this practice causes the overall bridge rating to be conservative, it provides a margin of safety in case the condition of the bridge worsens. Table 2.1 shows the PennDOT recommendations for noncomposite prestressed concrete adjacent box beams *(2)* that have since been adopted in common practice in PennDOT when inspecting PC box-beam bridges.

Recommendations for strand area reduction based on the observed condition of the beams was provided by the researchers in this study. These area reductions decrease the moment capacity and allow engineers to estimate any weight restrictions, if needed, to increase the level of confidence that the deteriorated bridge can remain in service. The recommended procedure by Naito *(2)* is summarized as follows:

- Visually observed strands +25%. Deduct 100% of all exposed strands plus an additional 25% (125% of the total cross-sectional area of exposed strands) from capacity calculations.
- Strands adjacent to or intersecting a crack shall be considered ineffective in the region immediately adjacent to the crack.
- If significant strand loss (i.e., in excess of 20% of the total number of beam strands) is noted especially for fascia beams, contact the Bridge Quality Assurance Division for further instruction.
- For beams with no exposed strands but which appear to have internal damage (as evidenced by bottom flange cracking with rust and/or delamination), contact the Bridge Quality Assurance Division for further instruction.

- For fascia beams with Capacity/Dead Load <1.5 or an Operating Rating <1.5 based on conventional analysis, an analysis that considers biaxial stress will be performed.
- Based on the limited research of beams with longitudinal cracks in the bottom flange the strand above the crack as well as two adjacent lower layer strands may be deteriorating. For this condition, a parametric study of strand loss should be performed to determine the sensitivity of the beam capacity to strand loss.

Table 2.1: PennDOT superstructure condition rating guidelines

Condition rating	Condition level	Strands exposed per beam (%)	Other deterioration of P/S concrete beams
9–Excellent	—	0	No cracks, stains, or spalls
8–Very good	No problems noted	0	No cracks, stains, or spalls
7–Good	Some minor problems	0	Map cracks and miscellaneous hairline cracks
6–Satisfactory	Structural elements show some minor deterioration	0	Spalls–Minor spalls/delaminations <5% Cracks–Maps cracks and miscellaneous hairline cracks
5–Fair	All primary structural elements are sound but showing minor cracks and signs of deterioration	1–5	Spalls– Spalls/delaminations <15% Transverse cracks–none Longitudinal cracks–Hairline longitudinal cracks in bottom flange Longitudinal joints–Leakage at joints with light efflorescence
4–Poor	Deterioration of primary structural elements has advanced	6–15	Spalls–Spalls/delaminations, 15–20% Transverse cracks–Hairline flexural cracks across bottom flange Longitudinal cracks–Minor efflorescence and/or minor rust stains Longitudinal joints–Heavy efflorescence and/or minor rust stains Transverse tendons–Loose or heavily rusted Web cracks – Initiation of vertical or diagonal cracks in P/S beam near open joints in barrier (<3-in. length)
3–Serious	Deterioration has seriously affected the primary structural components	15–20	Spalls – Spalls/delaminations >25% Transverse cracks–Open flexural cracks in bottom flange Transverse tendons–Broken or missing Web cracks–Vertical or diagonal cracks in P/S beam near open joints in barrier Camber–Sagging/loss of camber
2–Critical	Deterioration of primary structural components has advanced and bridge will be closely monitored, or closed, until corrective action can be taken	>20	All–Any condition worse than detailed above
1–Imminent Failure	Major deterioration in critical structural components. Bridge is closed but corrective action may put the bridge back into light service		
0–Failed	Bridge is out of service and beyond corrective action		

2.1.2 Virginia

The Aden Road Bridge located near Quantico, Virginia, was a PC box-beam bridge that was decommissioned due to extensive damage. Three of the beams were salvaged for testing to determine their flexural capacity. The beam tests were conducted at Virginia Tech. To accomplish this, the researchers focused on quantifying the deteriorated condition of the extracted beams by determining the amount of corrosion of the longitudinal strands in the beams, by testing the in situ compressive strength of the concrete through compression testing of extracted cores, by determining the tensile strength of the corroded strands, and by measuring chloride concentration in selected areas of the deteriorated beams.

The amount of corrosion in the strands was initially determined using two methods: concrete resistivity tests and half-cell potential tests. The concrete resistivity test was subsequently abandoned because beams were dry and current was unable to travel through the entirety of the beam. The half-cell potential test was primarily used to identify the possibility of active corrosion in different areas of the beams. Maps representing the potential for corrosion in different areas were developed to indicate potential areas where corrosion may or may not be active. Figure 2.2 shows an example of the mapping of the corrosion from the side view of a beam that was tested. The contours represent different probabilities of corrosion. The contours drawn along the center region from 0 ft to approximately 42 ft (blue) represent the lowest probabilities of corrosion, while the contours on the edges (red) at approximately 6 ft, 23 ft, 28 ft and 44 ft represent the highest probabilities of corrosion *(3)*.
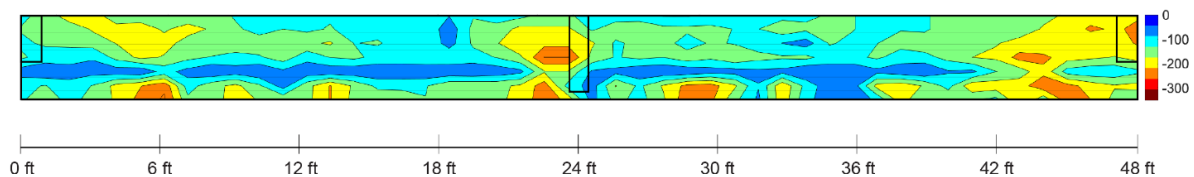
Figure 2.2: Mapping corrosion example

Flexural strength was determined by conducting tests to failure in the Virginia Tech laboratory. The testing protocol consisted of applying a concentrated load at the center of each beam that was simply supported at both ends. Load was applied in ascending increments until the beam failed. The strength of concrete was determined by testing cores extracted from the beams and testing them to failure using a compression testing machine following ASTM C39 *(4)*. To determine tension strength of corroded strands, tension tests followed ASTM A1061 *(5)*.

For damage estimation, two methods were used: a method developed by the researchers and the method developed by Naito et al. *(2)*. This method was recommended, producing reasonably accurate estimates of cross-sectional areas and estimates of strength. This method was developed from the same study done to determine load rating procedures. Flexural strength was computed using the AASHTO LRFD *(6)* method and a method based on strain compatibility and material stress-strain laws. Recommendations were to use the AASHTO LRFD method to estimate strength.

Other research conducted was to show the distribution between beams using shear keys *(7)*. Bridges are supposed to transfer some of the load from one bridge beam to another if they are

designed in an adjacent format using shear keys. Ways to improve the efficiency of shear keys and load distribution were found. Transverse post-tensioning would allow for greater transfer due to the confinement of the shear keys. Using ultrahigh performance concrete (UHPC) would reduce the likelihood of the failure of these shear keys.

2.1.3 New York

A substantial number of problems with PC bridges of all types in New York were not identified from the literature collected, but a review is included to investigate the rating procedures that the NYSDOT uses. NYSDOT relies on the condition states stipulated in the AASHTO *Manual for Bridge Element Inspection (8)* based on the condition states listed in Table 2.2. Given the large variation in deterioration or damage that may be present in PC bridges, the condition states listed are broad and do not give specific actions the NYSDOT should take that might be useful for use in bridge rating. These condition states could be useful to document progression of damage noted in a routine inspection.

Table 2.2: AASHTO condition state definitions for PC bridges

Defect/action	Condition State 1	Condition State 2	Condition State 3	Condition State 4
Exposed rebar	None	Moderate spall or patch areas that are sound	Severe spall or patched area showing distress	The condition is beyond the limits established in condition state three (3) and/or warrants a structural review to determine the strength or serviceability of the element or bridge
Exposed prestressing	None	None	Corrosion without section loss	
Cracks	Hairline cracks only	Narrow size or density	Medium size or density	
Efflorescence	None	Moderate but without rust	Severe with rust staining	
Load capacity	No reduction	No reduction	No reduction	
Feasible actions	Do nothing Protect	Do nothing Protect	Do nothing Protect Repair Rehab	Do nothing Rehab Replace

Note: Definitions provided in AASHTO for hairline, minor, narrow, moderate, medium, severe.

2.1.4 Ohio

The Ohio DOT (ODOT) developed methods of in situ testing of PC bridges to determine the level of corrosion in internal reinforcement (longitudinal or stirrups) *(9)*. ODOT identified two methods recommended to detect corrosion of reinforcement: magnetic flux leakage (MFL) and induced magnetic field (IMF). MFL is used to detect hidden corrosion and fractures in the steel reinforcement within a concrete member. IMF is used to detect the amount of "healthy" steel that is present in the member and determine corrosion by subtracting the amount of healthy steel from the expected steel. Both methods were evaluated as proof-of-concept methods, and MFL is currently in a more advanced state. Both methods still need development before they can be commonly used for inspection. However, the

potential for these methods warrants consideration to identify corrosion of internal reinforcement for this research project.

ODOT has also performed full-scale testing of in-service bridges using loaded trucks *(10)*. The goal of the research was to show the distribution of load from one member to the adjacent members. It was shown that the loads were adequately transferred between adjacent members through the transverse tie rods. These same beams later underwent destructive testing, which then confirmed the load sharing through the tie rods *(11)*. Examination of certain bridges from their in-service condition revealed that most of the deterioration was concentrated on the sides of the beams and that bridges with corroded strands could still carry appreciable load *(12)*. The recommendations focused on methods to get an accurate estimation of the strand areas, ultimate capacity, and service-level capacity. To gain an accurate estimate of the corrosion of strands, it is important to remove any loose or spalled concrete so that any strands could be exposed. For the ultimate capacity, any strands that are exposed have no contribution to the strength and are corroded. Any strand directly adjacent to those strands that are exposed are assumed to be ineffective. The service-level capacity should be based on the area of the effective strands and the effective eccentricity of the strands.

During a recent personal communication (Culmo 2023), it was pointed out that Ohio has a significant number (about 6,000) of adjacent box-beam bridges as part of the county highway system. Of these bridges, 95% of them are noncomposite and may require replacement in the next few decades.

2.1.5 Indiana

The Indiana DOT (INDOT), identified several PC box-beam bridges that exhibited signs of deterioration due to corrosion of internal reinforcement by using the NBI Database *(13)*. Most of these bridges exhibited damage caused by chlorides used for deicing roads. Correlations between bridge deterioration and age, location, or bridge span were studied and identified. The goal of attempting to establish these correlations was to identify any common causes of deterioration. INDOT found a strong correlation between age of the bridge and deterioration. Location of the bridge was also strongly correlated with deterioration, with bridges located in the northern part of the state more susceptible to deterioration, most likely due to the temperature difference. Length of the spans of bridges and deterioration was not strongly correlated. A common deficiency in the INDOT bridges was fracturing of shear keys, which exacerbated water leakage between PC box units. A lack of drain holes forced water penetrating into the box beams to flow through the concrete boxes and further promote corrosion of internal reinforcement.

2.1.6 Michigan

Michigan (in the Great Lakes Region and northern United States) experiences many of the same issues as the prior states listed. One primary focus was on how to use preventative measures for future bridges by examining existing bridges or bridges that have been demolished *(14)*. Like other states, they recommended improved inspection techniques and a more uniform system. One of the primary goals of the research was to find ways to protect

the concrete and steel inside. They recommend extensive evaluations of sealants that are used, since the effectiveness from bridge to bridge varies based on the substrate.

2.1.7 Illinois

One of the concerns of prestressed concrete is that, when the strand area is lost and its effectiveness diminished, beams with deteriorated strand will crack while under service loads leading to undesirable behavior. This could in turn lead to a reduced capacity, given that further loading could result in crack propagation. Indeed, AASHTO LRFD *(6)* already has specific guidelines on reductions that can be used to estimate the capacity. AASHTO LRFD also has a recommendation on serviceability calculations, and that should be the controlling factor of the bridge. The findings in Illinois show that these reductions should be used with caution. Simply sticking with the AASHTO LRFD recommendations of keeping the strand stress within 80%, its serviceability estimate, of the ultimate stress, is conservative *(15)*. There are no recommendations whether to keep the strand stress down to 80% or to go with the capacity reduction and that these should be left up to the owner of the bridge.

2.2 Materials and Modeling Practices

Modeling of prestressed concrete or reinforced concrete beams has been extensively researched and the materials for both concrete and reinforcement have been extensively researched. While most of the research, particularly for finite-element modeling (FEM), has focused around reinforced concrete members, most of the modeling techniques can be extended to prestressed concrete. Other analysis techniques are also extremely important to analyze the section capacity of PC beams, such as moment-curvature analysis. Previous researchers *(16)* developed a simple, analytical model of deteriorated prestressed concrete members. The model was validated by FEM and experimental results, particularly in estimates of the load-deflection behavior of beams.

2.2.1 Material Modeling

Concrete has been given many different mathematical representations. To conduct moment-analysis of prestressed concrete sections, stress-strain models that capture the uniaxial behavior of concrete in compression have been used *(17)*. Hognestad proposed a parabolic stress-strain relation up to its compressive stress f'_c at a value ε_o. In the Hognestad model, post-peak stresses decrease linearly as a function of increased strain until reaching the assumed crushing strain of 0.0038 *(17)* (Eq. 2.1). In Eq. 2.1, f'_c is the compressive strength of concrete, ε_o is the corresponding strain at peak stress, often taken equal to 0.002, and ε_u is the crushing strain of concrete.

$$f_c = f'_c \left[2\frac{\varepsilon}{\varepsilon_o} - \left(\frac{\varepsilon}{\varepsilon_o}\right)^2 \right] \text{ for } \varepsilon \leq \varepsilon_o \qquad (2.1a)$$

$$f_c = f'_c - (f'_c - 0.85f'_c)\frac{\varepsilon - \varepsilon_o}{\varepsilon_u - \varepsilon_o} \text{ for } \varepsilon > \varepsilon_o \qquad (2.1b)$$

Instead of describing the stress-strain relation using two curves (one to peak stress and one for the post-peak behavior), concrete can be modeled using a parabolic relation up to the crushing strain with little loss in accuracy. To verify the accuracy of these models, tests on reinforced concrete members subjected to combined axial load and flexure were performed *(17)*. Further discussion of the moment-curvature analysis procedure is presented in Section 6.0.

A stress-strain model for confined and unconfined concrete was proposed *(18)*. The stress-strain model uses the initial tangent modulus of elasticity of concrete; the concrete modulus of elasticity in ACI 318 *(19)* AASHTO *LRFD Bridge Design Specifications (6)* correspond to secant modulus at $0.5f'_c$. The Mander stress-strain relation has been used extensively in concrete research and it matches closely with the Hognestad model for unconfined concrete. This stress-strain model can also be used for fiber-reinforced concrete (FRC) and UHPC with some modification. An attractive feature of this model is that it is defined using a single equation that can be more easily programmed into general purpose finite-element software.

$$f_c = \frac{f'_c x r}{r - 1 + x^r} \tag{2.2a}$$

$$x = \frac{\varepsilon}{\varepsilon_o}, r = \frac{E_{tan}}{E_{tan} - E_{sec}}, E_{sec} = \frac{f'_c}{\varepsilon_o} \tag{2.2b}$$

The bond-slip relationship of strand embedded in concrete is also a very important aspect of the behavior that should be included when there are concerns of strain slippage in prestressed concrete members. The CEB-*fib* Model Code 2010 *(20)* provides a nonlinear bond-slip relationship between steel and concrete. Murcia-Delso and Shing *(21)* described the three-dimensional bond-slip relationship of reinforcement in concrete. Wang et al. *(29)* proposed a simplified version of the bond-slip model between prestressing strand and concrete. The proposed parameters of the model are very similar to those for mild reinforcement in concrete. Along with the model, Wang et al. *(29)* also proposed a degradation factor related to the loss of strand area to reduce the bond between the strand and concrete. These factors were determined from physical experiments conducted on deteriorated strands exhibiting corrosion.

To model the stress-strain behavior of mild reinforcement and prestressing strands, there are two types of models that are commonly used: elastoplastic material models and Ramberg-Osgood models. For mild reinforcement it is quite common to use elastoplastic material models; some include strain hardening depending on the expected maximum steel strain. Ramberg-Osgood models (Eq. 2.3) are well suited to model the stress-strain behavior prestressing strands because the model may be used to capture the yielding behavior of reinforcing that does not exhibit a sharp transition from the linear range to post-yield range. The *PCI Design Handbook (22)* provides a stress-strain equation to estimate stresses in prestressing strand as a function of strain, based on an asymptotic behavior near ultimate stress.

$$f_{ps} = E_{ps}\varepsilon \left[A + \frac{1-A}{\left(1+(B\varepsilon)^{1/C}\right)^C}\right] \tag{2.3}$$

The stress-strain properties are likely to change with corrosion of strands. One of the primary corrosion mechanisms is pitting in the strands *(23)* (Figure 2.3). Lu et al. *(23)* proposed a procedure to account for the degradation of the stress-strain behavior for strands that have undergone corrosion. The proposed modification is related to the reduced area of the strand. The strand stress-strain proposed by Lu et al. consists of a bilinear model that can incorporate reduction factors. Deng *(24)* proposed a model for the reduced area that is based on experimental models and from FEM modeling.
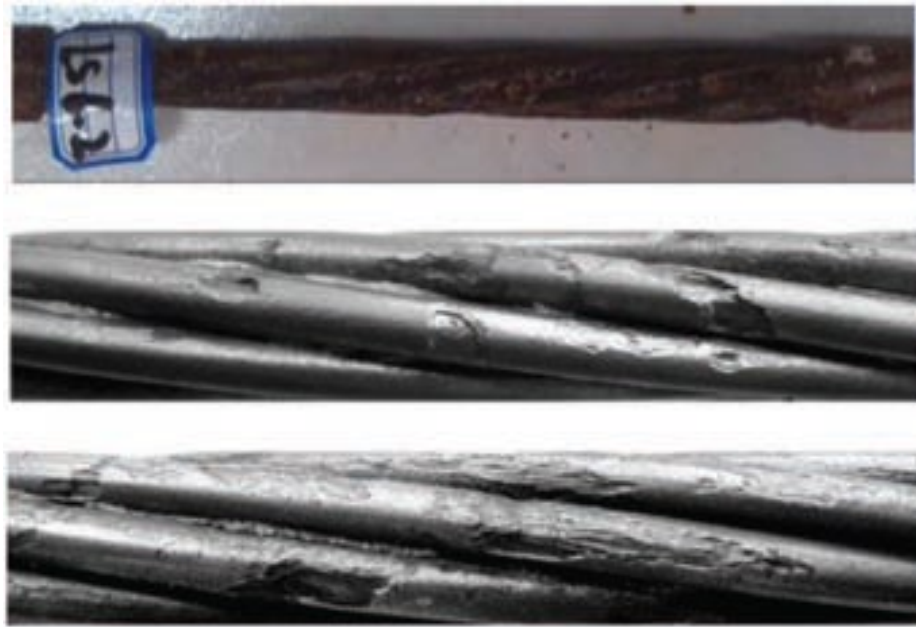
Figure 2.3: Examples of pitting corrosion

3.0 NBI Database and Inspection Report Analysis

3.1 NBI Database Mapping and Distribution

In Massachusetts, condition ratings in the inspection reports are based on the guidelines of FHWA coding and recording manual *(25)*, where items are given a rating from 1 to 10 for their condition, where 1 is the worst and 10 is the best. However, there are no discernible details in the MassDOT *Bridge Inspection Handbook (30)* on how inspectors are to give a consistent rating based on condition of the bridges. Although the FHWA and the inspection reports give some indication on how this is done, there are no details on how to inspect particular types of bridges, only how to give an overall assessment. There should be more details regarding how to inspect different types of bridges, such as what inspectors should be looking for in terms of deterioration (i.e., spalling, cracking, etc.) and how that might affect the condition rating. Table 2.1 presents an example of what MassDOT could consider to incorporate so that more detailed guidance is given to inspectors.

Information about every bridge in Massachusetts listed in the NBI Database was downloaded and used to obtain the distribution of precast prestressed bridges in the state. Only data in the NBI Database that was relevant to the project scope was analyzed in detail.

Data corresponding to only PC bridges was first identified to obtain information on the total number of this type of bridges in Massachusetts. Subsequently, the data were trimmed down to study those bridge cases that corresponded to a deck and superstructure conditions rating of 5 or less to provide a subset of deteriorated structures. The rating scale from the NBI coding of superstructure and deck condition (items 59 and 58, respectively) is shown in Table 3.1 for condition rating.

For precast prestressed bridges with a superstructure and deck rating of 5 or below, the data were obtained that could be used to study the distribution of these bridges in comparison with the entire PC bridge population in Massachusetts. Data collected included Bridge Identification Number (BIN), location (longitude and latitude), highway district, span length, road category carried by the bridge (interstate highway, state highway, local road), age, and type of feature crossed by the bridge. The types of bridges that are the focus of this research typically have the same rating for deck and superstructure because the deck is integral with the superstructure. However, some data for PC beam bridges with cast-in-place deck were also included.

According to the NBI Database, there are 5,229 bridges in Massachusetts, with 403 of these recorded as PC slabs, 135 as PC box beams, and 415 as PC beams. Of these bridges, 97, 32, and 44 PC slab, PC box-beam and PC beam bridges, respectively, currently have a superstructure rating of 5 or less.

Table 3.1: Condition rating guide (MassDOT inspection reports)

Code		Condition	Defects
N	—	Not applicable	—
G	9	Excellent	Excellent condition.
G	8	Very Good	No problems noted.
G	7	Good	Some minor problems.
F	6	Satisfactory	Structural elements show some minor deterioration.
F	5	Fair	All primary structural elements are sound but may have minor section loss, cracking, spalling or scour.
P	4	Poor	Advanced section loss, deterioration, spalling or scour.
P	3	Serious	Loss of section, deterioration, spalling or scour have seriously affected primary structural components. Local failures are possible. Fatigue cracks in steel or shear cracks in concrete may be present.
C	2	Critical	Advanced deterioration of primary structural elements. Fatigue cracks in steel or shear cracks in concrete may be present or scour may have removed substructure support. Unless closely monitored it may be necessary to close the bridge until corrective action is taken.
C	1	"Imminent" Failure	Major deterioration or section loss present in critical structural components or obvious vertical or horizontal movement affecting structure stability. Bridge is closed to traffic but corrective action may put it back in light service.
—	0	Failed	Out of service: beyond corrective action.

The location of these types of PC bridges with a superstructure rating of 5 or less was mapped using latitude and longitude data from NBI. Geolocation data were imported into ArcGIS and used to create a series of maps to indicate the location of bridges in relation to different parameters such as district, superstructure condition, and type of roadway (Figure 3.1 through Figure 3.10). These were created to visualize bridge locations relative to MassDOT districts.

A visual comparison between Figure 3.1, which illustrates the location of all bridges in Massachusetts, with Figure 3.2, which illustrates all PC bridges in the state, does not illustrate a markedly different distribution of PC bridges relative to the general distribution of all bridges throughout the state. The distribution of PC bridges in the state seems to follow a similar pattern as for all bridges with a higher density of PC bridges in District 6.
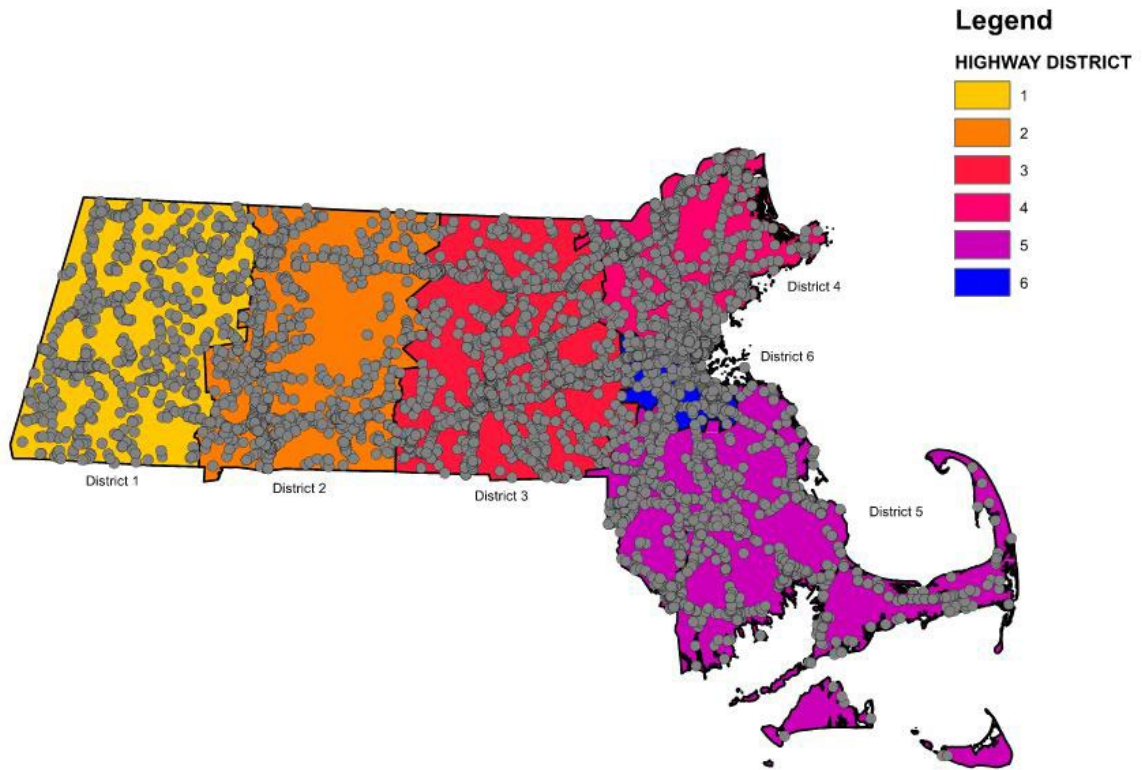
Figure 3.1: All bridges in Massachusetts
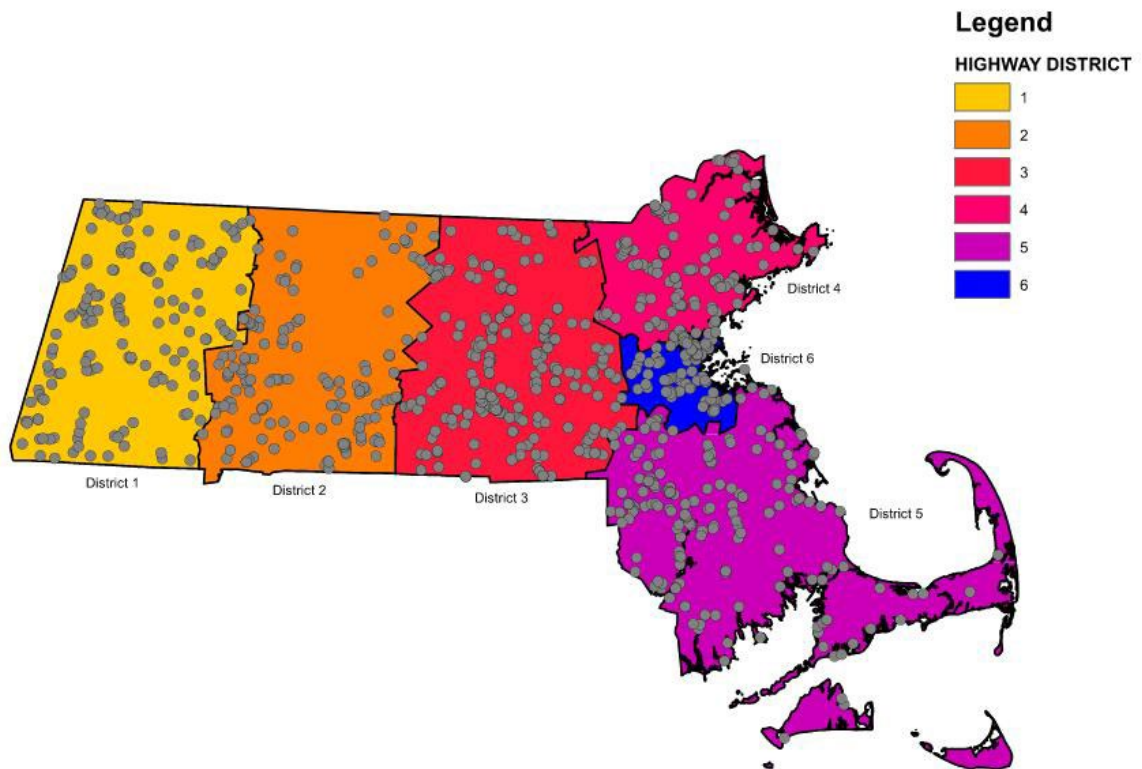
Figure 3.2: All PC bridges in Massachusetts

15
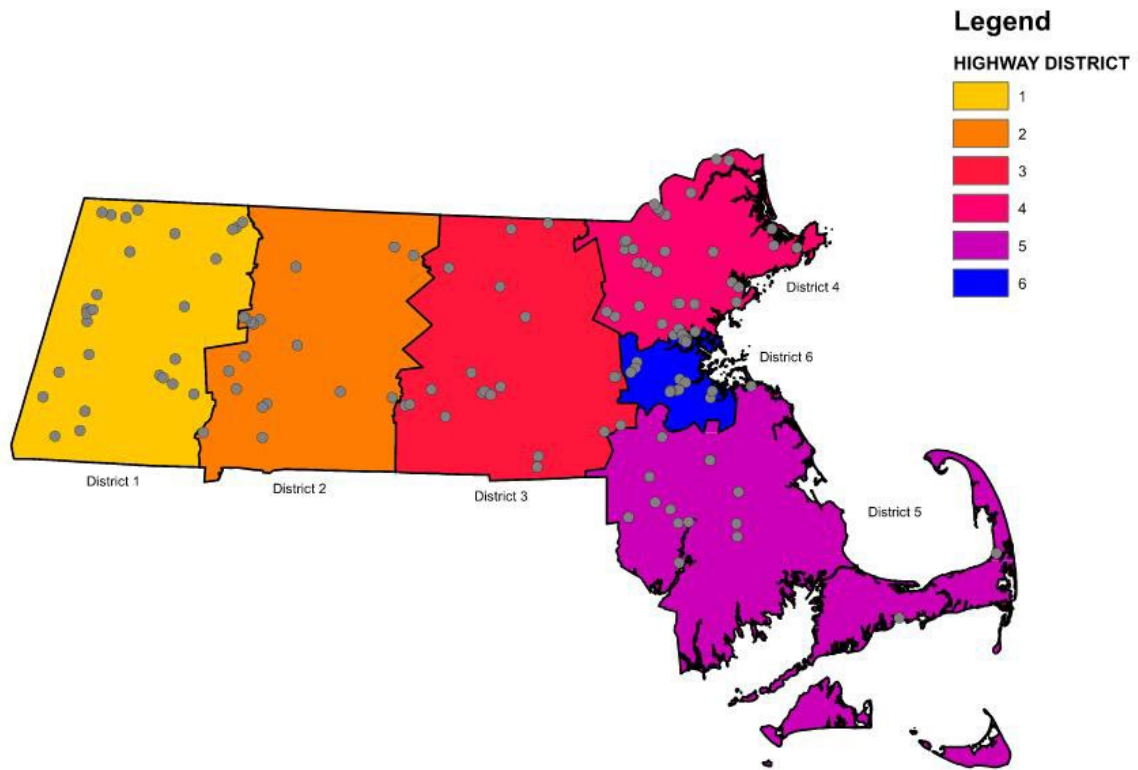
Figure 3.3: All PC box-beam bridges in Massachusetts
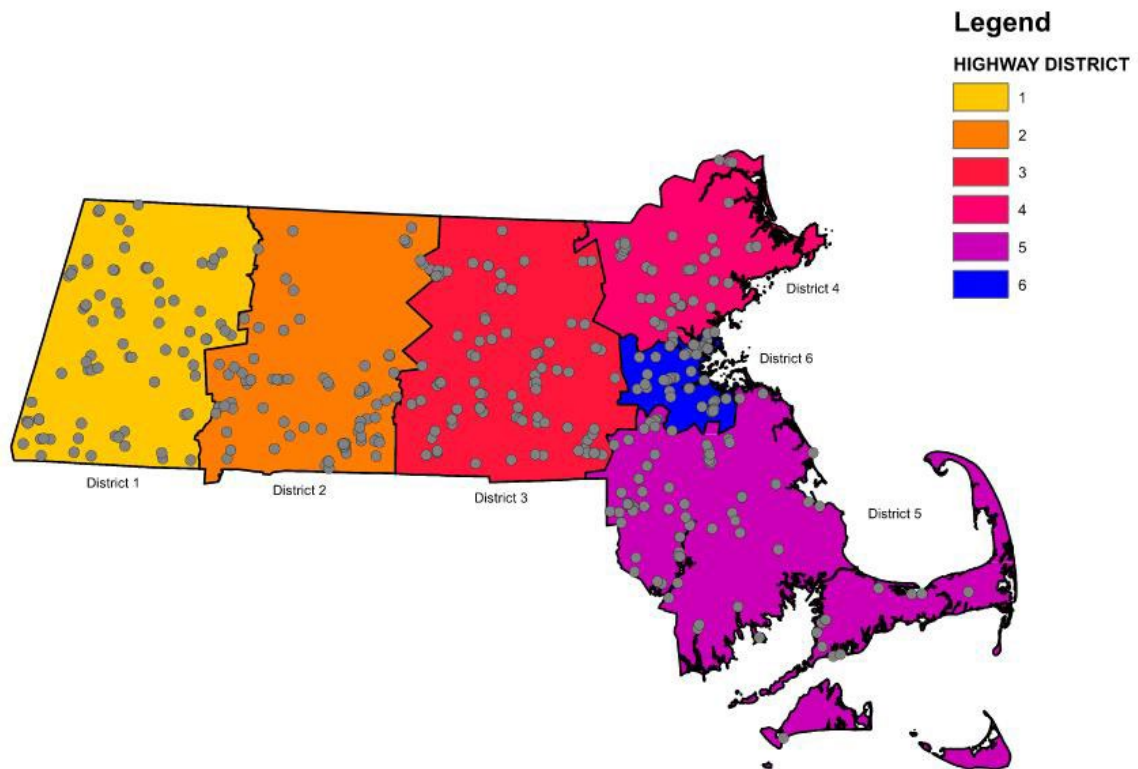
Figure 3.4: All PC slab bridges in Massachusetts

16
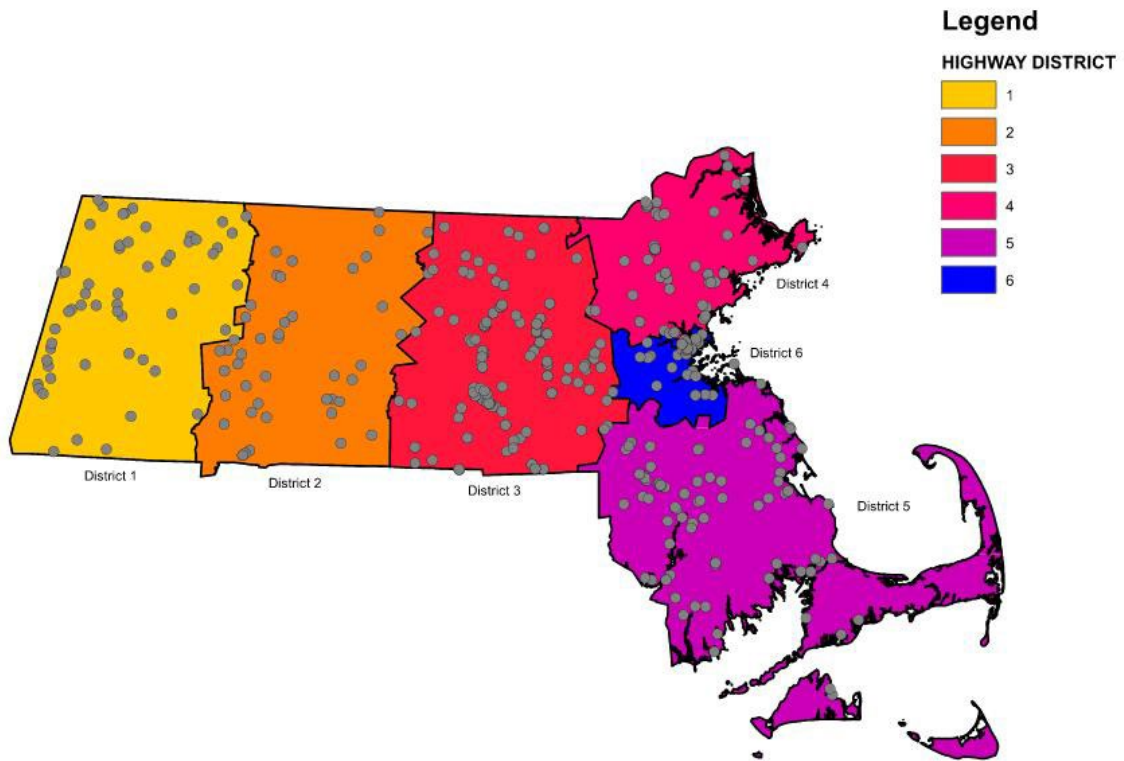
Figure 3.5: All PC beam bridges in Massachusetts
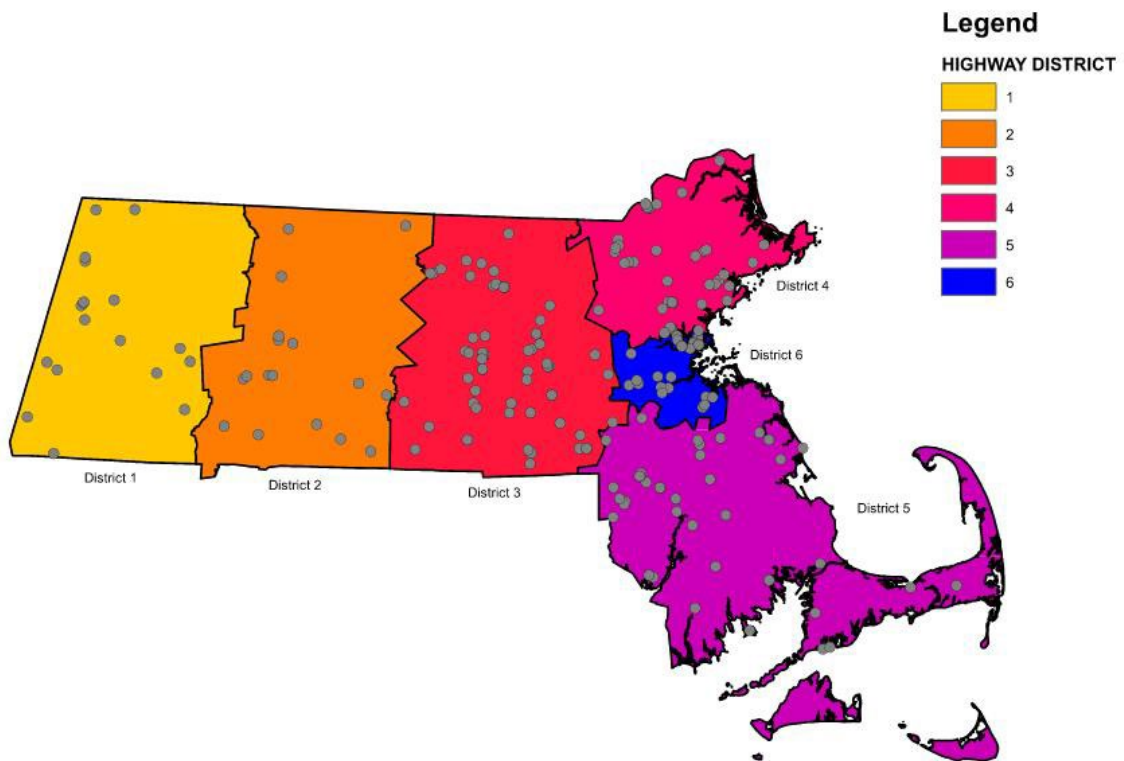
Figure 3.6: All PC bridges with a deck and superstructure rating ≤ 5
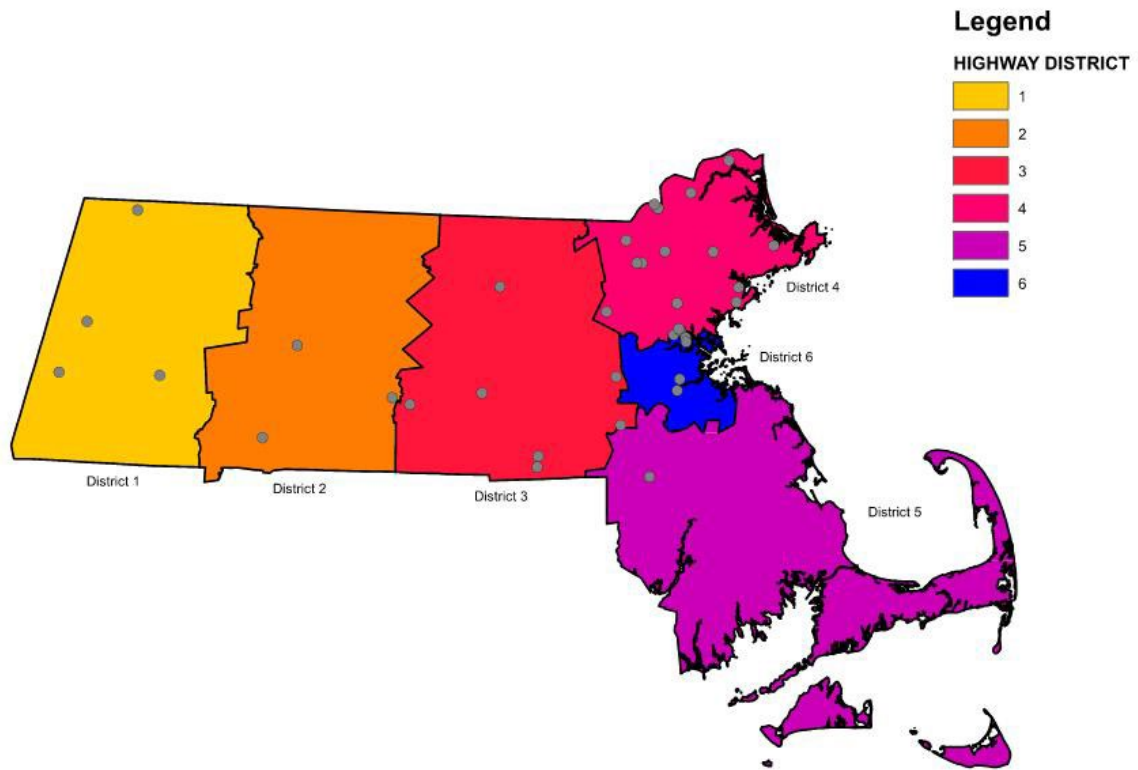
Figure 3.7: PC box-beam bridges with a deck and superstructure rating ≤ 5
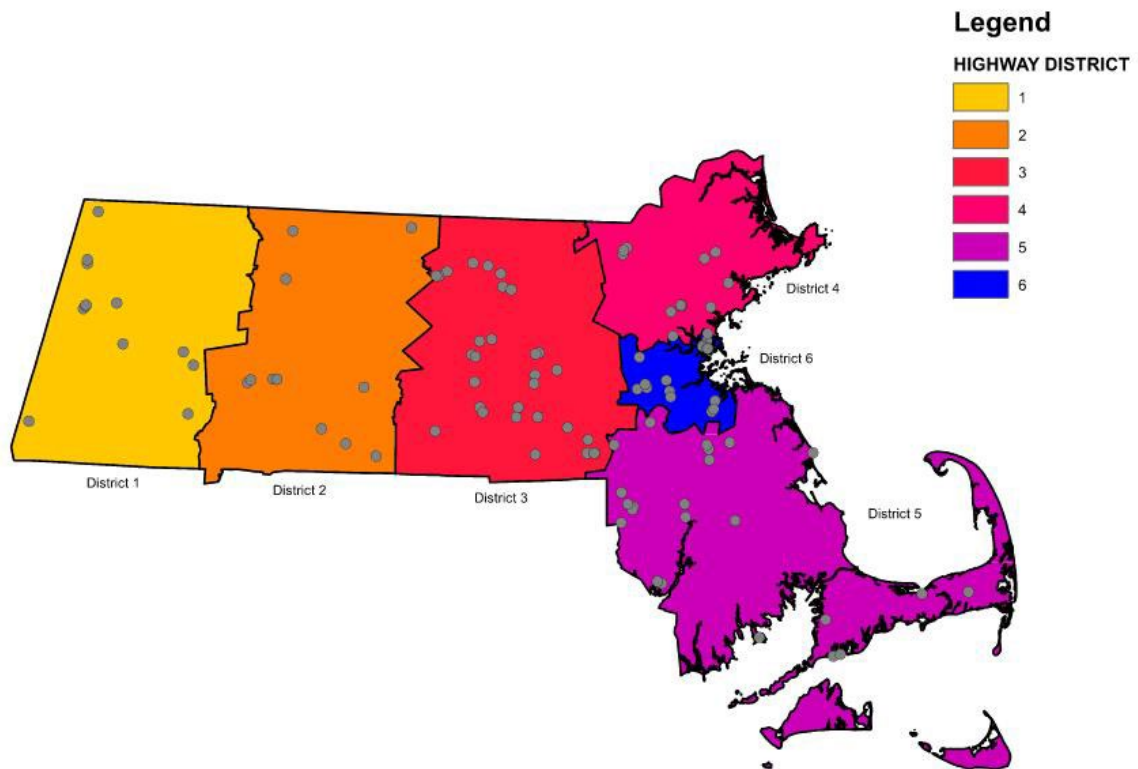
Figure 3.8: PC slab bridges with a deck and superstructure rating ≤ 5
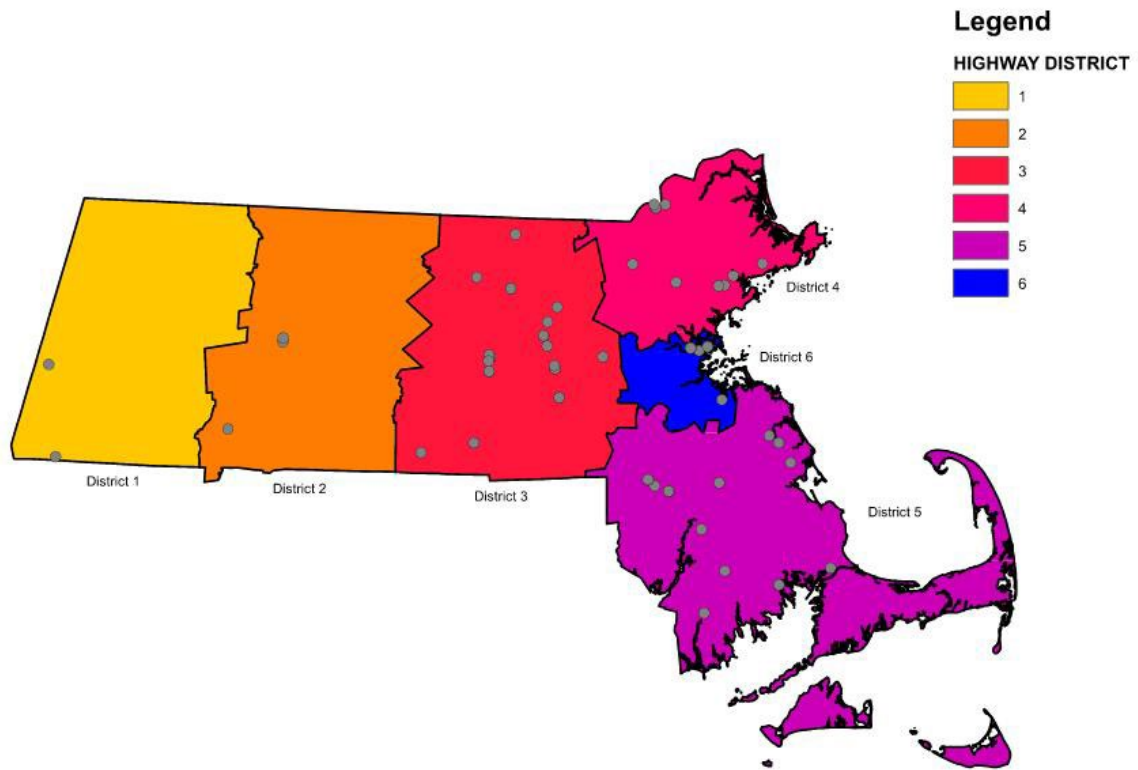
Figure 3.9: PC beam bridges with a deck and superstructure rating ≤ 5
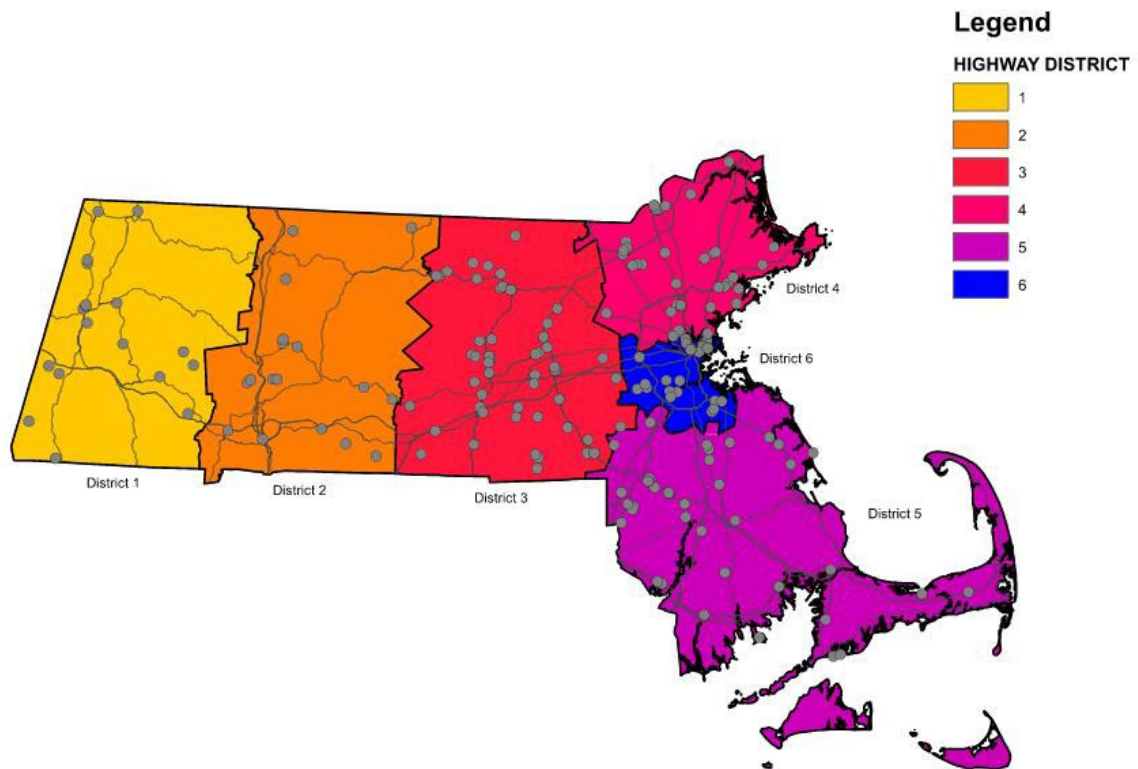
Figure 3.10: All PC bridges with a rating ≤ 5 overlain on highway map

19

Data from the maps give a qualitative perspective of location and distribution of PC bridges throughout the state and any general trends in deterioration as a function of location. Clustering of bridges was investigated to identify potential trends. From the maps, higher bridge clustering seems to occur around cities as would be expected, such as near Boston and Worcester; deterioration of bridges follows this same trend. Quantification of these data was conducted to provide measures of deterioration as a function of the following parameters: (1) deterioration by district; (2) deterioration by construction decade; (3) deterioration by type of roadway carried, and (4) deterioration by maintenance responsibility. The quantified data are presented in Figure 3.1 through Figure 3.9.

Figure 3.11 indicates the number and distribution (percentage) of PC bridges by MassDOT district. In Figure 3.12, the number and percentage of PC bridges of the total number in the state with a superstructure rating of 5 or less is presented by district. The highest percentages of deteriorated bridges occur in Districts 3 and 4 for PC beam and box bridges, whereas they occur in Districts 3, 5, and 6 for PC slab bridges. For example, 14.3% of all PC beam bridges in the state with a deck and superstructure rating less than or equal to 5 occur in District 6. The PC box-beam bridges with a rating less than or equal to 5 are predominantly located in District 4, whereas the other two are spread out more evenly across the other districts.

Figure 3.13 shows how many bridges in each district have a rating less than or equal to 5 (also shown in Figure 3.12) and the percentage this represents of the total bridges of this type in that district. For example, 25.0% of PC box bridges in District 6 have a deck and superstructure rating less than or equal to 5, whereas 41.5% of PC slab bridges in this district have that superstructure rating. The highest percentages of bridges with superstructure rating less than or equal to 5 occur for PC box or PC slab bridges in all districts, with the highest percentage for PC slabs (41.5 %) occurring in District 6, and the highest percentage for PC box-beam (41.5%) occurring in District 4.

In general, Districts 3, 4, 5, and 6 all tend to exhibit a greater number of bridges with damage. Districts 3, 4, and 6 have the highest amount of damage within their districts. District 5 shows more damage with PC slab bridges only.

Figure 3.14 shows how many bridges were built in each decade per bridge type. Figure 3.15 shows how the damaged beams are spread out for each decade. For example, 10.3% of all PC beam bridges with a deck and superstructure rating less than or equal to 5 occur in the 1990s. Figure 3.16 shows how many bridges in each decade have damage. For example, 46.9% of all PC box bridges built in the 1980s have a deck and superstructure rating less than or equal to 5.

PC box-beam bridges constructed in the 1980s have the greatest number of ratings that are less than or equal to 5, but by percentage of total bridges of that type in the inventory the condition of these structures from 1950 through 1989 are all similar (46.9% to 60%). For PC beam bridges, they seem to be evenly spread out amongst the other decades as seen in Figure 3.16. The PC beam bridges are spread out over the 1950s, 1960s, and 1970s. The PC slab bridges are spread out relatively evenly over the 1950s through the 1980s with some coming in the later decades and more being focused in the 1970s.

Overall, what is noticed is that all of the bridges built between the 1950s and the 1980s have the highest amount of damage. That should be expected because objects deteriorate with age, and the evidence seems to suggest that certain bridges are more prone to deterioration in different decades than others.

Figure 3.17 shows how the bridges are split up by different street types. Figure 3.18 shows how the damaged beams are distributed into the different street types. For example, 42.9% of all PC beam bridges with a deck and superstructure rating less than or equal to 5 are an interstate. Figure 3.19 shows how many bridges in each decade have damage. For example, 75.0% of PC slab bridges that are a US numbered highway have a deck and superstructure rating less than or equal to 5. However, the total number of US numbered highways that are PC slab bridges is 8. So, the total number is low, but the overall percentage is high.

City streets seem to have the greatest number of bridges with damage throughout the state, but US numbered highways have the greatest proportion of damage. We are not able to make any definitive statements on city streets because different cities may treat their roads differently and certain jurisdictions maintain their roads at varying degrees of regularity. Maintenance might not be consistent in some areas but highly consistent in others. The only thing we can say is that the US highways are prone to more damage, as seen in the next paragraph, and further investigation would be needed to definitively say that their treatment is directly related to damage.

Each different road type experiences a certain amount of traffic. City streets could experience either a high or a low amount of traffic, depending on where the bridge is. The overall utilization is a factor. US numbered highways as well as state highways and interstates tend to experience a significant amount of traffic as they are some of the quickest ways to traverse the state.
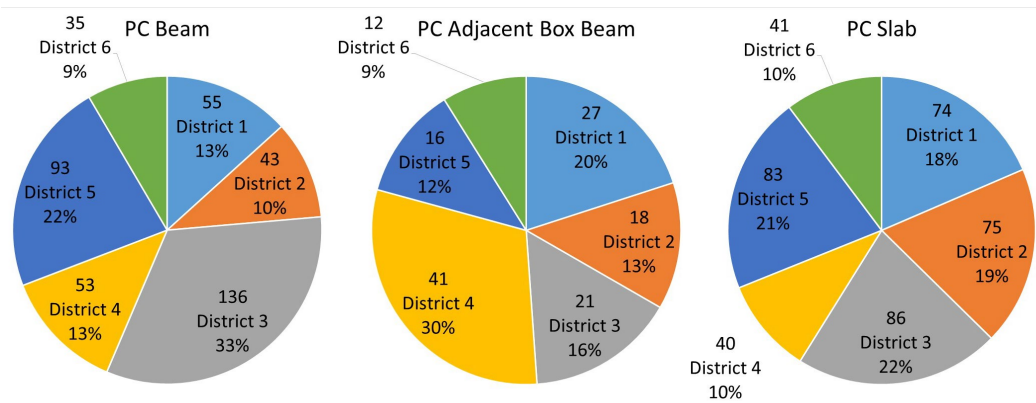
Figure 3.11: Total bridges by district
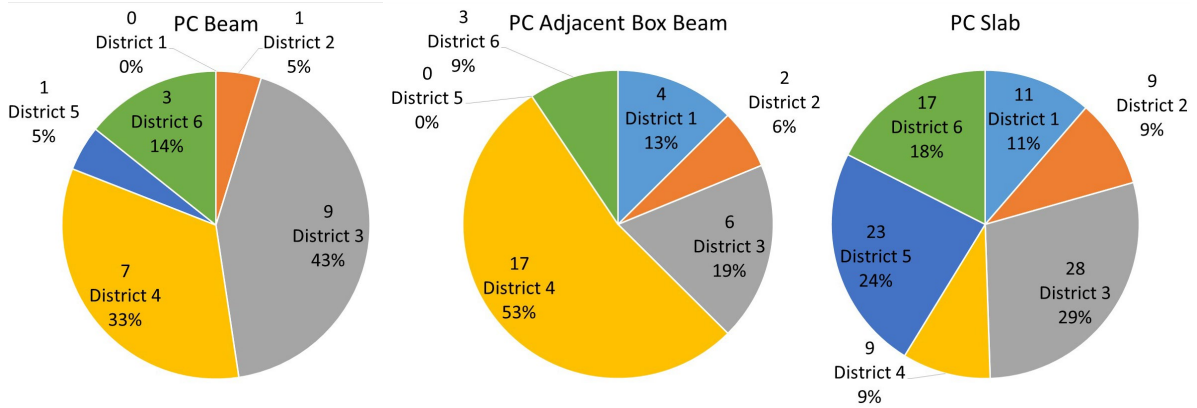
Figure 3.12: Bridges per district with a deck and superstructure rating ≤ 5
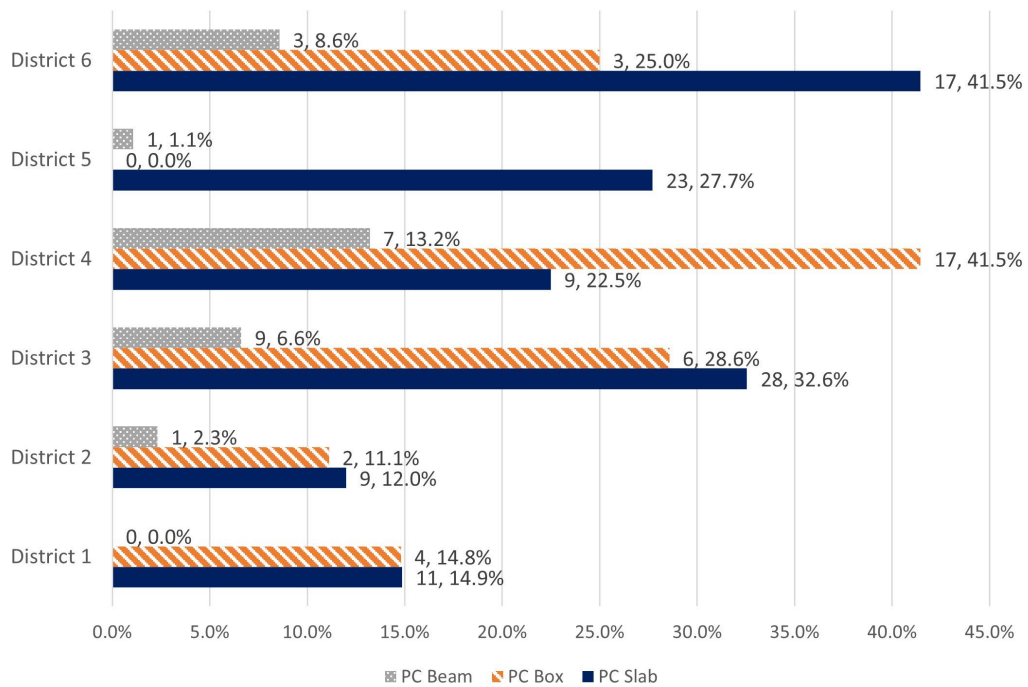
Figure 3.13: Bridges with a deck and superstructure rating ≤ 5 by district
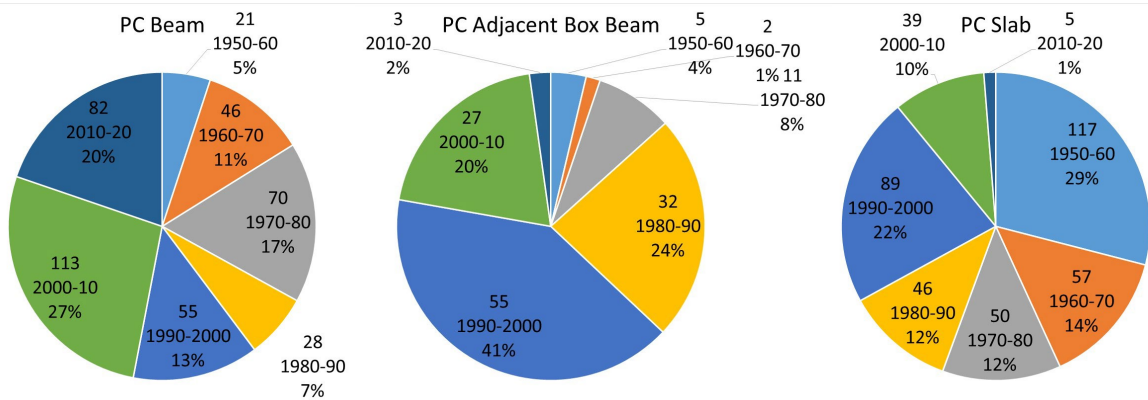
Figure 3.14: Total bridges by decade

22
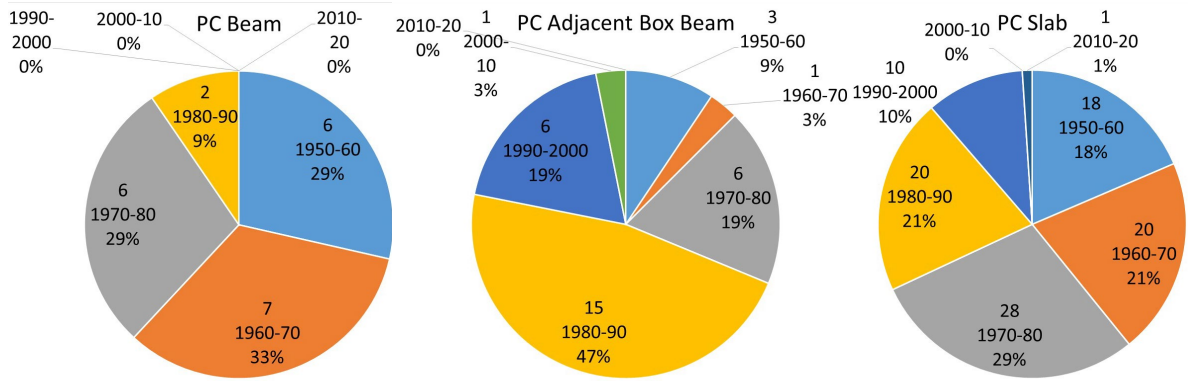
Figure 3.15: Bridges in each decade with a deck and superstructure rating ≤ 5
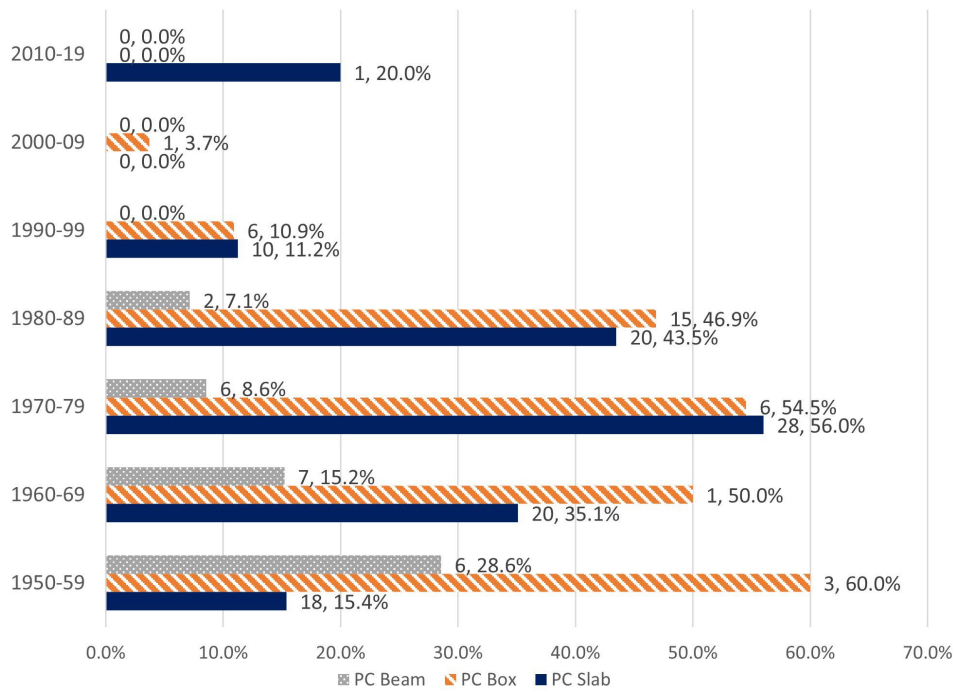
Figure 3.16: Bridges with a deck and superstructure rating ≤ 5 by decade

23

PC Beam

Other, 2.2%
Interstate, 22.4%
US # HW, 4.1%
State HW, 24.1%
City Street, 47.2%

- ■ Interstate
- ■ US # HW
- ■ State HW
- ■ County HW
- ■ City Street
- ■ Other

PC Box

Other, 1.5%
US # HW, 2.2%
State HW, 20.7%
City Street, 75.6%

- ■ Interstate
- ■ US # HW
- ■ State HW
- ■ County HW
- ■ City Street
- ■ Other

PC Slab

Other, 1.7%
Interstate, 4.2%
US # HW, 2.0%
State HW, 15.6%
City Street, 76.4%

- ■ Interstate
- ■ US # HW
- ■ State HW
- ■ County HW
- ■ City Street
- ■ Other
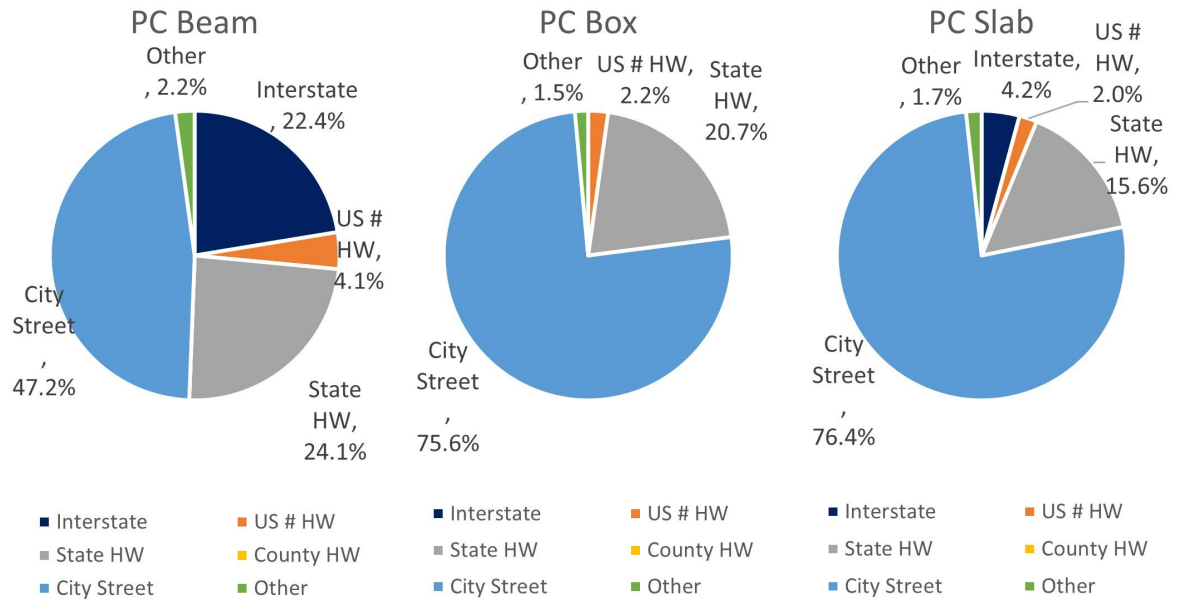
Figure 3.17: Total bridges by street type

PC Beam

City Street, 23.8%
Interstate, 42.9%
State HW, 23.8%
US # HW, 9.5%

- ■ Interstate
- ■ US # HW
- ■ State HW
- ■ County HW
- ■ City Street
- ■ Other

PC Box

US # HW, 6.3%
State HW, 31.3%
City Street, 62.5%

- ■ Interstate
- ■ US # HW
- ■ State HW
- ■ County HW
- ■ City Street
- ■ Other

PC Slab

Interstate, 6.3%
US # HW, 6.3%
State HW, 14.6%
City Street, 72.9%

- ■ Interstate
- ■ US # HW
- ■ State HW
- ■ County HW
- ■ City Street
- ■ Other
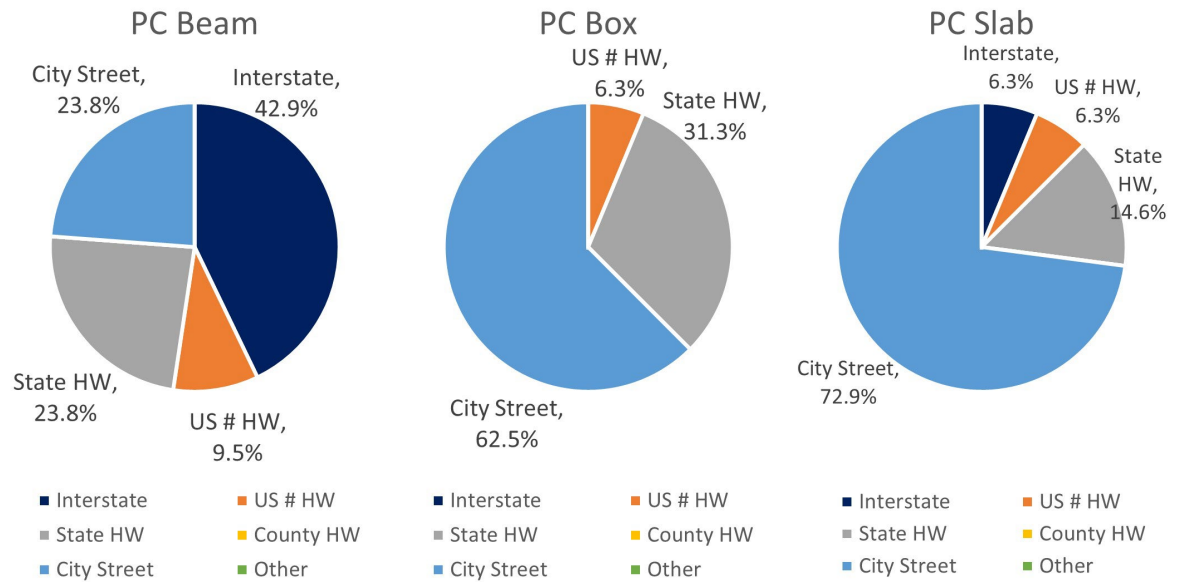
Figure 3.18: Bridges with deck and superstructure rating ≤ 5 by street type

24
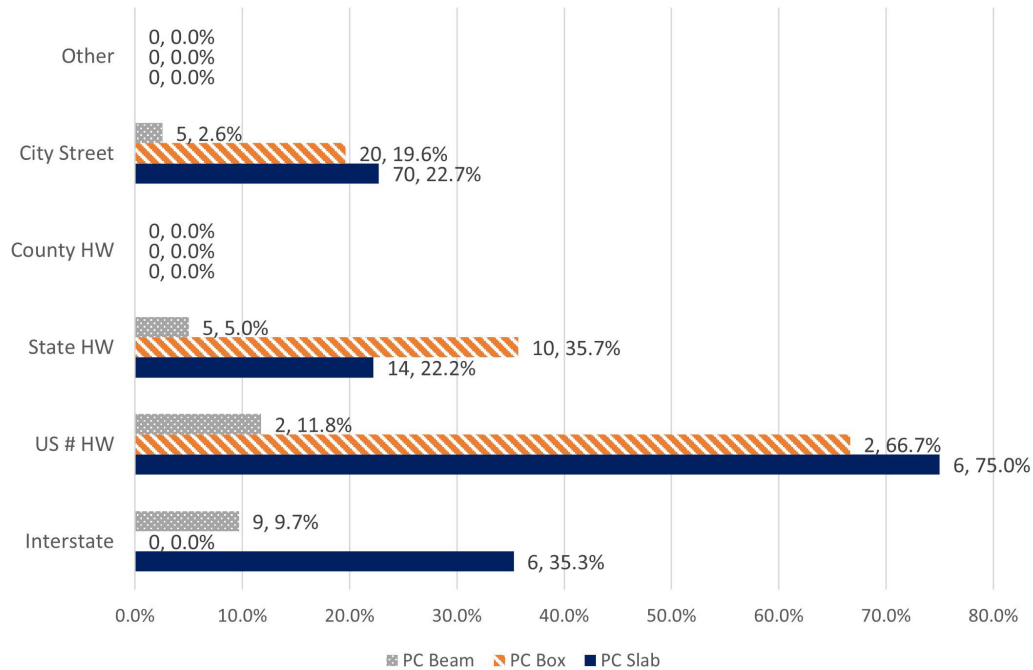
Figure 3.19: Bridges with a deck and superstructure rating ≤ 5 by street type

From the maps, there is no discernible trend between the level of deterioration observed and the location of the bridge. More bridges appear to exhibit deterioration on the eastern side of the state than on the western side of the state, but this could be attributed to a higher population density and higher roadway traffic causing the bridges to be subjected to a larger number of load cycles than those on the western side of the state. This is predominantly due to Boston and Worcester being on the eastern part of Massachusetts. This is also shown in the district data, where the bridges located in eastern districts appear to exhibit higher deterioration (Figure 3.12 and Figure 3.13). It would seem then that bridge deterioration can be directly correlated with population density; consequently, bridges need to be treated during winter to keep them in operation. Average daily traffic (ADT) was also investigated to determine if the superstructure ratings are influenced by the amount of traffic the bridge experiences. After looking at the series of box and whisker plots for the ADT of prestressed concrete bridges with different superstructure ratings (Figure 3.20), bridges with lower condition rating (3 to 5) correspond with those having highest ADT. ADT is also influenced by population density; that data indicate that bridges with higher ADT (those in the eastern side of the state) exhibit lower condition rating.
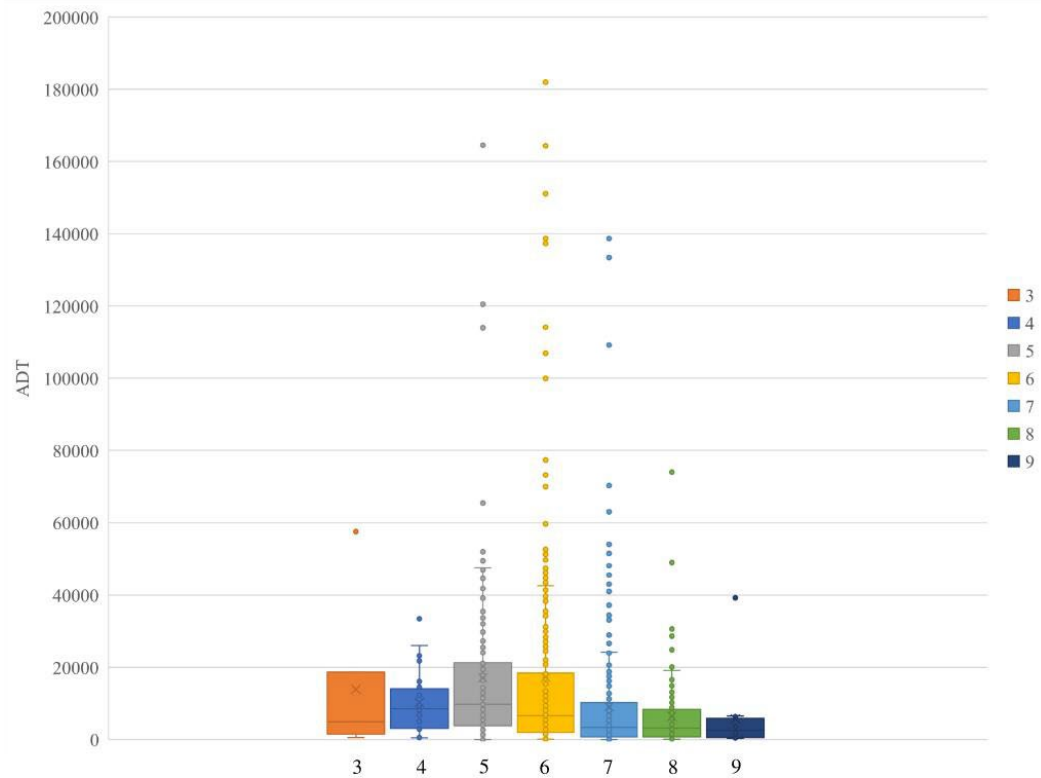
Figure 3.20: ADT of bridges with different superstructure ratings

There seems to be a correlation between age and the rating of the bridge. The 1960s, 1970s, and 1980s are the decades that are exhibiting the greatest number of low ratings both proportionally and totally. The theory that was given to us was there was a bad batch of concrete that was given in the 1960s and 1970s. This theory currently holds water for those decades, but it does not account for the 1980s. More research would be needed to expand this theory. The city streets seem to account for most of the damaged bridges in terms of total numbers, but proportionally, the US numbered highways have the highest percent of damage. Based off this, there does not seem to be a huge correlation between jurisdiction and damage, but more information would be needed to make a definitive declaration on the US numbered highways.

3.2 Individual Bridge Deterioration Analysis

A total of seven different deterioration metrics were identified as either showing or being a possible identifier of deterioration. These metrics are as follows: concrete staining, hairline cracking, wide cracking, differential deflection, concrete spalling, strand corrosion, and strand severing. Sections 9.7.3 and 9.10.3 of the FHWA *Bridge Inspectors Reference Manual (26)* gives a list of common deficiencies than can occur with prestressed slabs and prestressed box beams, respectively. However, we believed that some of these deficiencies would likely not contribute to structural behavior, would be presented with other levels of deterioration, or

would be a result of external forces that would not contribute to the natural deterioration of structures.

3.2.1 Inspection Report Data Collection

After studying a few of the inspection reports, it was decided to determine deterioration individually for each beam of each bridge and collect that information in tabular format by dividing each beam longitudinally into thirds. Because of lack of sufficiently detailed information, data was summarized simply by indicating whether the type of deterioration was present or not (yes/no) (Figure 3.21).

To determine presence of deterioration, photographic evidence and condition descriptions (notes, sketches, etc.) collected by inspectors were studied in detail and used to populate the deterioration tables. Some of the inspection reports included detailed information including detailed drawings, a variety of clear photographs, and excellent descriptions of conditions that could not be seen through the photographs or drawings alone. Other reports provided very little information or no information at all. Whenever information was lacking, it was assumed that no deterioration occurred within that region of the beam.

In very few cases, the research team did not have access to the inspection reports because their access was restricted (two bridges around Logan Airport). Three other inspection reports did not contain deterioration information that could be used for this project. In total, of the 132 bridge inspection reports (adjacent box-beam bridges and deck slab bridges), the team could not access information for two, and three others did not contain any useful deterioration information. The total number of inspection reports that were included in this part of the study was 127.

Figure 3.21 shows an example of deterioration data collected for beams of a particular bridge. The first column was used to identify the bridge (structure number is also included in the spreadsheet). The second column was used to identify the beam number in the bridge. The third column was used to report location along each one-third beam section. The subsequent seven columns were used to report if deterioration of any type was present within that portion of each beam. An additional column was created to add comments about the beam in question.

	#1	1st Third (East)	N	Y
		2nd Third	N	Y
		3rd Third (West)	Y	Y
	#2	1st Third (East)	N	N
		2nd Third	N	N
		3rd Third (West)	N	N
	#3	1st Third (East)	N	N
		2nd Third	N	N
		3rd Third (West)	N	N
	#4	1st Third (East)	N	N
		2nd Third	N	N
		3rd Third (West)	N	N
	#5	1st Third (East)	N	Y
		2nd Third	N	N
		3rd Third (West)	N	N
	#6	1st Third (East)	N	N
		2nd Third	N	N
		3rd Third (West)	N	N
	#7	1st Third (East)	Y	Y
		2nd Third	N	N
		3rd Third (West)	N	N
	#8	1st Third (East)	N	Y
		2nd Third	N	Y
		3rd Third (West)	N	Y

Figure 3.21: Deterioration data collected by bridge

Several spreadsheets were created to summarize data obtained from bridges by DOT district to make data more manageable. These spreadsheets were then merged into a larger spreadsheet (Figure 3.22) that contained information from all the bridges for which inspection data were collected to calculate the percentage of beams in a bridge with a particular deterioration in a particular location. Histograms were created to present data collected.

Cond_Rat	Structure Number	B.I.N.	Bridge Type	Latitude	Longitude	ADT	District	Number of Beams	% Beams w/ Staining	% Beams w/ Hairline Cracking	% Beams w/ Wide Cracking	% Beams w/ Differential Deflection	% Beams w/ Spalling	% Beams w/ Corrosion	% Beams w/ Severed Strands
5	C1100303MMUNNBI	03M	PC Box	42.27968333	72.98123333	260	1	20	25.00%	5.00%	5.00%	0.00%	55.00%	30.00%	10.00%
5	C150010C4DOTNBI	0C4	PC Box	42.71748333	73.07239167	2665	1	12	8.33%	16.67%	0.00%	0.00%	100.00%	8.33%	0.00%
5	P100020DYDOT634	0DY	PC Box	42.41944444	73.24638889	11429	1	10	50.00%	20.00%	0.00%	0.00%	60.00%	50.00%	50.00%
5	S2600402MMUNNBI	02M	PC Box	42.28304722	73.34241389	1940	1	20	35.00%	35.00%	0.00%	0.00%	30.00%	35.00%	10.00%
5	W19002187MUNNBI	187	PC Box	42.22843333	72.14856667	6069	2	10	40.00%	30.00%	20.00%	60.00%	50.00%	30.00%	20.00%
5	B2600421GDOT634	21G	PC Box	42.21078056	72.08518056	2200	3	10	100.00%	0.00%	0.00%	0.00%	30.00%	0.00%	0.00%
5	L080081GCMUNNBI	1GC	PC Box	42.52496944	71.76471389	1600	3	12	0.00%	100.00%	0.00%	100.00%	0.00%	0.00%	0.00%
5	N0300429RDOT634	29R	PC Box	42.28582778	71.34655556	1300	3	10	10.00%	30.00%	0.00%	0.00%	30.00%	10.00%	0.00%
5	U020081J2MUNNBI	1J2	PC Box	42.07521389	71.62532778	780	3	9	11.11%	100.00%	22.22%	0.00%	0.00%	11.11%	0.00%
5	U020521MWDOTNBI	1MW	PC Box	42.046375	71.62937222	1614	3	8	37.50%	0.00%	0.00%	37.50%	50.00%	37.50%	12.50%
5	W440111DWMUNNBI	1DW	PC Box	42.24178056	71.82774167	2239	3	11	54.55%	18.18%	0.00%	18.18%	27.27%	54.55%	0.00%
3	E110012TVDOTNBI	2TV	PC Box	42.63197222	70.77856944	18620	4	11	36.36%	36.36%	18.18%	0.00%	36.36%	36.36%	18.18%
4	A09015332DOT634	332	PC Box	42.61866111	71.17088333	3500	4	30	20.00%	20.00%	20.00%	0.00%	23.33%	16.67%	6.67%
4	H12025310DOTNBI	310	PC Box	42.77270278	71.07598611	26000	4	17	0.00%	100.00%	0.00%	0.00%	100.00%	0.00%	0.00%
4	M170262RWDOTNBI	2RW	PC Box	42.73191389	71.19531111	33400	4	11	36.36%	9.09%	0.00%	0.00%	36.36%	36.36%	36.36%
5	A070032QUMUNNBI	2QU	PC Box	42.85851389	70.93835556	3400	4	8	0.00%	100.00%	0.00%	0.00%	100.00%	0.00%	0.00%
5	A100252DQDOTNBI	2DQ	PC Box	42.39743056	71.14350833	9700	4	10	40.00%	60.00%	0.00%	0.00%	40.00%	20.00%	20.00%
5	B120152MUDOT634	2MU	PC Box	42.58774722	71.25422778	5400	4	12	100.00%	100.00%	0.00%	0.00%	0.00%	0.00%	0.00%
5	B120162MTDOT634	2MT	PC Box	42.58791389	71.27155	4500	4	11	0.00%	100.00%	0.00%	0.00%	18.18%	0.00%	0.00%
5	C190222DUDOTNBI	2DU	PC Box	42.458075	71.381375	46900	4	20	0.00%	100.00%	5.00%	10.00%	10.00%	0.00%	0.00%
5	M12012AN4DOT634	AN4	PC Box	42.40737778	71.11638889	14100	4	11	0.00%	45.45%	0.00%	0.00%	0.00%	0.00%	0.00%
5	M170262RXDOTNBI	2RX	PC Box	42.73205	71.19538056	33600	4	11	18.18%	0.00%	0.00%	0.00%	36.36%	18.18%	18.18%
5	M1702831KDOTNBI	31K	PC Box	42.743	71.20836111	4900	4	9	44.44%	55.56%	44.44%	0.00%	33.33%	11.11%	11.11%
5	M200022RBMUNNBI	2RB	PC Box	42.61643889	70.99694722	3000	4	9	0.00%	100.00%	22.22%	44.44%	33.33%	0.00%	0.00%

Figure 3.22: Partial view of deterioration spreadsheet

3.2.2 Inspection Report Data Analysis

From the collected data, it was clear that discerning any trends was going to be a challenge for some of the deterioration types we had previously identified. For the lower levels of deterioration (i.e., hairline cracking, concrete staining, differential deflection between adjacent beams), trends were very difficult to discern. With higher levels of deterioration intensity, some trends began to emerge, but some were weak trends.

The graphs in Figure 3.23 show the data in histogram form for concrete staining as the deterioration condition. For example, for 92% of bridges with a condition rating of 4, between 0 and 33% of the beams had rust staining, whereas only 8% of bridges with a condition rating of 4 had more than two-thirds of the beams with concrete staining. A lower condition rating (presumably more deterioration) did not correspond to a higher percentage of beams with rust staining as an indicator of deterioration. Bridges with a condition rating of 3 have a larger percentage of the beams with rust staining. When examining concentration of beams with condition ratings of 4 or 5, data do not seem to support an inverse relation between condition rating and percentage of beams with staining. Some bridges that rated a 5 exhibit more concrete staining than all that are rated with a condition rating of 3. It should be made clear that staining could have been caused by exposed reinforcing bar chairs, making it difficult to use rust staining as a reliable deterioration parameter. Furthermore, there is a large amount of spread among the different ratings, showing that there is not much concentration of the ratings in a specific percentage of beams.

Figure 3.24 shows the relationship between differential deflection and the condition rating. Again, a 3 would be expected to exhibit more deflection than the others, but that is simply not the case. In fact, all the bridges that exhibit differential deflection, although it cannot be shown in this figure, are rated at a 5. There is no discernible difference between whether this deterioration has an impact on the condition rating.
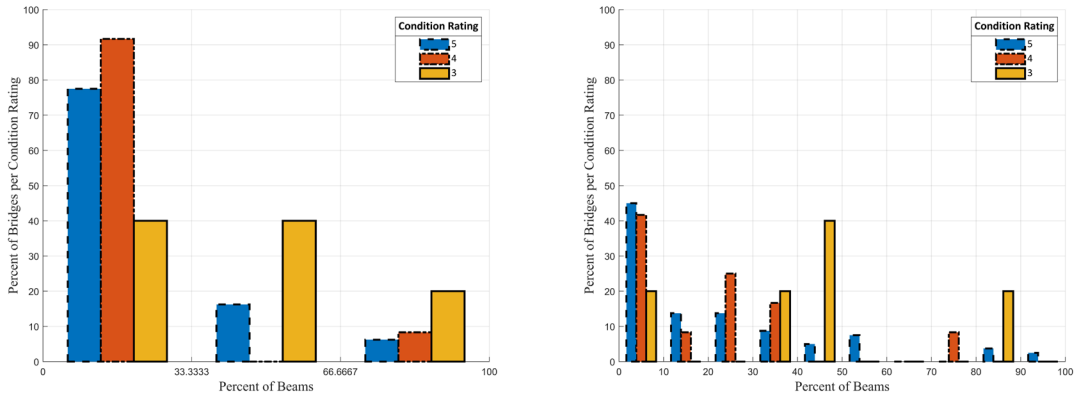
Figure 3.23: Voided slabs containing concrete staining at any location
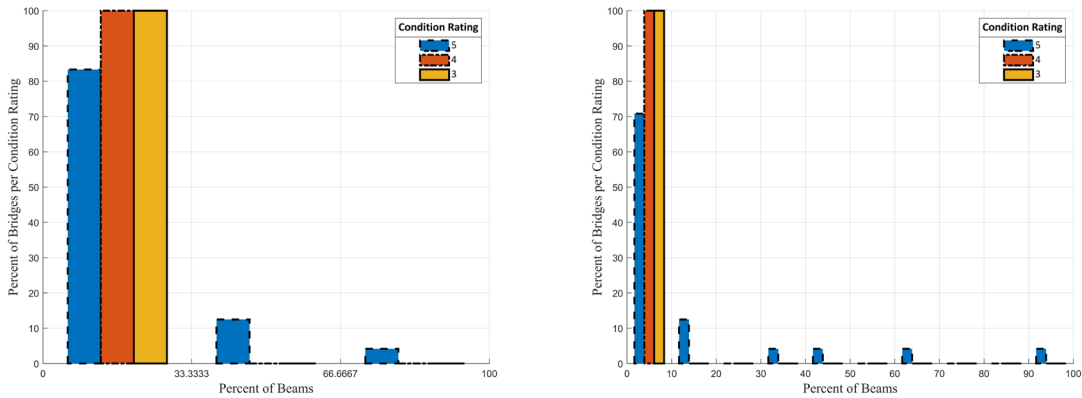
Figure 3.24: Adjacent box beams with differential deflection at midspan

Other deterioration metrics showed more trends than those with less severity. Strand severing, corrosion, and concrete spalling had the most consistency, but there were still some graphs that showed few trends. The other things that we tried to look for were the totality of deterioration among all the beams, meaning that we would look at a combination of metrics in order to see if inspectors took those into account.

In Figure 3.25, we can see most of the 3s exhibit more strand severing than those rated a 4 or 5. In fact, it even seems that 5s exhibit less strand severing than 4s. There are not, however, many things to differentiate some of the condition ratings from each other. In fact, 40% of the slab bridges rated a 3 exhibit around as much strand severing as about 90% of bridges that had a condition rating of 4 or 5. What we can also see is that there are still bridges rated a 4 or 5 that have more strand severing than those that are rated a 3. This shows that while some trends can be identified, there is still some room for interpretation on what constitutes a condition rating of 3, 4, or 5.

Figure 3.26 shows an example of the importance of including both data representations. The graph on the left shows the difference between the 3s and the other condition ratings while the one on the right shows us where the other condition ratings are concentrated. Again, we

can see that 3s have more corrosion than the other ratings. The problem arises with the spread of the 3s and the very similar and rather inconsistent numbers of the 4s and 5s.
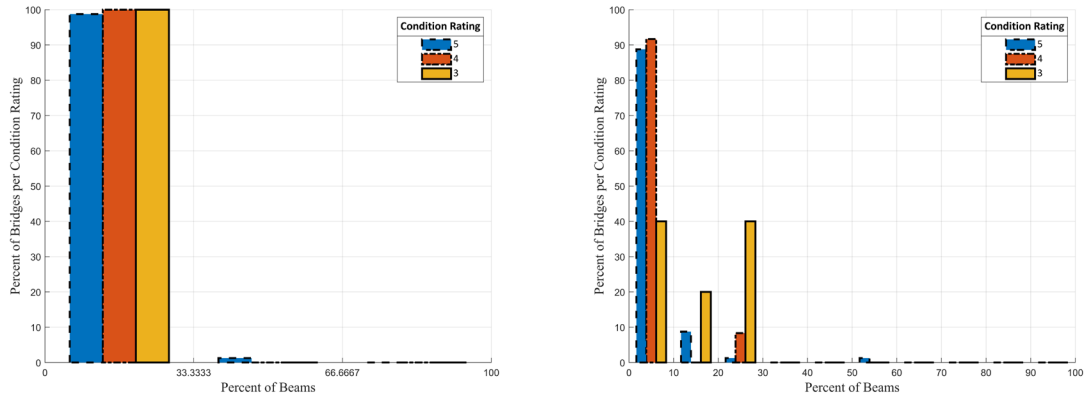
Figure 3.25: Voided slabs containing ruptured strand in middle third of slab
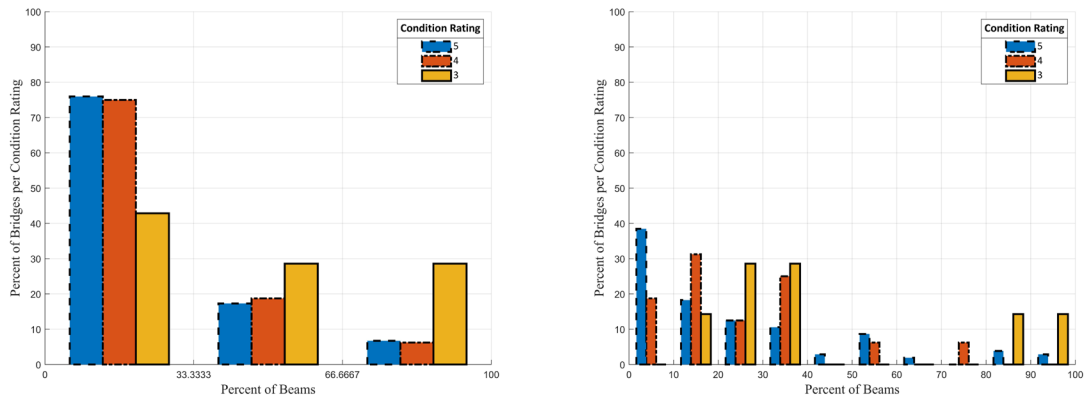
Figure 3.26: Voided slab/box-beam bridges with corrosion present

In Figure 3.27, combinations of deterioration metrics were examined, specifically for this figure, combinations of concrete spalling and strand deterioration such as corrosion or rupture in the middle third of the beam. These are the most severe levels of deterioration, so it would be expected to identify trends. Furthermore, strand corrosion leads to concrete spalling indicating that the linked phenomena might provide trends in data. There does seem to be consistency that 4s and 5s have less deterioration than those that are rated 3. Issues again arise when we try to look at the difference between 4s and 5s. They both have very similar numbers, and the 5s have a few bridges that exhibit more deterioration than both the 4s and 3s.
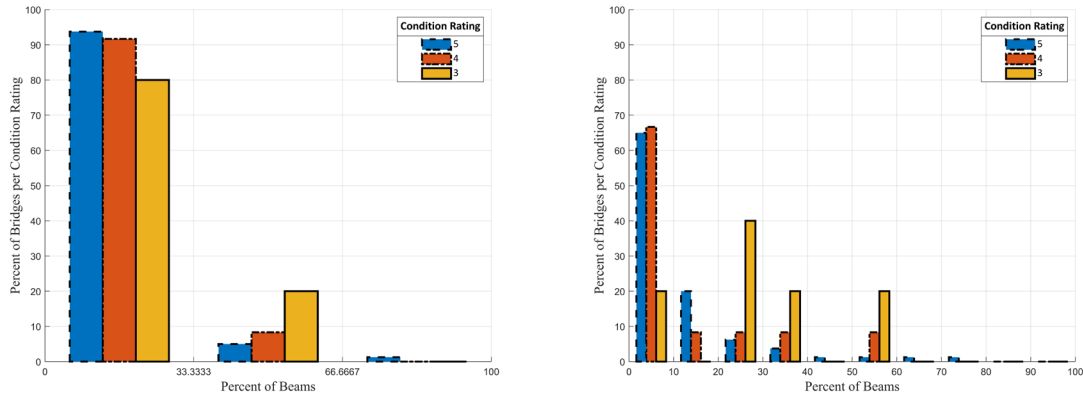
Figure 3.27: Voided slabs/box beams containing concrete spalling and strand distress

The discussion above reveals that, while certain trends can be identified, there are inconsistencies with the way certain bridges are assigned a condition rating for the superstructure. We have not seen anything that would indicate inspectors are to assign a condition rating based on a certain amount of deterioration. This seems to suggest that the condition ratings are primarily based on individual analysis of the deterioration of the superstructure based largely on judgment.

3.2.3 Nonnumerical Analysis of Inspection Reports

There were other things that were noticed about the inspection reports that showed a wide variability in how the information was presented. The most common way the information was presented was through verbal information. The inspectors tried to encapsulate the information with writing where the deterioration was located. The problem was, because of how descriptive their information was, they missed some key information on the severity of the deterioration. They also only chose to make descriptions on a certain number of beams, specifically those that they thought had the most deterioration.

They also tried to use pictures to show the deterioration, which was often more helpful than reading about the deterioration. There were some drawbacks to many of the inspection reports. Some of them contained no pictures, making it hard to gauge the extent of some of the deterioration and forced us to rely heavily on the descriptions the inspectors provided to us. Others only contained a few images and missed pictures of deterioration that they had described earlier.

Another thing that was done, although it was not common, was drawings of the deterioration observed were provided. These drawings allowed us to get a more accurate picture of the deterioration present. While they typically provided information on wide cracking, spalling and strand severing, the accuracy in the drawings in providing the precise location of the deterioration allowed us to get a more accurate picture of what the inspectors saw.

4.0 Description of Bridge Beams and Laboratory Setup

Two bridges were identified for replacement: Bridge No. R-04-004(3LW), herein after referred to as Rehoboth Bridge, and Bridge No. E-11-001(2TV), herein after referred to as Essex Bridge. The Rehoboth Bridge was decommissioned and scheduled for replacement because of poor substructure condition. The abutments of this bridge were exhibiting extensive scour caused by the Palmer River flowing downstream from a dam. The Rehoboth Bridge superstructure had little to no deterioration.

The Essex Bridge superstructure exhibited significant corrosion-induced deterioration in the prestressed box beams. Its poor condition can be attributed to periodic contact with flooding waters. The bridge is located over the Essex River. Three beams from each bridge were selected for testing at UMass to evaluate the bridge rating procedures contained in the MassDOT *Bridge Design Manual*. This section describes details of the beams.

4.1 The Bridge Candidates

4.1.1 Description of the Rehoboth Bridge

The Rehoboth Bridge, constructed in 1964, consists of 10 voided slab beams, six of which support road traffic lanes, two served as transition from traffic lanes to pedestrian sidewalks, and the two fascia beams were used for the sidewalks. The original plans are shown in Figure 4.1, and clarification closeup view of the bridge span and superstructure is presented in Figure 4.2 and Figure 4.4 respectively for better clarity. The bridge span was 33 ft, 5 1/2 in. as seen in Figure 4.2 with the original drawings. The roadway was 30 ft wide to carry the traffic of Reed Street over the Palmer River in Rehoboth, Massachusetts. The bridge skew was 47°−30′ from the longitudinal axis of the bridge.

4.1.2 Description of the Essex Bridge

The Essex Bridge, constructed in 1970, consisted of 11 adjacent box beams. Seven of those beams were placed on traffic lanes and four were used to support sidewalks and utilities across the bridge. The bridge was used for local traffic in Essex, MA to cross the Essex River. The bridge was not constructed on a skew angle. The bridge span was 71 ft to centerline of bearings at each abutment (Figure 4.3). There were two 15-ft long approach slabs on either side. The roadway was 32 feet long with two 5-ft sidewalks. The original plans are shown in Figure 4.3 and a closeup view of the bridge superstructure is shown in Figure 4.5.

33
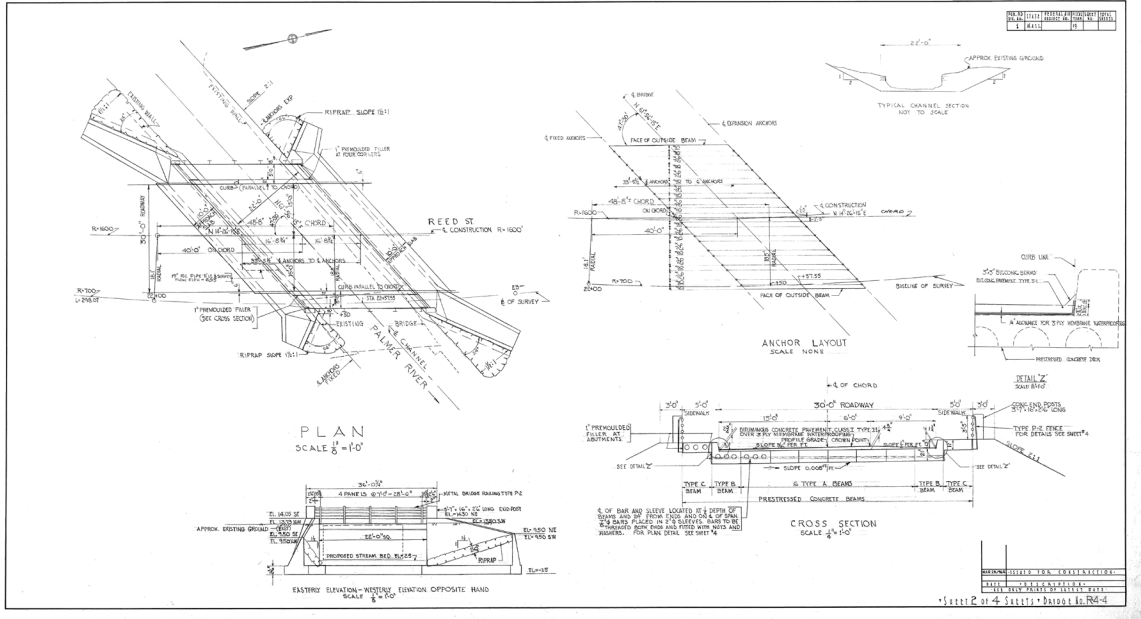
Figure 4.1: Rehoboth Bridge original drawing
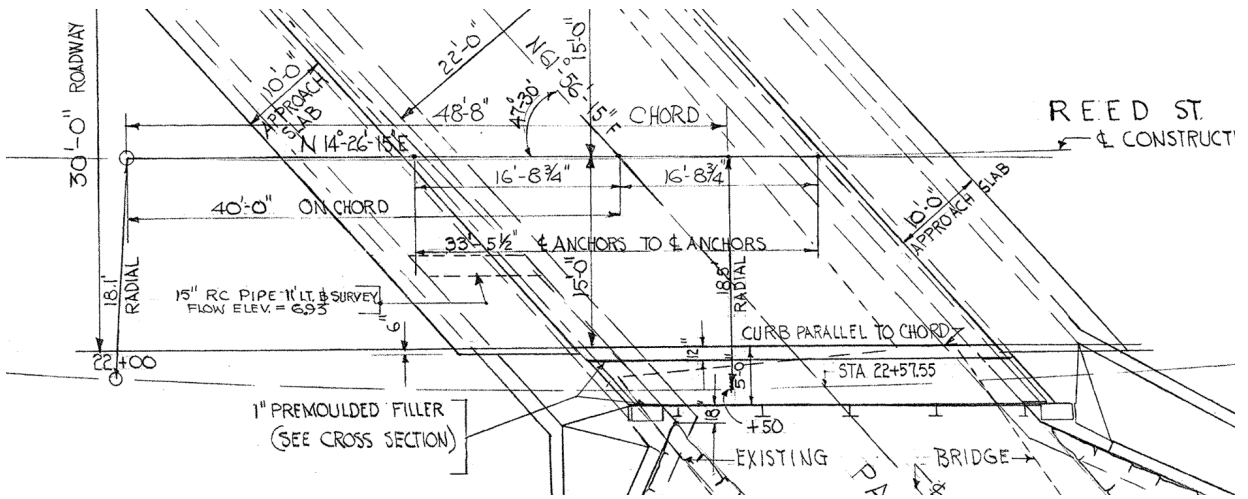
Figure 4.2: Closeup of Rehoboth Bridge span

34
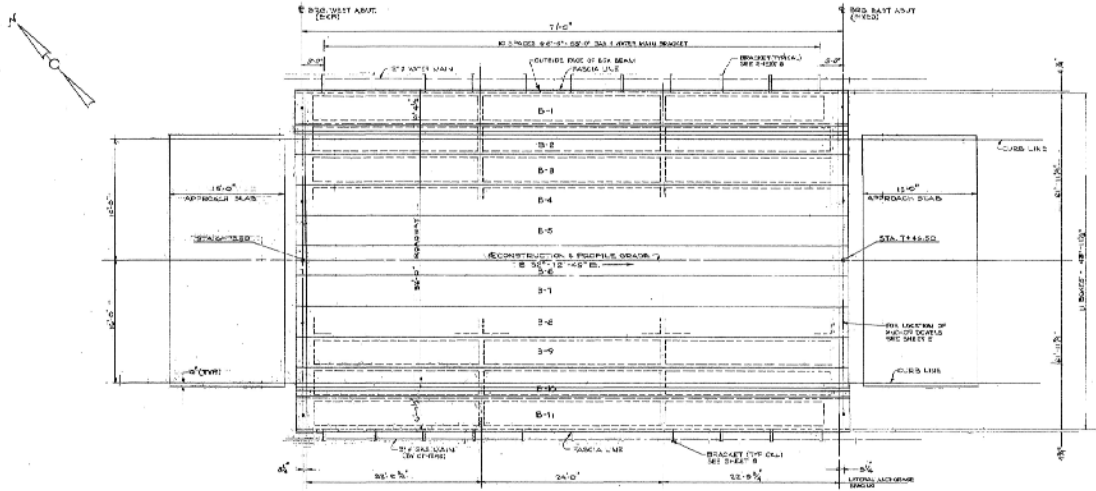
Figure 4.3: Essex Bridge original drawing

A

1C

1B

1A

2A

3A

Reed St.

4A

5A

6A

2B

2C

A

Palmer River

Plan View

Type C Type B   Type A   Type B Type C
Cross Section View at A-A
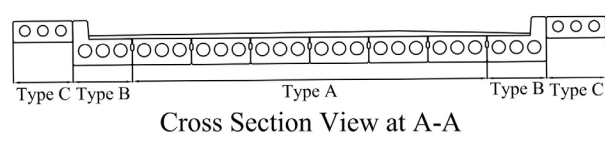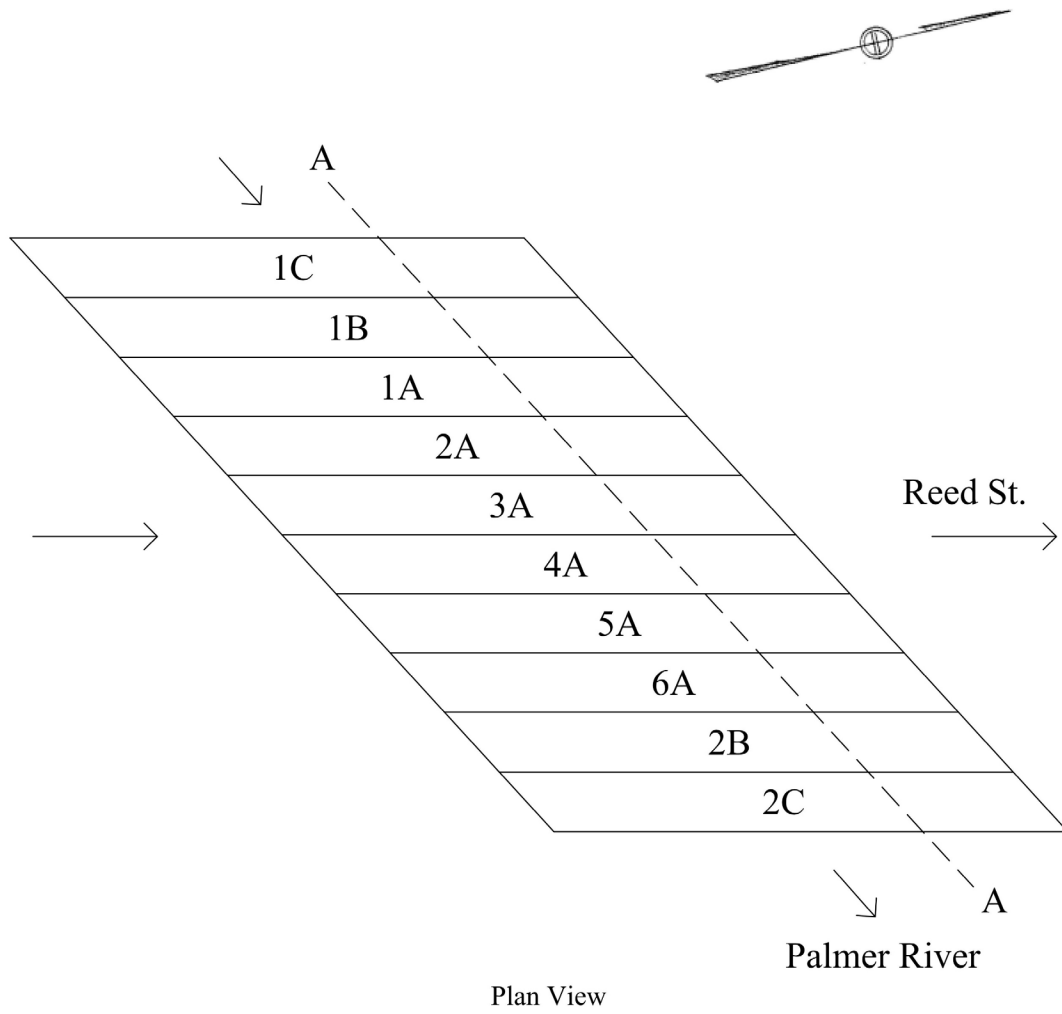
Figure 4.4: Rehoboth Bridge superstructure detail plan and cross section

Main St.

B-1 B-2 B-3 B-4 B-5 B-6 B-7 B-8 B-9 B-10 B-11

Essex River

A — — — — — — — — — — — A

Plan View

Cross Section View at A-A
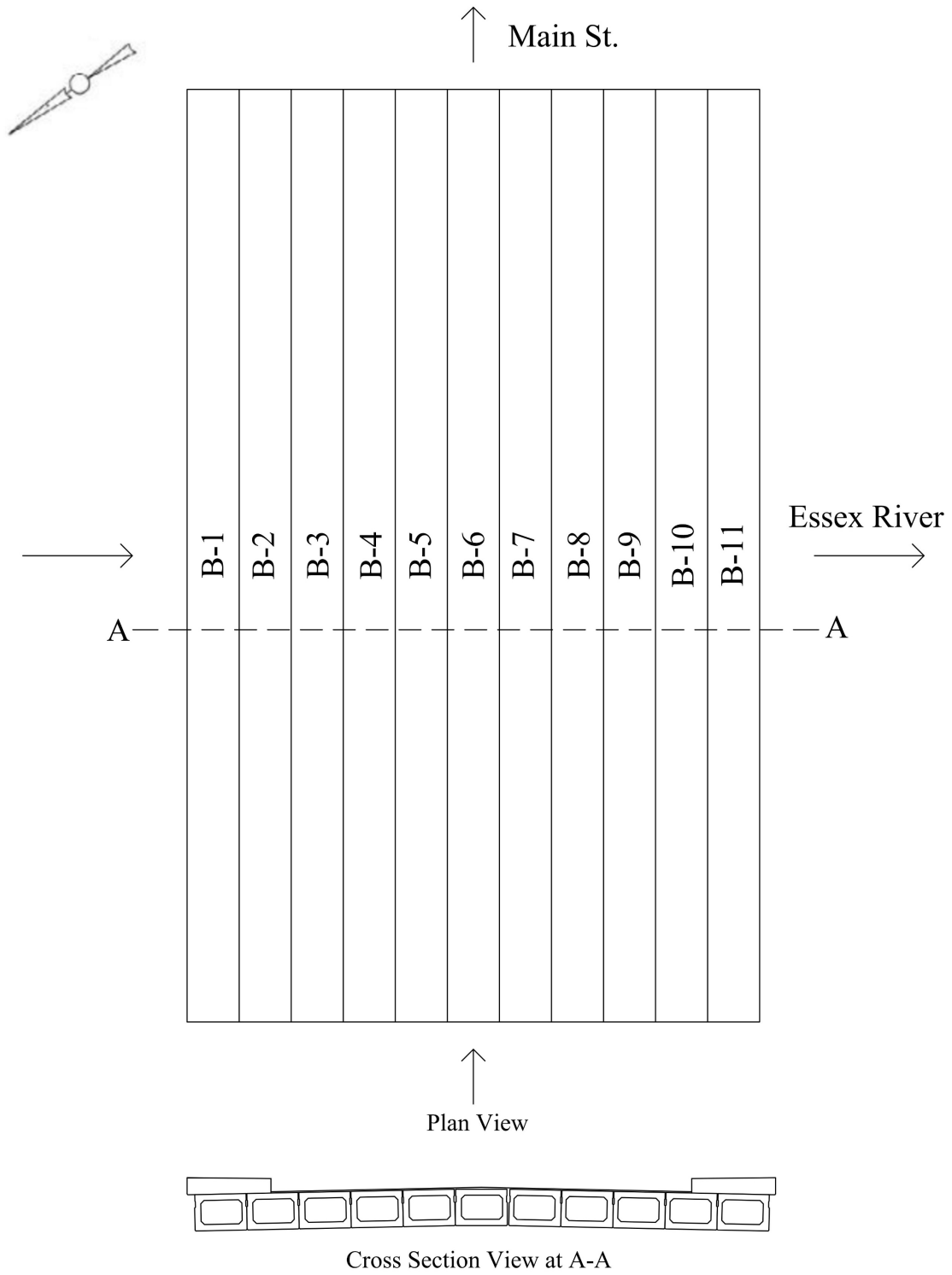
Figure 4.5: Essex Bridge superstructure plan and cross section

4.2 Bridge Beam Selection and Details

4.2.1 Rehoboth Bridge Beams

The edge beams in the Rehoboth Bridge were used to support a sidewalk on either side. The first inboard beam on either side contained an integral curb to allow the beams supporting the sidewalks to be placed higher than beams supporting the roadway. Because these two beams had details which were different from other interior beams, only beams corresponding to those placed underneath the roadway were considered for testing. These beams are designated as Type A beams (Figure 4.4). In Figure 4.4, each beam is referenced by the type of beam using a letter (A, B, or C) and a number to identify their placement beginning from the left on the figure. Beams 2A, 3A, and 4A were selected for testing to failure in the laboratory. Each beam specimen will be designated using a letter corresponding to the bridge name (R in this case), and a number corresponding to the beam number in the bridge (all beams were Type A).

On April 15, 2022, beams 2A, 3A, and 4A were delivered to the Brack Structural Testing Laboratory at Umass Amherst. These beams are denoted as specimens R2, R3, and R4 when reporting laboratory information and data. Each beam was delivered by a private contractor on a separate trailer and stored in the laboratory yard until the date of testing. During storage, the beams were stacked on top of each other using dunnage at the beam ends to avoid damaging the beams as shown in Figure 4.6. The numbers at the ends of these beams represent the beam numbering scheme used at the bridge site.

Original plans and drawings of the bridge were provided, and all known or assumed properties of the bridge were taken from these drawings. Each beam contained 56 0.375 in. straight strands along the full length. Forty-six of those strands were placed along the bottom of the beams and 10 near the top surface of the beam. All dimensions and reinforcement were obtained from the drawings as shown in Figure 4.7.

Beams 2A, 3A, and 4A were 32 ft 5 in. long. Figure 4.7 and Figure 4.8 display the dimensions of the beam along with the strand layout and location of the voids of the beam. The beams were designed for a nominal concrete compressive strength of 5,000 psi, Grade 270 (f_{pu} = 270 ksi) 0.375-in. diameter low-relaxation strands, and mild Grade 60 reinforcing bars for no. 4 stirrups (f_y = 60 ksi). Beams were placed on skewed abutments with a 47.5 degree angle. To allow for transfer of forces between beams, beams contained a 10-in. deep shear key along each side. The wearing surface topping of each beam was removed prior to delivery to the laboratory. The voids in these beams were formed using three circular holes that ran continuously along the entire length of each beam, commonly used to decrease the beam weight and make their load-carrying capacity more efficient.

Figure 4.6: Rehoboth Bridge beams at Brack Structural Engineering Laboratory
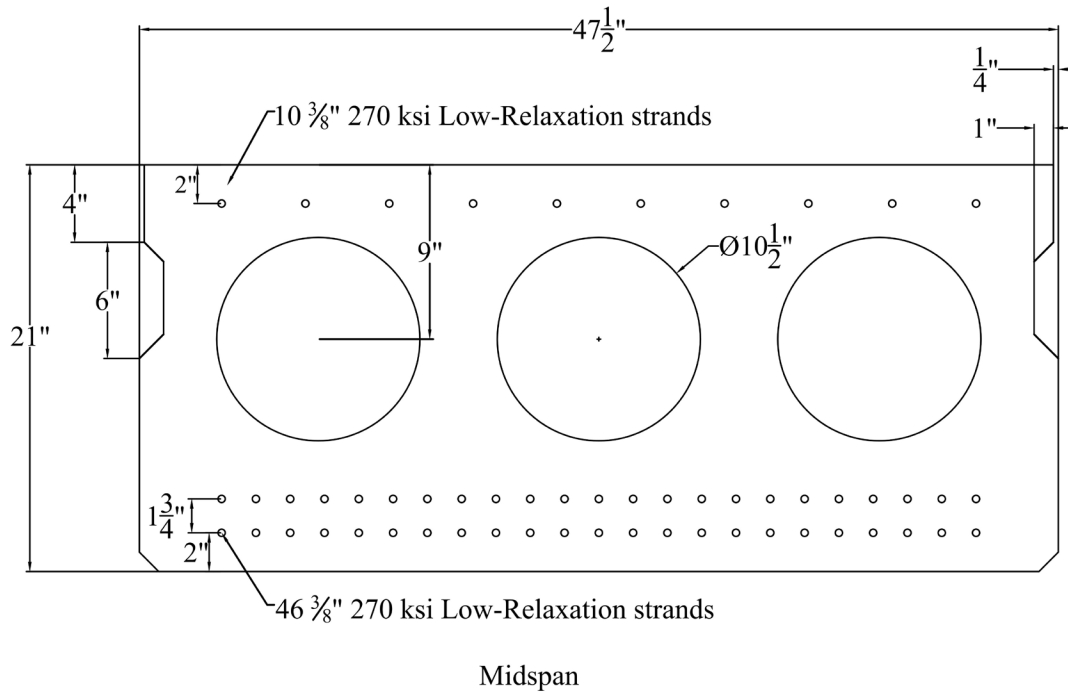
Figure 4.7: Rehoboth Bridge beam (Type A) cross section
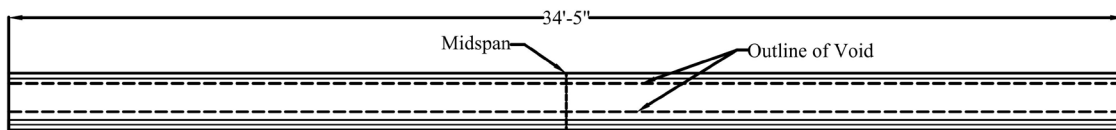
Figure 4.8: Rehoboth Bridge strand layout (side elevation)

4.2.2 Essex Bridge Beams

Delivery to the Brack Structural Engineering Laboratory (UMass Amherst) and storage of Essex Bridge beams is shown in Figure 4.9. The Essex Bridge superstructure consisted of 11 adjacent rectangular box beams placed on straight abutments. The beam span was 71 ft long to centerline of supports on abutments. The beam cross-sectional dimensions are 33 in. deep by 47.5 in. wide (Figure 4.10). Due to the limitations of the laboratory testing space, each beam had to be cut to a total length of approximately 41 ft to fit inside the testing space. The research team decided to test beams to potentially develop a flexural failure and to avoid the potential for a shear failure. To preserve symmetry of the strand pattern about the beam centerline, beam ends were cut 15 ft symmetrically from each end. Original plans for the bridge were used to estimate material and beam properties. The bridge was designed using concrete with a nominal compressive strength of 5,000 psi, 22 0.5-in.-diameter Grade 270 low-relaxation strands, and Grade 60 (f_y=60 ksi) mild reinforcement for no. 4 stirrups and 10 no. 5 top longitudinal reinforcement within the top flange of the beams. Of the 22 prestressing strands, six strands located within the beam webs were harped 9 ft from the center of the beam toward the top flange as shown in the end section (Figure 4.10). The beams had grouted 6-in.-deep shear keys along the entire span and were post-tensioned

40

transversely at two locations along the bridge to promote transverse load distribution (Figure 4.10). Beams contained interior concrete diaphragms where the transverse post-tensioning ducts were located.

Due to corrosion deterioration that had occurred over the years, the top surface of each beam had been patched using either an asphalt overlay or a concrete overlay of varying thickness. Beam patches were not uniform in location or material. Patches or beam topping on the beams remained in place during the test, except for localized places where the loading frame was supported.

On August 8, 2022, three of the Essex Bridge beams were delivered to the Brack Structural Testing Laboratory. Just as for the Rehoboth Bridge beams, each beam was delivered by a private contractor and on separate flatbed trailers. As shown in Figure 4.9, each beam was identified and marked prior to shipping using a number depending on the beam location on the bridge (Figure 4.5). In the original drawings, each beam was identified using the letter B, followed by the beam number. Each specimen was designated only using the beam number identifier used in the bridge drawings (i.e., Essex Bridge Beam 3).

Using the nomenclature in Figure 4.5, beams B-3, B-4, and B-9 were chosen for testing and delivered to the Brack Structural Engineering Laboratory. These beams were chosen because they showed moderate to significant amounts of deterioration and were believed to represent a range of deterioration conditions of beams in the bridge. Beams B-1, B-2, B-10, and B-11 were placed on the two bridge edges and supported a monolithic sidewalk that was cast onto them. Therefore, they were not representative of beams used to support the traffic lanes of the bridge. For the purpose of reporting laboratory data, the beams shipped to the laboratory will be referenced by a letter corresponding to the bridge name (E for the Essex Bridge) along with the beam number from the drawings (i.e., Specimen E4).

The Essex Bridge beams have a rectangular cross section and contain a rectangular void that runs along the beam length. Dimensions of the beam and void are shown in Figure 4.10, and a side elevation of the beams that illustrates the prestressing strand pattern is shown in Figure 4.11.

Figure 4.9: Essex Bridge beams at the Brack Structural Engineering Laboratory

- Harped Strands

Midspan

End Section
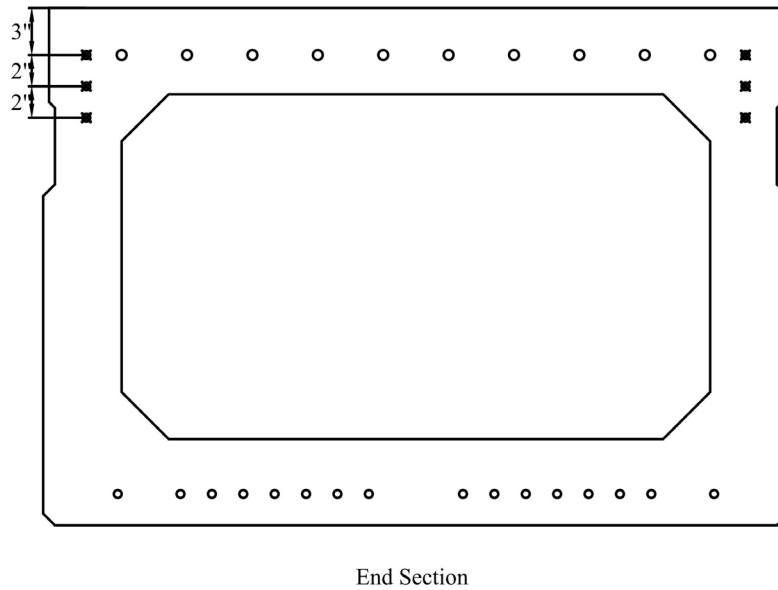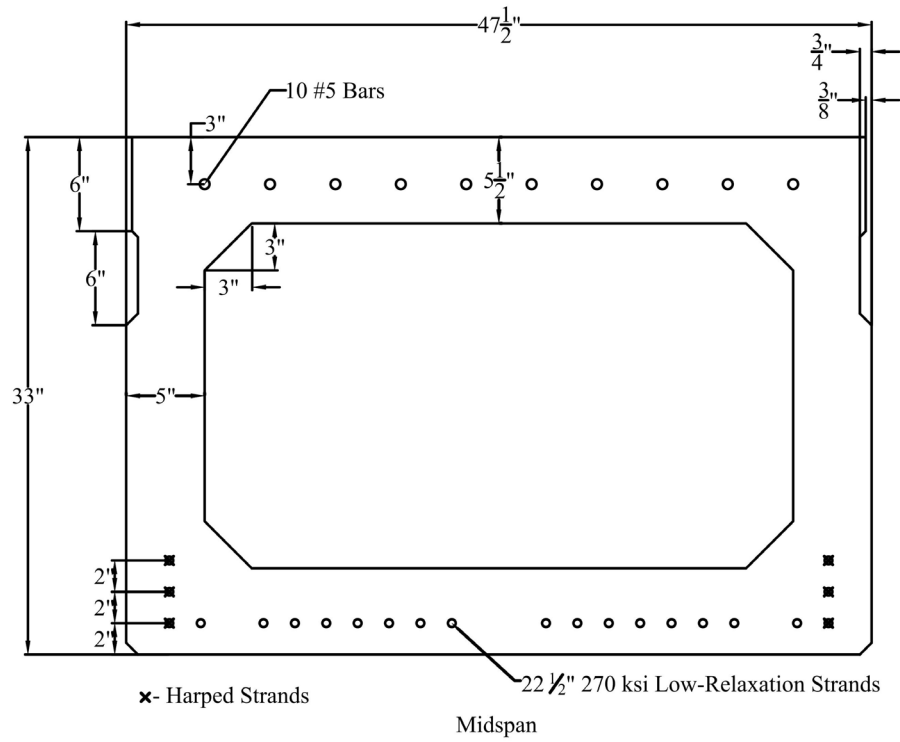
Figure 4.10: Essex Bridge Beam cross sections
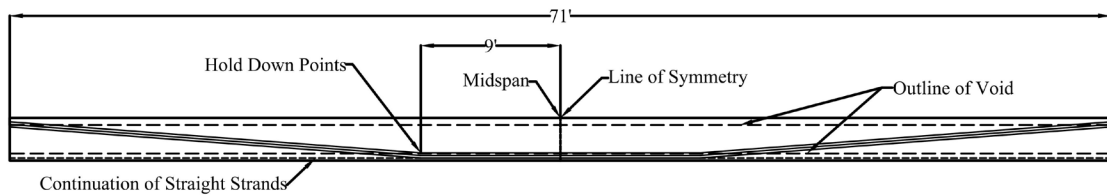
Figure 4.11: Essex Bridge beam strand layout (side elevation)

43

4.3 Bridge Beam Condition

4.3.1 Rehoboth Bridge Beams

Specimens R2, R3, and R4 exhibited no signs of significant deterioration on the bottom surface of the beam. They showed minor signs of deterioration at the acute corners of the beams, which could have been caused during beam removal. Representative conditions of the end of each beam are shown in Figure 4.12 through Figure 4.14. Figure 4.12 shows damage to the top of the beam and exposed strand in Specimen R2. Similar damage was observed in Specimen R4 (Figure 4.14). Vertical and horizontal cracking was observed at the southeast corner of Specimen R3 (Figure 4.13).

Figure 4.12: Northwest corner of Specimen R2

Figure 4.13: Southeast corner of Specimen R3

Figure 4.14 Northwest corner in Specimen R4

4.3.2 Essex Bridge Beams

Specimen E4 Deterioration

Specimen E4 exhibited evidence of strand corrosion on the bottom surface of the beam, along the sides of the beam, and even at the top surface of the beam. On the bottom surface, all the deterioration was concentrated at the south end of the beam as placed in the laboratory. The only visible signs of deterioration were localized spalls and longitudinal cracks (Figure 4.15). After removing the beam from the test setup, it was observed that one of the cracks ran through the entire bottom flange right at the location of one of the strands (Figure 4.16).

Along the sides of the beam at the south end, full-thickness cracks near the bottom flange-web connection were observed on both webs (Figure 4.16). It was also evident that that the form used to create the void in this box beam shifted during construction, causing one web to be significantly thinner than the other. The difference in web thickness was observed on both ends of the beam.

The top surface of the beam also showed deterioration and concrete spalling. Patching of the top surface had taken place as shown to improve rideability. The concrete patch repair along the beam and a thick concrete overlay that was present along the beam are shown in Figure 4.17.

Crack and spall mapping was conducted for the bottom of the beam as shown by the sketch in Figure 4.18. Only the bottom of the beam was documented to this detail as it was the most likely to affect the performance of this specimen during testing.

Figure 4.15: Bottom surface deterioration (Specimen E4)

Figure 4.16: Effect of form void shifting in web thickness (Specimen E4)

Figure 4.17: Longitudinal cracking at south end of Specimen E4

Figure 4.18: Cracking and spalling on bottom surface of Specimen E4

Specimen E3 Deterioration

Specimen E3 showed minor cracks, spalls, exposed stirrups, and exposed or severed strands throughout the length of the beam, predominantly along both bottom edges of the beam. An example of the degree of strand exposure and the loss of strand and stirrup section is shown in Figure 4.19. There was also significant spalling of the corner and bottom of the beam corresponding to the laboratory supports setup for testing the beam (about 15 ft from the end of the original beam). These spalls needed patching with grout prior to testing, as shown in the bottom-left corner of Figure 4.20.

No splitting cracks were observed along the strands in this beam, either along the length of the beam or at the ends. It was observed that the form void shifted during construction causing variation of web thickness. The top surface of the beam had also been patched at several locations. In some cases, these patches extended down into the top flange of the beam (Figure 4.21). The deterioration of the bottom surface was mapped to use for later calculations (Figure 4.22). Stirrups and strands are shown as orthogonal lines within hatched regions that represent spalled concrete.

Figure 4.19: Exposed and corroded strand in the bottom of Specimen E3

Figure 4.20: South end of Specimen E3

Figure 4.21: North end of Specimen E3
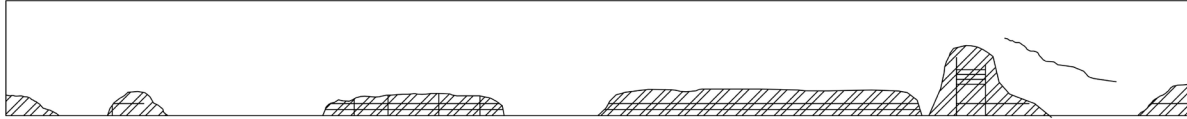
Figure 4.22: Deteriorated regions on the bottom surface of Specimen E3

Specimen E9 Deterioration

The deterioration condition observed in Specimen E9 was concrete spalling, exposed stirrups, and exposed or severed strands. Most spalling and exposed strand was predominantly evident along one of the bottom edges of the beam (Figure 4.23). A concrete spall was located directly under the location of one of the load points from the test apparatus. This location had to be grouted to ensure the loading beams were horizontal and stable during testing.

For this beam, the void form also shifted during construction, which created webs of uneven thickness. Figure 4.24 shows the significantly different thickness of the web on the right and left side of the figure. Although this posed a concern because of the possibility of localized web shear crushing, there was no evidence of this occurring during testing as discussed later in this report. A horizontal crack at the level where a concrete overlay was added to the top of the bridge can also be observed in this figure.

The top surface of the beam had deteriorated extensively over the years. This required concrete patching to be made to the beam (Figure 4.25). Figure 4.26 shows the mapping of deterioration of the bottom surface as described for Specimen E9.

Figure 4.23: Spalled concrete corner in Specimen E9 exposing fractured strand

Figure 4.24: North end of Specimen E9

Figure 4.25: Concrete patching along top of Specimen E9
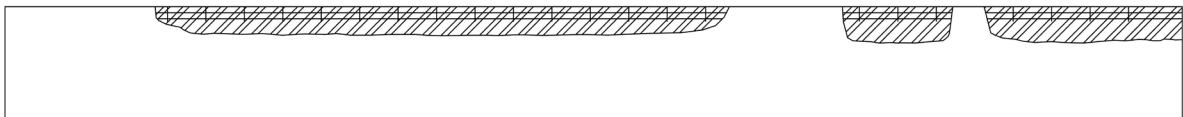
Figure 4.26: Deterioration along bottom corner of Specimen E9

This page left blank intentionally.

5.0 Laboratory Testing

This section presents a description of the laboratory tests conducted on beams from the two bridges described in Section 4. The section begins with a description of the test setup, continues with a discussion about the instrumentation used in the specimens, and discusses the test procedures used. Observations on the qualitative behavior during testing, supported by selected photographs taken during the tests, is also presented in this section. Analysis of each individual specimen, along with specific deterioration presented in Section 4, will be examined in Section 6.

5.1 Description of Testing Setup

The beams were tested using a 4-point bending configuration to generate a constant moment region in the center of the beam. A load frame was used to transfer load to the two load points using structural steel spreader beams. Because of the presence of voids, loads were applied along the edge of the beams where beam webs are located. This loading scheme prevented loading the top flange, which would have induced transverse bending to the top flange; it minimized the potential for a localized transverse failure prior to reaching the capacity of the beam in bending. Each of the spreader beams was supported on random-oriented-fiber (ROF) bearing pads to transfer the loads from the spreader beams to each of the specimens.

Each of the specimens was supported at each end on 2 × 2 × 8 ft concrete blocks. These blocks were heavily reinforced so that they could withstand the required reaction forces. ROF bearing pads were set between the top surface of the support concrete blocks and the bottom surface of the test beams to distribute bearing stresses while allowing rotation of the beam ends.

Load during testing was applied using two 60-ton hydraulic rams, one on each side of the loading beam (Figure 5.1). The rams were connected by hydraulic hoses to an electric hydraulic pump that was operated manually. Load was applied in predetermined increments as described in Section 5.3.

The loading beam was a built-up section made from two MC channels spaced 1.5 in. apart to allow rods to pass between each MC section. These channels were connected by welded steel plates to the top and bottom flanges of the channels. The channels were provided with stiffeners along their length, particularly in regions where concentrated forces were generated. Spreader beams to distribute forces in the longitudinal direction consisted of I-beams placed between the loading beam and the test specimens. Spreader beams were also stiffened at locations of concentrated forces. The loading beam was connected to a tie-down steel block on each side, which was bolted to the strong floor in the laboratory, using 1-in.-diameter high-strength threaded steel rods.

Figure 5.1: Loading beam assembly

5.1.1 Laboratory Setup for Rehoboth Bridge Beams

The specimens from the Rehoboth Bridge were positioned in the laboratory following the bridge skew. The loading beam was also placed at the bridge skew angle to minimize twisting of the concrete beam during testing (Figure 5.2). Load points were equidistant to the end of the beam measured along their corresponding beam edge.
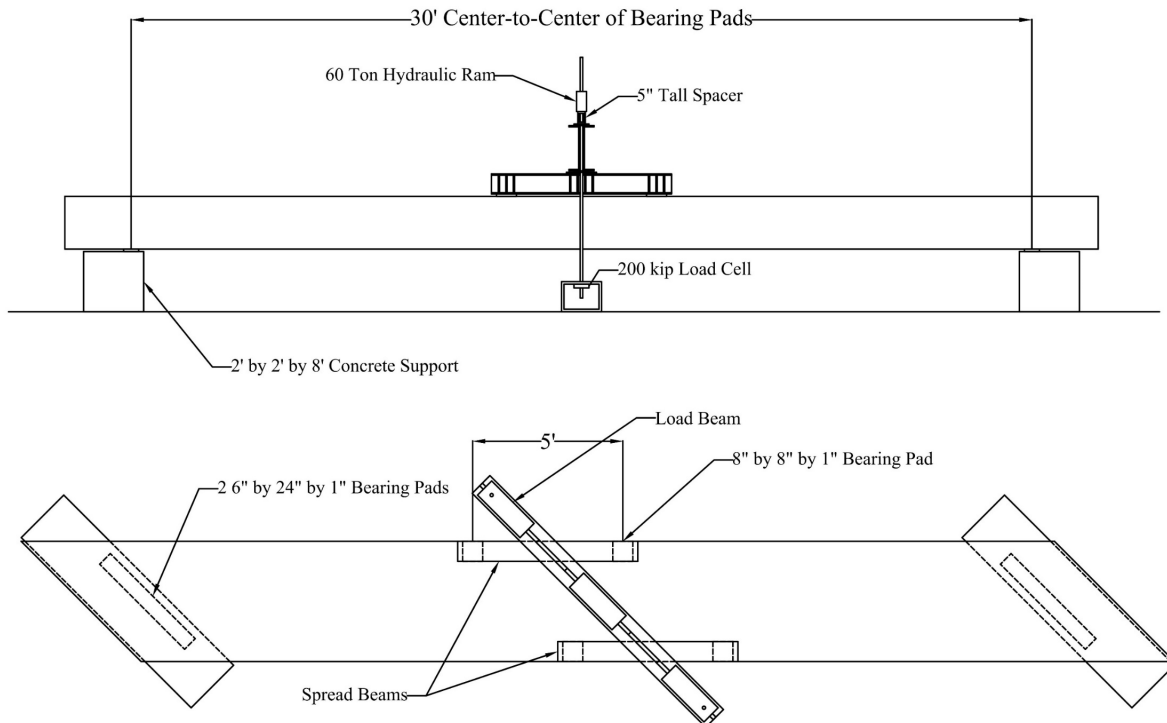
Figure 5.2: Laboratory setup for Rehoboth Bridge beams

5.1.2 Laboratory Setup for Essex Bridge Beams

Because the Essex Bridge was not constructed on a skew, beams obtained from this bridge were positioned on concrete blocks in the laboratory set perpendicular to the beam axis. All loading components were the same as those used for Rehoboth Bridge beams, with the exception of the threaded rods connecting the loading beam to the tie-down blocks. For the Essex Bridge beams, 1 ¼-in.-diameter rods were needed because of the higher applied loads anticipated in these specimens. The actual test span length varied slightly for each of the specimens in this group because of differences in the cut length of each beam as provided by the contractor. The span length of Specimens E3, E4, and E9 are 489 in., 486 in., and 490 in., respectively. The test setup for the Essex Bridge beams is shown in Figure 5.3.
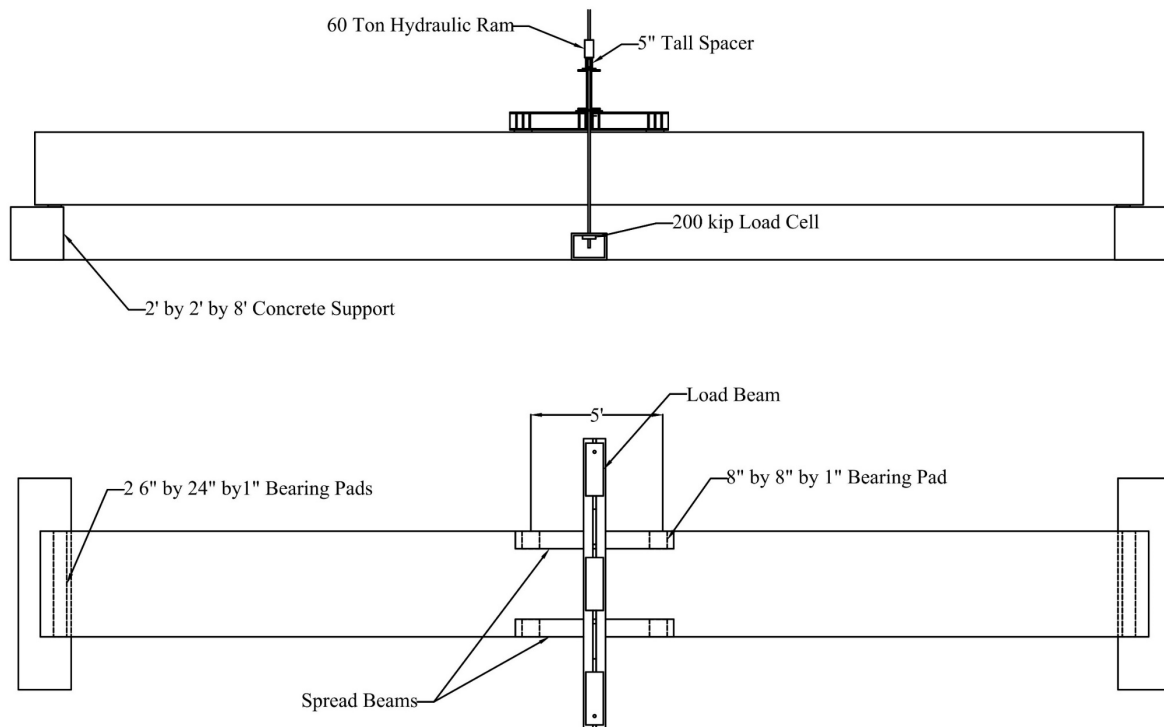
Figure 5.3: Laboratory setup for Essex Bridge beams

5.2 Description of Instrumentation

Each beam was instrumented using a similar instrument layout. Applied load during the tests was measured using two 200-kip capacity load cells placed between the high-strength rods and each tie-down block. For backup purposes, a pressure transducer was connected to the hydraulic lines at the pump end as an indirect measurement of applied load.

Beam displacements were measured using linear potentiometers at selected locations to capture details of the beam deflection profile during the tests. Five locations along the beam span were established to construct the longitudinal displacement profile: midspan, sections under the two load points, and displacements at the centerline of bearing pads on beam

supports. Instrumented sections corresponding to the two load points were selected to allow displacement measurement where most of the inelastic action in the beams was expected to occur given the testing configuration. To measure twist of the beams during testing, instruments were placed along both beam edges. The linear potentiometers were connected to angle brackets that were attached to the beams at each instrumented location prior to testing (Figure 5.4).

Linear potentiometers were labeled in reference to their position relative to the laboratory cardinal direction and their location on the beam. The first letter in the potentiometer labeling represents the cardinal location of the face of the beam onto which the potentiometer was connected, and the second letter corresponds to the section along the beam. Instrumented potentiometer locations and labeling can be seen in Figure 5.5 and Figure 5.6 for the Rehoboth and Essex Bridge beams, respectively.

The Rehoboth beams predominantly ran in the east–west direction, meaning that they had a north (N) and south (S) face. The second letter designated where along the length of the beam the potentiometer was located. For the Rehoboth beams, the second letter would either be a E (east), W (west), or M (midspan).

The Essex beams ran in the north–south direction, meaning that they had an east (E) and west (W) face. For the Essex beams, the second letter would either be a N (north), S (south), or M (midspan). For the potentiometers at the ends of the beam, "End" was added for its designation.

Strains were measured at selected sections along the beams and different depths to allow constructing strain profiles. All strain gauges were mounted on the concrete surface at different depths to allow construction of strain profiles at instrumented sections. Strain gauges were used to estimate stresses at different depths for various load levels and the corresponding neutral axis location as a function of moment throughout testing.

For sections instrumented using strain gauges, a notation similar to the one used for sections instrumented with potentiometers was used along the length of the beam. Since four gauges at different depths were used at each instrumented section, a third letter was added to the gauge designation to identify gauge depth (Figure 5.7). Letter A was the label assigned to the strain gauge located closest to the top of the beams, and letter D was added to the label assigned to the strain gauge located closest to the bottom of the beams. A list of sections and depths of strain gauges for each specimen is provided in Table 5.1.

Figure 5.4: Typical attachment of potentiometer at supports
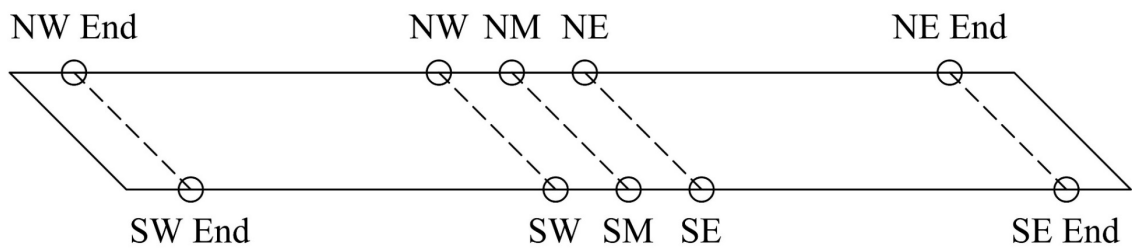
Figure 5.5: Instrumented potentiometer sections for Rehoboth Bridge beams
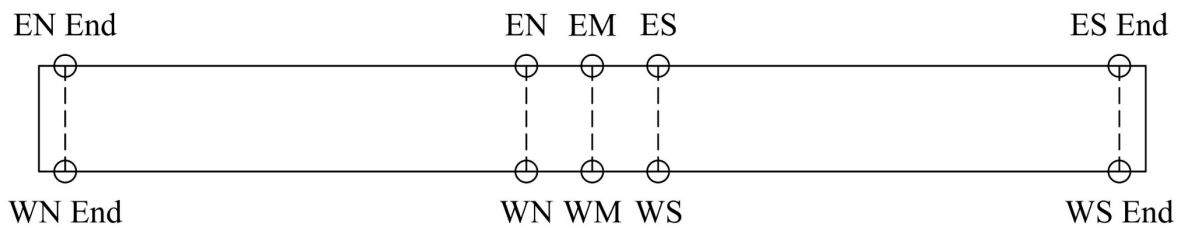
Figure 5.6: Instrumented potentiometer sections for Essex Bridge beams
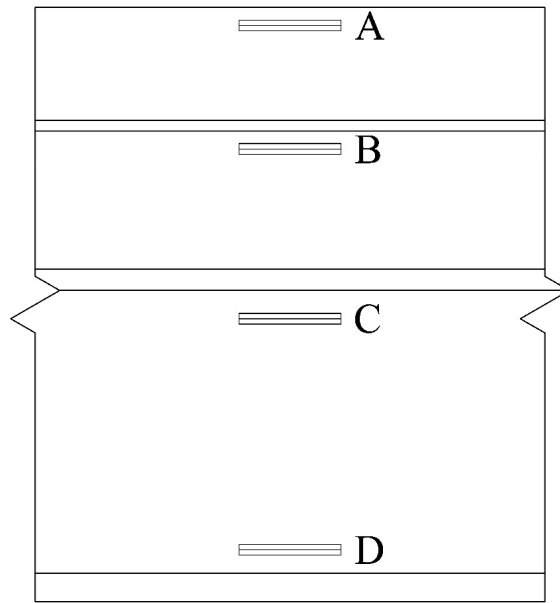
Figure 5.7: Strain gauge labels at each section

Table 5.1: Strain gauge depths*

Sections	A	B	C	D
Specimen R2				
NE	20.40	15.5	10.38	2.31
NM	20.38	15.5	10.25	2.31
NW	20.44	15.5	10.00	2.31
SM	20.28	15.5	10.28	2.31
Specimen R3				
NM	20.50	15.50	10.06	2.63
SE	19.28	15.44	9.91	2.75
SM	19.44	15.50	9.84	2.69
SW	19.28	15.38	10.00	2.50
Specimen R4				
NM	20.53	15.38	9.72	2.75
SE	20.66	15.34	10.06	2.88
SM	20.56	15.69	10.16	2.88
SW	20.31	15.50	10.38	2.88
Specimen E3				
EM	31.00	26.00	20.00	3.00
WN	31.00	26.00	20.00	3.00
WM	31.00	26.00	20.00	3.00
WS	31.00	26.00	20.00	3.00
Specimen E4				
EM	32.00	25.50	19.00	2.50
WN	32.00	25.50	19.00	2.50
WM	32.00	25.50	19.00	2.50
WS	32.25	25.50	19.00	2.50
Specimen E9				
EM	32.00	28.00	23.00	8.00
WN	32.00	25.00	19.00	4.00
WM	32.00	23.00	19.00	2.00
WS	32.00	23.00	19.00	5.00

*Depths are measured from the bottom surface of the beam (in inches).

5.3 Testing Procedure and Loading Protocol

Loads acting on specimens prior to application of test loads were considered for the interpretation of results presented in Section 6. These loads included self-weight; wearing surface or topping, if present; laboratory setup components that were supported on top of the beams; and any water that was entrapped inside the voids (this was only observed for one specimen: Essex Bridge Beam 3).

For any asphalt or concrete overlay present on the specimens, a unit weight of 140 lb/ft^3 was assumed based on the AASHTO *LRFD Bridge Design Specifications (6)* Table 3.5.1-1 for bituminous wearing surfaces to estimate the dead load for the overlay. Thickness and width measurements of each wearing surface were taken for each specimen to estimate the load acting on the beams.

The weight of the laboratory test setup components was estimated for the transverse spreader beam, the longitudinal spreader beams, the hydraulic rams, and other ancillary elements supported on the beams. These loads were considered as concentrated forces applied at the load points.

During testing of Essex Beam 3 (E3), entrapped water in the center cell of the box beam leaked out onto the laboratory floor after cracking occurred in the beam. This water weight was estimated by assuming a depth of entrapped water in this center cell between diaphragms and a water unit weight of 62.4 lb/ft^3.

5.3.1 Loading Protocol

Each specimen experienced a very similar loading protocol to determine the ultimate load-carrying capacity of each beam. Load was initially applied incrementally until flexural cracking was first observed. After cracking was observed, cracks were marked, and the load was released gradually down to zero to estimate the loading-unloading behavior under low loads. Specimens were then loaded in increments to a maximum load corresponding to flexural failure mode or other mechanisms (shear, strand rupture) that prevented beams from safely reaching higher loads. After reaching the maximum load, the load was gradually released to zero force.

For the Rehoboth Bridge beams, the beams were first loaded to cracking by increasing the pressure in 12.3-kip increments. The pressure was then fully released. After, the beams were then loaded in 24.6-kip increments to their ultimate strength. For Specimen R2, testing was stopped prior to the concrete crushing to avoid damaging the test apparatus, although the load was similar to those experienced for the two subsequent specimens. Specimens R3 and R4 were loaded to the crushing of the concrete.

Loading of the Essex Bridge beams differed slightly from each other. Specimen E4 was first loaded in three 24.6-kip increments and then in 12.3-kip increments until the beam reached its failure load. The webs in the south end were experiencing diagonal tension cracks, indicative of impending failure of the webs. This will be further explored in Section 5.4.4 and Section 6.

Specimen E3 was first loaded in three 24.6-kip increments and then 12.3-kip increments until cracking was observed. The beam was then loaded in nine 12.3-kip increments. The beam was subsequently unloaded and reloaded to see if the same load could be achieved. After, the beam was loaded in additional 12.3-kip increments until the test was stopped when the observed load-deflection curve reached a plateau.

Specimen E9 was first loaded in three 24.6-kip increments and then 12.3-kip increments until cracking was observed. After fully unloading from the cracking load, the beam was loaded in 24.6-kip increments until the beam reached its peak strength. The test was stopped when the observed load-curves began to plateau.

5.4 Observed Behavior during Testing

5.4.1 Specimen R2

On January 12, 2023, Specimen R2 was tested using the setup shown in Figure 5.2. An overall view of the specimen prior to testing is shown in Figure 5.8. The maximum load applied to this specimen was 211.3 kip. The beam was loaded in 12.3-kip increments until flexural cracks were observed at 112.2 kip. Upon reaching this load, the test was halted to mark cracks and make any observations of the beam. After finishing the visual observations, the beam was unloaded gradually to 0 kip. The beam was subsequently reloaded without pausing to the cracking load previously reached. After reaching the cracking load, loads were applied in 24.6-kip increments until 211.3 kip was reached. During these load increments, any new cracks or crack extensions were marked, and photographic evidence was recorded as needed. After reaching the peak load, the beam was then unloaded back to 0 kip. Loading of the beam was stopped as concrete in the top face of the beam started flaking, indicating impending crushing. At this point, a small misalignment in one of the threaded rods was noticed, which induced bending in the rod. To avoid damaging one of the load cells, the team decided to stop the test knowing that the peak load had been nearly reached.

Each of the linear potentiometers was observed during the experiment to identify the displacements at the supports and to notice the overall deflection of the beam. At the applied load points, there was a distinct difference in the measured displacement on opposing faces of the test specimen, indicating that the specimen was twisting. The clearest evidence of beam twisting was observed at specimen ends; the ends were closely monitored to ensure the specimen did not come into contact with the support blocks.

Cracks tended to follow similar patterns on the two faces of the beams. Sections under the northwest and southeast load points experienced similar crack patterns, as did the southwest and northeast load points (184 kips) (Figure 5.9). The northeast and southwest load points first experienced flexural cracks and, as loading increased, experienced flexure-shear cracks extending further out toward the beam ends. The northeast and southwest corners primarily experienced flexural cracks.

Figure 5.8: Specimen R2
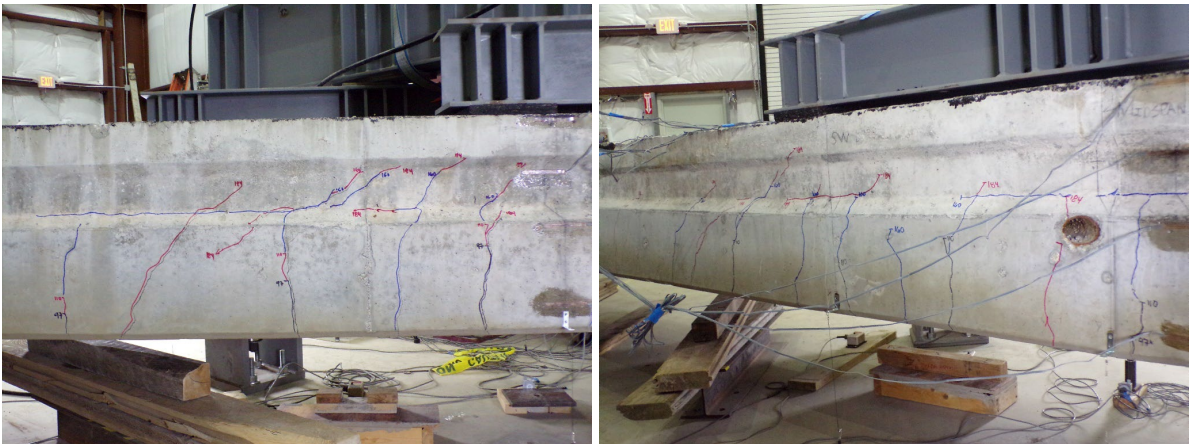
Figure 5.9: Specimen R2: northeast and southwest load points

Figure 5.10 shows the load-displacement curve measured during the test and a comparison of the load measured by the two individual cells. It can be observed that despite the rod bending, the load cells measured approximately the same load throughout testing with a maximum difference of 8.1%.
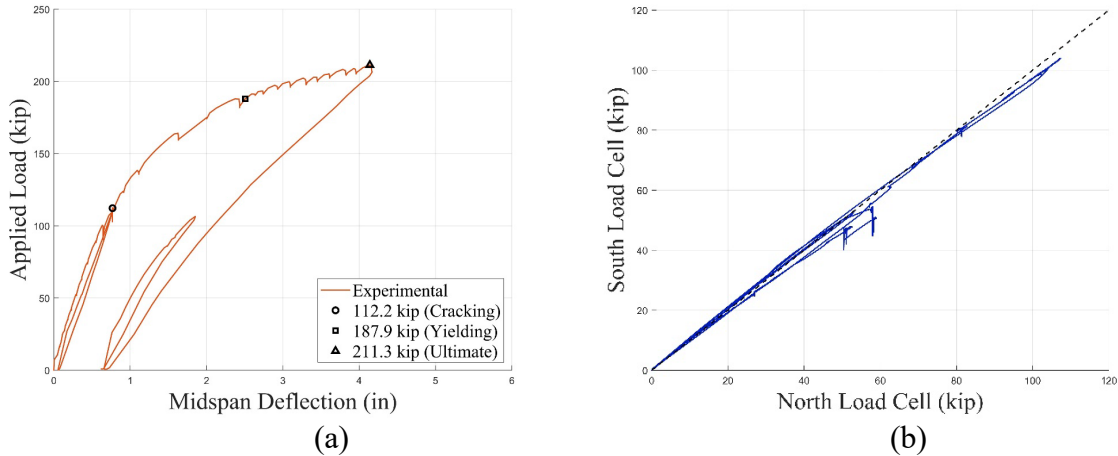
Figure 5.10: Specimen R2: (a) load-deflection response; (b) north and south load cells

5.4.2 Specimen R3

On February 2, 2023, Specimen R3 was tested using the test setup shown in Figure 5.2. An overall view of the specimen prior to testing is shown in Figure 5.11. The maximum applied load to this specimen was 196.7 kip. As for other specimens in this group, loading proceeded in steps of 12.3 kip until the first flexural cracks were observed at a cracking load of 99.25 kip. The specimen was subsequently unloaded, reloaded to cracking, and subsequent load increments of 24.6 kip were taken until reaching the peak load of 196.7 kip. Flexural cracks formed in the region between the two load points (constant moment region); these extended into flexure-shear cracks outside the constant moment region of the beam. A view of the loading apparatus is shown in Figure 5.11.

At the peak load, the top surface of the beam exhibited concrete crushing across the entire width of the beam at a section adjacent to the west load points (north and south), as can be seen in Figure 5.12 and Figure 5.13. After crushing, the top strand was exposed and buckled (Figure 5.13).

Specimen R3 experienced twisting during the test as evidenced by differences in readings between the potentiometers located along the north edge and those located along the south edge. Twist occurred with acute corners rising relative to the obtuse corners of the specimen. The cracking patterns noticed in the beam during testing also reflected beam twisting in a very similar manner to Specimen R2 (Figure 5.12).

Figure 5.14 shows the load-deflection curve measured during the test and a comparison of the load cell values recorded throughout testing. The readings on the north load cell were higher than those in the south load cell. The slight differences in load cell reading could have been caused by beam twisting or slight loading beam misalignment, although differences did not exceed approximately 10%.

Figure 5.11: Specimen R3 setup

Figure 5.12: Cracking of Specimen R3 at concrete crushing (northwest load point)

Figure 5.13: Concrete crushing at failure of Specimen R3

(a)	(b)
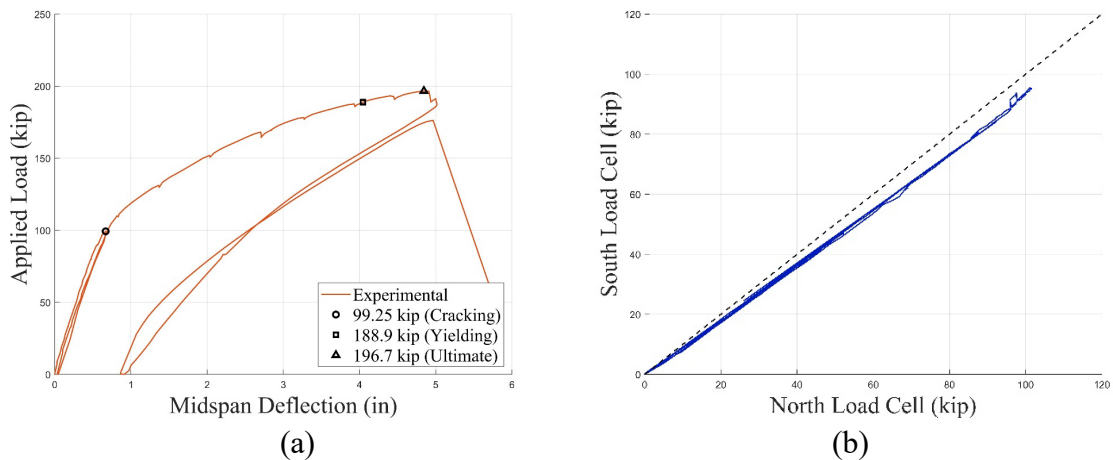
Figure 5.14: Specimen R3: (a) Load-deflection response; (b) north and south load cells

5.4.3 Specimen R4

Specimen R4 was tested on February 14, 2023, using the laboratory setup shown in Figure 5.2. Load was applied in 12.3-kip increments up to a cracking load of 111.7 kip, with flexure cracks forming in the constant moment region, and an ultimate load of 200.9 kip using the loading protocol described above with the same equipment shown in Figure 5.15. The

maximum applied load to this specimen was 200.9 kip. As for other specimens in this group, loading proceeded in steps of 12.3 kip until the first flexural cracks were observed at a cracking load of 99.25 kip. The specimen was subsequently unloaded, reloaded to cracking, and subsequent load increments of 24.6 kip were taken until reaching the peak load of 196.7 kip. Flexural cracks formed in the region between the two load points (constant moment region); these extended into flexure-shear cracks outside the constant moment region of the beam.

The beam exhibited concrete crushing at the peak load (200.9 kip) at a section adjacent to the load points located on the west side (Figure 5.17). The crushed surface extended across the beam width, indicating that the load was adequately distributed to the entire beam.

The linear potentiometer readings indicate that there was twist occurring in the beam, with the acute corners (SE and NW corners) rising above the obtuse corners (SW and NE corners). The cracking patterns also reflected the idea that the beam was twisting toward those corners in a very similar manner to each of the first two specimens (Figure 5.16).

Figure 5.18 shows the load-displacement curve of Specimen R4 and a comparison of the load cell readings. The load cell reading comparison indicated less deviation than that recorded for Specimen R3. The north load cell registered slightly higher loads in comparison with the south load cell; the maximum difference was approximately 10%.

Figure 5.15: Specimen R4
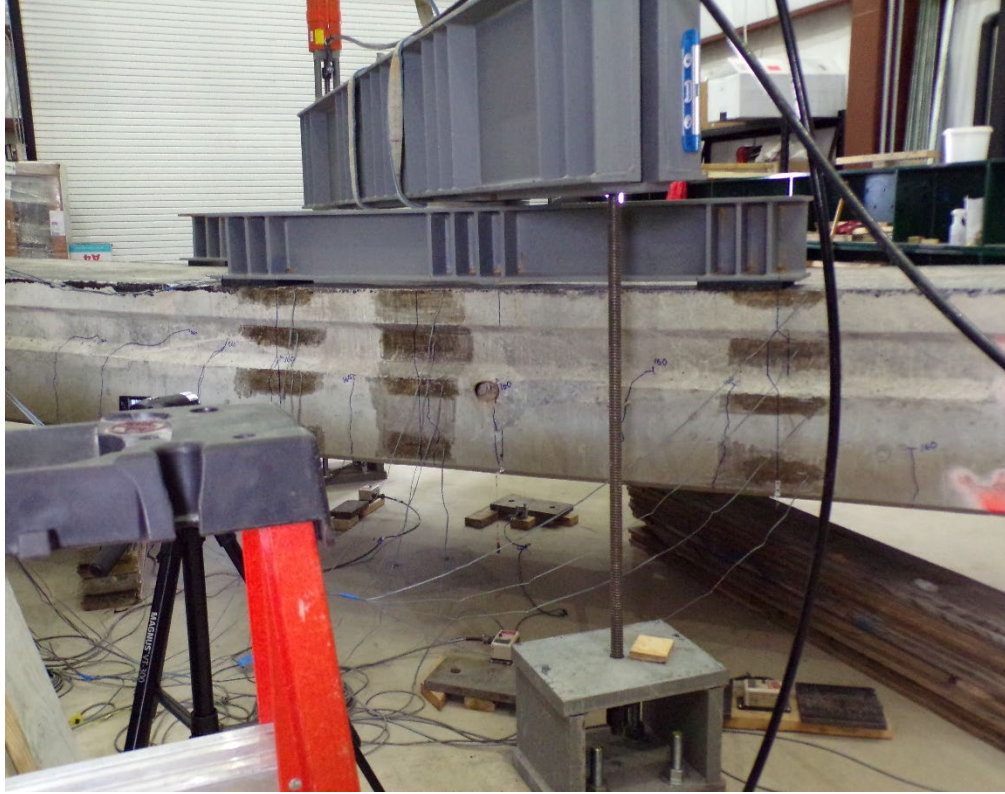
Figure 5.16: Cracking in Specimen R4 at 160 kip

Figure 5.17: Concrete crushing after failure of Specimen R4
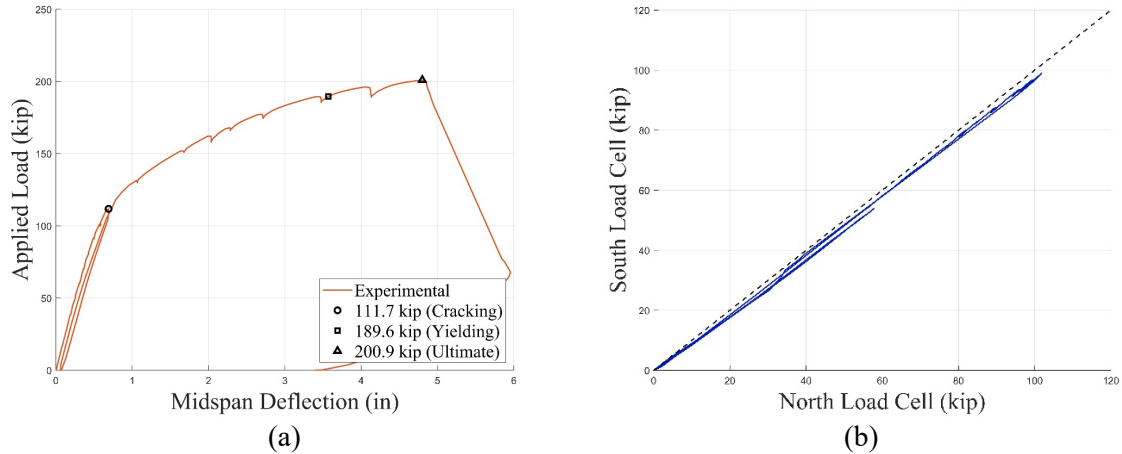
Figure 5.18: Specimen R4: (a) Load-deflection response; (b) north and south load cells

5.4.4 Specimen E4

Specimen E4 was tested on April 28, 2023, to failure with the testing configuration shown in Figure 5.3. An overall view of the specimen ready for testing is shown in Figure 5.19. It was load tested incrementally until the ultimate load was achieved. The beam was tested in 12.3-kip increments. The south end of this beam exhibited significant deterioration and web cracking (Figure 5.20), so this end was monitored closely during testing. At approximately 60 kip, it was observed that strands located in the web region were pulling in from the south end of the beam. The web located on the west face at the south end was significantly thinner than the web on the east face; diagonal tension cracks had formed and extended during testing, causing the strand to pull in because of bond distress. In addition to strand splitting cracks, a crack between the bottom flange of the box and the web on the west side formed as shown in Figure 5.21 and Figure 5.22. After loading to 83.2 kip, the crack between the flange and web at the south support widened; this was accompanied with a drop in load. Diagonal cracking of the web on the west face was also occurring at this time indicating the potential for shear failure of the beam. Because the beam was unable to develop higher forces, the test was stopped with failure induced by web diagonal tension cracking at the south end of the beam (thin web). The load-deflection curve measured during this test can be seen in Figure 5.23, which shows the loss of load after reaching the ultimate load of 83.2 kip.

68

Figure 5.19: Specimen E4

Figure 5.20: South end of Specimen E4 prior to testing

Figure 5.21: Cracking of Specimen E4 at south end triggering strand slip

Figure 5.22: South end failure of Specimen E4
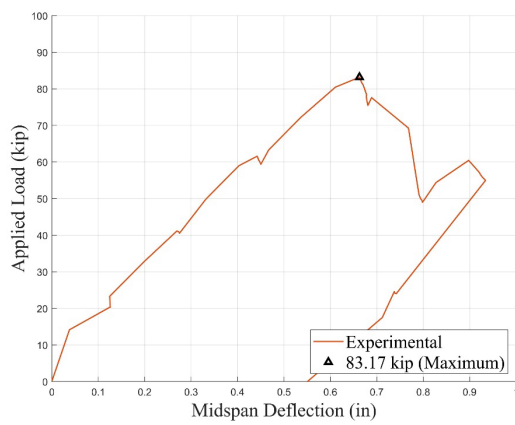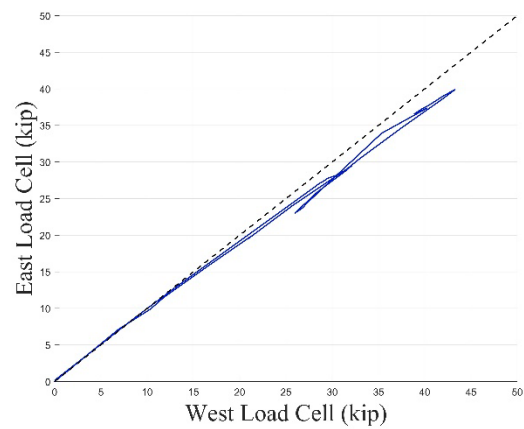
(a)   (b)

Figure 5.23: Specimen E4: (a) Load-deflection response; (b) east and west load cells

The difference in web thickness that was noticed in this specimen was considered a major contributor to the behavior observed during testing. At the south end, the east web was noticeably thicker than the west web; in contrast, at the north end, the west web was thicker than the east web. The void form shifted during construction of the beam, and the amount of movement that occurred during casting is difficult to quantify. This was not an isolated incident, because the other two Essex Bridge beams received at the laboratory for testing also exhibited differences in web thicknesses. Proper construction methods and inspection of the beams during fabrication to ensure uniformity in web thickness is quite important for this type of section. After fabrication, inspection is complicated because diaphragms typically hide the web thickness, although nondestructive methods could be used to estimate web thicknesses.

Using linear potentiometer data during the test, it was observed that there was no significant twisting occurring along the beam or at beam ends, as would be anticipated because of the lack of skew in this bridge. After unloading, the beam was observed to have a permanent deflection of 0.52 in.

5.4.5 Specimen E3

Specimen E3 was tested on May 18, 2023, to failure using the setup shown in Figure 5.3. Figure 5.24 shows the loading apparatus and the condition of the south end of the beam on the concrete support block. The bearing pad at the support block was extended throughout the bottom face to minimize the potential for cracking between the bottom flange and the webs. The beam exhibited severe strand corrosion throughout the span. The beam showed signs of concrete spalling, longitudinal cracking, exposed stirrups, exposed strands, and severed strands as previously stated in Section 4.3.3. During the test, water leaked from the bottom of the beam after flexural cracks had formed and widened (Figure 5.25). This prevented cracks from being adequately marked during testing after the water had begun to leak. The water was primarily trapped in between the two diaphragms in the center region of the beam.

The beam was tested in two stages, with unloading occurring at 114 kip and reloading occurring after the release of the load. The 114-kip load was chosen during the experiment as the unloading point due to substantial water leaking from the beam. To keep the instruments intact and for safety of all involved in the test, the load was released to be able to mop up the water. Initially, the beam was loaded using 12.3-kip increments. Flexural cracking occurred at 90.5 kip, coincident with the first significant drop in load. Popping sounds were heard after the cracking load, indicating that strands were slipping and strand wires were fracturing. The beam reached a maximum load of 127.7 kip. As loading values neared the maximum load, frequent snapping sounds were heard, indicating that strands were fracturing and slipping. At this point, the load-deflection curve had significantly flattened; so, because of concerns of strand fracture leading to sudden failure of the beam, the test was concluded. Cracking, yielding, and ultimate load are marked by points overlain in the load-deflection curve presented in Figure 5.27.

After the test, the bottom surface of the beam was examined to determine the number of strands that had become visible due to the loss of cover (Figure 5.26). Nine strands were exposed after concrete spalling; multiple sections exhibited strand exposure.

<p style="text-align:center">(a)   (b)</p>

Figure 5.24: Specimen E3: (a) loading beams; (b) south end

Figure 5.25: Flexural cracking of Specimen E3 and water leakage

Figure 5.26: Severely corroded strand exposed in Specimen E3 after concrete spalling

(a)   (b)
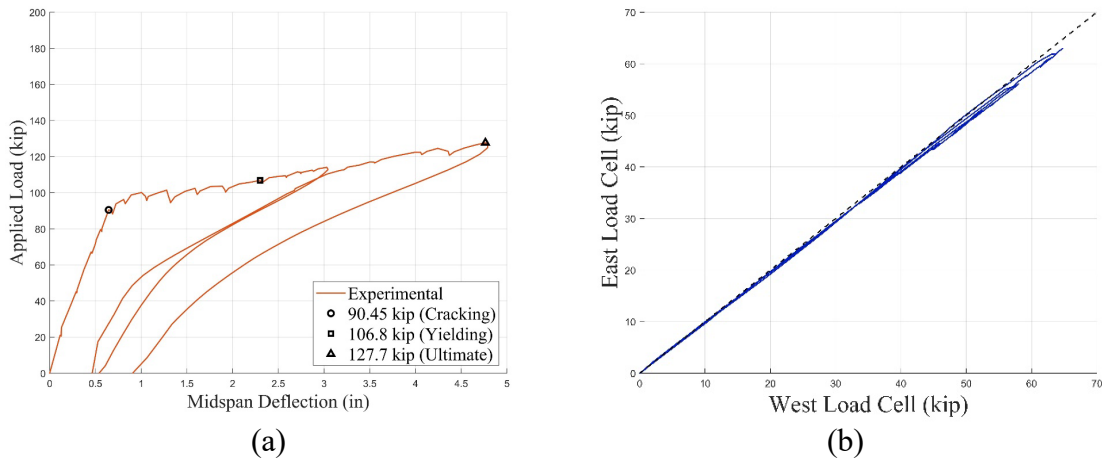
Figure 5.27: Specimen E3: (a) Load-deflection response; (b) east and west load cells

The location of the most significant corrosion deterioration occurred in a region approximately located 12 ft from the north support. During the test, it was observed that, in this region, concrete spalling occurred and sounds indicating strand slippage and strand wire fracture took place. This region was located well outside of the constant moment region of the beam.

The readings recorded by the two load cells during testing indicated a near even distribution of load to each side of the beam. Potentiometer readings revealed that very little beam twist

occurred as expected for a nonskewed loading arrangement. The beam exhibited a permanent deflection of 0.86 in. after unloading.

5.4.6 Specimen E9

On June 9, 2023, Specimen E9 was tested to failure using the setup shown in Figure 5.3. An overall view of the specimen prior to testing is shown in Figure 5.28. Weep holes were observed located in the bottom surface of the beam within the middle region between concrete diaphragms. Water did not leak from this area during testing, indicating that water was not trapped inside the beam because of the presence of weep holes. The original beam top surface had evidently undergone significant deterioration as indicated by the extensive patching and thick overlay on the beam. Patching, however, had not been applied or with the same materials; there were areas that had been patched with an asphalt overlay and others had a 5-in. thick concrete topping. The corners of the box section also showed signs of deterioration (chipping, spalling).

The beam was tested in two stages. The beam was first loaded until flexural cracking was observed at a load of 131.1 kip. The beam was first loaded in two increments of 24.6 kip, and subsequently in 12.3-kip increments until reaching the cracking load. After cracking, the beam was fully unloaded. The beam was reloaded in increments of 24.6 kip to get to the peak load. The load-deflection curve was monitored throughout the test, and when the curve flattened significantly, loading progressed gradually until higher loads could not be reached. At this point, the test was stopped, and the beam was fully unloaded to prevent damage to the laboratory equipment. Flexure-shear cracks had formed and widened near the north load points (Figure 5.29).

Popping sounds were heard just before the first flexural crack was observed. These sounds were a combination of strand slippage and concrete overlay debonding from the beam ends as confirmed by visual inspection (Figure 5.30). At approximately the cracking load, a louder sound was heard indicative of strand rupture. After inspecting the underside of the beam in one of the most severely deteriorated regions, one of the exposed strands was observed to have ruptured. All load was then released from the beam. The beam was subsequently reloaded in 24.6-kip increments until the ultimate load was achieved.

The beam reached an ultimate load of approximately 168.5 kip. At approximately 142 kip, more sounds were heard from overlay debonding, the concrete cover on regions along the bottom face of the beam was lost, existing cracks extended, and new cracks formed. At approximately 150 kip, cracks formed between the top of the beam and the overlay as debonding progressed primarily from the north end of the beam into the span, and cracks continued to form or propagate. At the ultimate load, part of the corner near the northwest load point popped off; cracks propagated to the compression face of the beam, causing a redistribution in load; and more of the topping was lost. This loss is shown in Figure 5.30. After reaching peak load, a gradual reduction in load was observed in the load-deflection curve that was being monitored throughout the test, indicating imminent failure.

The location of the most significant deterioration occurred around 14 ft from the north loading point. The section was located outside of the region of maximum moment.

The recorded loads in individual load cells were fairly even (Figure 5.31). Potentiometer readings at beam ends were nearly equal, giving evidence of nearly no beam twist as expected. The largest load deviation between load cells was near the ultimate load. The beam at the end of the test had a permanent deflection of 1.26 in.

Figure 5.28: Specimen E9

Figure 5.29: Flexure-shear cracking of Specimen E9 near peak load

Figure 5.30: Debonding of concrete overlay in Specimen E9 (north shear span)

	(a)	(b)
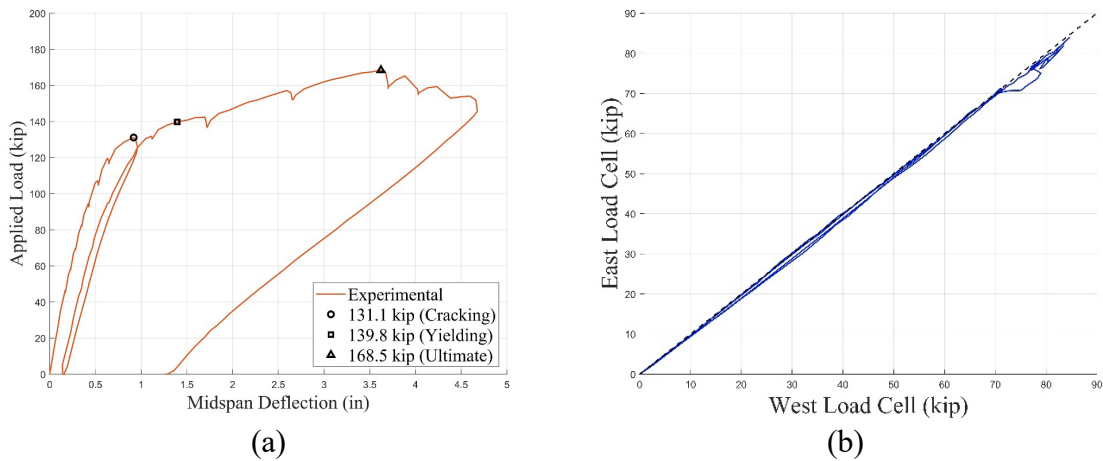
Figure 5.31: Specimen E9: (a) Load-deflection response; (b) east and west load cells

In Section 6, the results of the experiments will be compared with estimates of the nominal moment strength. Moment strength will be calculated using established practices provided in the AASHTO *LRFD Bridge Design Specifications (6)* and from moment-curvature analysis, which will be discussed in Section 6.

6.0 Results and Analysis

The data collected during the tests was used in part to compare measured strength with available analytical models for strength and available design equations. In this section, the data reduction is presented and the strength calculations that were conducted for comparison with experiments are presented. Analysis techniques will be thoroughly discussed along with any assumptions used in these calculations. These strength calculation techniques will be compared with results obtained using calculations commonly conducted using AASHTO LRFD specification procedures *(6)*. The calculation methods presented in this section will be used to assess adequacy of current MassDOT *LRFD Bridge Manual (1)* procedures for deteriorated prestressed concrete bridge girders. Modifications to existing MassDOT methods are discussed in Section 7.

6.1 Description of Moment-Curvature Analysis

One of the primary goals of the research project was to evaluate current procedures to estimate strength of deteriorated prestressed concrete girders contained in the MassDOT Bridge Manual and develop recommendations for their modification as supported from laboratory test results. To allow estimation of moment strength of deteriorated prestressed beams, a method based on estimating the moment-curvature response of the section was used. Moment-curvature analysis was selected because moment strength at a given cross section can be calculated using uniaxial material models for the concrete and prestressing strand that better reflect the field conditions of the tested elements. These models could, in theory, be modified to include effects of deterioration caused by corrosion of the prestressing strand at a given section.

A moment-curvature analysis is based on using uniaxial stress-strain models for the constituent materials making up a cross section. For a given strain distribution across the cross section, internal stresses are calculated using uniaxial stress-strain models. Therefore, selection of appropriate material stress-strain models to adequately capture the behavior of the prestressed beams had to be performed. Uniaxial models for concrete and prestressing strand available in the literature were used to calculate sectional strength using moment-curvature analysis.

Concrete in compression was modeled using a uniaxial model developed by Hognestad *(17)*. The model assumes the concrete stress-strain relation is initially parabolic until reaching the peak compressive stress, f_c', followed by a linearly decreasing relation until reaching the concrete crushing strain, assumed equal to 0.003 (Figure 6.1; Eqs. 6.1 through 6.5). The tensile behavior of concrete was captured using a linear-elastic model until reaching a stress equal to the modulus of rupture of concrete, f_r. A total loss of tensile strength was assumed

for concrete at higher strain than that corresponding to f_r. The elastic modulus of concrete was assumed equal to E_c as defined in AASHTO *LRFD Bridge Design Specifications (6)*.

The uniaxial material model for concrete in compression was calibrated by using AASHTO LRFD *(6)* equations, which define parameters including the modulus of elasticity, E_c, and the modulus of rupture, f_r. A linear behavior was assumed using E_c up to a concrete stress of $0.5f'_c$. A complete description of the concrete stress-strain curve, was obtained using Eqs. 6.1 and 6.2, using a value for ε_o obtained from Eq. 6.3. Note that the value ε_o was determined to be consistent with f'_c, satisfying that the stress-strain curve passes through $0.5\,f'_c$ at a strain value equal to $0.5\,f'_c\,/\,E_c$. The maximum attainable compression strain, ε_{cu}, was taken equal to 0.003. Eqs. (6.1 through 6.5) provide the stress-strain model used for concrete in compression. For analysis purposes, compression was assumed to be positive, and tension was assumed to be negative. The uniaxial stress-strain model for concrete with a 28-day compressive strength equal to 5 ksi is depicted in Figure 6.1.

$$f_c = f'_c \left[2\frac{\varepsilon_c}{\varepsilon_o} - \left(\frac{\varepsilon_c}{\varepsilon_o}\right)^2 \right] \text{ for } (\varepsilon_c \leq \varepsilon_o) \text{ (ksi)} \tag{6.1}$$

$$f_c = f'_c \left[1 - 0.15\left(\frac{\varepsilon_c - \varepsilon_o}{\varepsilon_{cu} - \varepsilon_o}\right) \right] \text{ for } (\varepsilon_c > \varepsilon_o) \text{ (ksi)} \tag{6.2}$$

$$\varepsilon_o = \frac{f'_c}{E_c(2-\sqrt{2})} \tag{6.3}$$

$$E_c = 1{,}820\sqrt{f'_c} \text{ (ksi)} \tag{6.4}$$

$$f_r = -0.24\sqrt{f'_c} \text{ (ksi)} \tag{6.5}$$
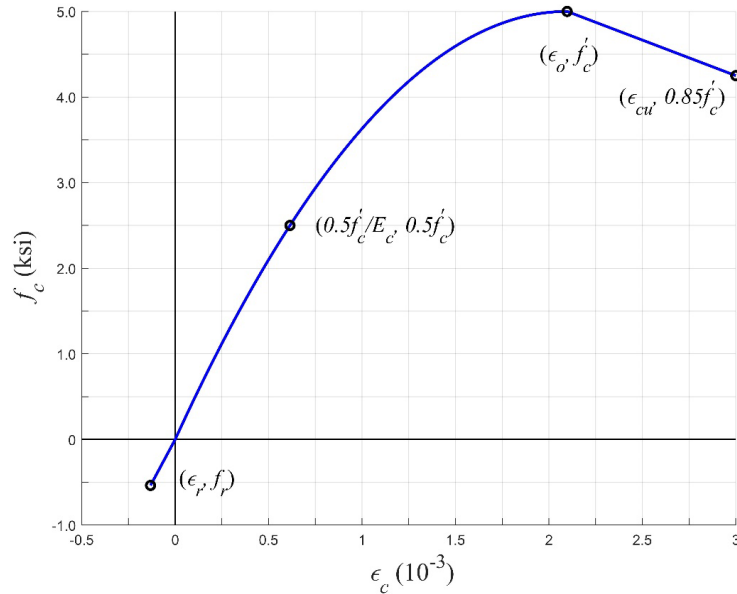
Figure 6.1: Concrete stress-strain curve

A Ramberg–Osgood model was used to model the uniaxial tensile behavior of prestressing strand. The Ramberg–Osgood model was compared with the *PCI Design Handbook (22)* approximate equation for 7-wire low-relaxation strand. Eq. 6.6 corresponds with the *PCI Design Handbook* equation, and Eq. 6.7 represents a generalized version of the Ramberg–Osgood model.

$$f_{ps} = \begin{cases} (28{,}800\ ksi)\varepsilon_{ps} & \left(\text{for } \varepsilon_{ps} \leq \frac{243}{28{,}800}\right) \\ 270\ ksi - \dfrac{0.04}{\varepsilon_{ps}-0.007}\ ksi & \left(\text{for } \varepsilon_{ps} > \frac{243}{28{,}800}\right) \end{cases} \tag{6.6}$$

$$f_{ps} = E_{ps}\varepsilon_{ps}\left[A + \frac{1-A}{\left[1+(B\varepsilon_{ps})^C\right]^{1/C}}\right] \leq 270\ ksi \tag{6.7}$$

The values for A, B, and C in Eq. 6.7 were calibrated for this research to match closely the PCI handbook stress-strain curve for strands (Table 6.1), and E_{ps} was taken as 28,800 ksi. The strand was assumed to reach a minimum yield stress of $0.9f_{pu}$ equal to 243 ksi as defined using the 0.01 offset method. The elongation at failure of the strand was assumed equal to 3.5%. A comparison of Eqs. 6.6 and 6.7 is presented in Figure 6.2.

Table 6.1: Calibration constants for the Ramberg-Osgood model (Eq. 6.7)

E_{ps} (ksi)	A	B	C
28,500	0.0125	110.46	0.075
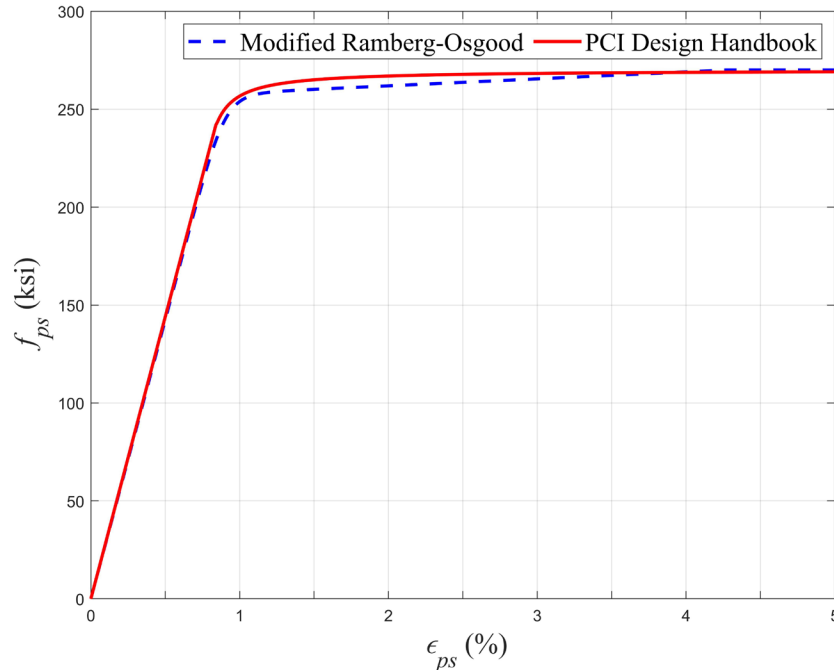
Figure 6.2: Prestressing strand stress-strain curves

Stress-strain behavior of mild reinforcing bars was modeled using a bilinear model. The initial linear-elastic behavior was defined by adopting a line with a slope equal to the modulus of elasticity of steel, taken as 29,000 ksi up to a stress corresponding to the yield stress of reinforcement. Because of lack of more detailed information, all mild reinforcement was assumed to have a yield stress of 60 ksi (Grade 60). The post-yield behavior was assumed to be perfectly plastic, and strain hardening was neglected.

AASHTO *LRFD Bridge Design Specifications (6)* estimates on prestress losses were used to determine the effective prestressing stress in the strand prior to loading. Creep, shrinkage, relaxation, and elastic shortening were considered as sources for loss of prestressing force, with Eqs. 6.8(a–c). All variables can be found in AASHTO *LRFD Bridge Design Specifications*. The approximate methods set in AASHTO LRFD specifications for all long-term losses were used for calculations. The results are summarized in Table 6.2. These values are used to determine the effective prestress force in the beam, which is important for determining the initial curvature given that the prestress influenced the beam initial camber. Figure 6.3 and Figure 6.4 show results of the moment-curvature analyses of each bridge beam cross section, including the effects of initial curvature caused by the existing prestressing force. The calculations were conducted for nominal material properties and sections, that is, they excluded material overstrength and any section loss caused by bridge beam deterioration from corrosion or concrete spalling.

$$\Delta f_{pES} = \frac{E_p}{E_c} f_{cpg} \tag{6.8a}$$

$$\Delta f_{pLT} = 10.0 \frac{f_{pi} A_{ps}}{A_g} \gamma_h \gamma_{st} + 12.0 \gamma_h \gamma_{st} + \Delta f_{pR} \tag{6.8b}$$

$$\Delta f_{pT} = \Delta f_{pES} + \Delta f_{pLT} \tag{6.8c}$$

Table 6.2: Prestress loss calculations

Bridge	f_{pi} (ksi)	Δf_{pT} (ksi)	f_{pe} (ksi)	Losses (%)
Rehoboth	164.7	20.6	144.1	12.5
Essex	188.9	25.8	163.1	13.6

A moment-curvature analysis was conducted for different areas of prestressing strands based on observed deterioration. The prestressing strand areas were adjusted to better fit the measured response during the tests as will be discussed later.

6.1.1 Moment-Curvature Analysis Procedure

The moment-curvature analysis was conducted by incrementally increasing the value of extreme compression strain in the compression face of the concrete. Each point in the moment-curvature curve was determined by assuming a strain in the extreme compression fiber of the concrete and calculation of the corresponding neutral axis by iteration. To determine if the neutral axis location was correct in each iteration, the section was discretized

into thin slices to determine concrete stress within each slice based on the concrete stress-strain relation. Similarly, internal forces in the strand and mild reinforcement were calculated from using the strain values for this assumed neutral axis location and the corresponding stress-strain relation of the reinforcing bars or strand. Stresses were used to compute internal forces and verify if internal force equilibrium was achieved within a prescribed tolerance. The neutral axis depth was adjusted until internal force equilibrium was satisfied. Moment and curvature were calculated after satisfying force equilibrium for this assumed value of extreme strain in compression. The extreme compression fiber strain was increased, and the analysis repeated until enough points were determined to construct the moment-curvature response of the section. The maximum attainable compressive strain in the concrete was set at 0.003, a typical value used for unconfined concrete in design (the actual value of peak strain of unconfined concrete could be slightly higher but was not determined).

6.1.2 Results of Moment-Curvature Analysis

A baseline was taken for all the individual beams by calculating their design nominal capacity. The moment-curvature analysis of the intact sections for the Rehoboth and Essex Bridge specimens are shown in Figure 6.3 and Figure 6.4, respectively. The Ramberg–Osgood stress-strain curve with the Whitney stress block, the PCI stress-strain curve with the Whitney stress block, and the AASHTO prestressing stress equation with the Whitney stress block were used to compare the moment-curvature analysis to techniques that bridge engineers might be more likely to use. All these methods were also used for the approximation of the capacity of the deteriorated beams to assess the validity of current procedures and to develop modifications to existing rating procedures.

The moment strength of the nondeteriorated Rehoboth Bridge beam section was estimated equal to 1,317.5 kip-ft when the moment-curvature analysis was used. This value is used as baseline for strength comparisons that follow. When using the AASHTO prestressing stress equation (Eq. 6.9) in combination with the Whitney stress block, the resulting moment capacity was 1,242.9 kip-ft (5.7% lower than moment-curvature analysis), a conservative estimate of capacity. Use of the Ramberg–Osgood equation (Eq. 6.7) or the PCI handbook equation (Eq. 6.6) to estimate prestressing strand stress in combination with the Whitney stress block resulted in moment strengths of 1,306.1 kip-ft and 1,318.3 kip-ft, respectively (0.9% lower and almost identical to moment-curvature analysis, respectively).

$$f_{ps} = f_{pu}\left(1 - k\frac{c}{d}\right)\ (ksi) \tag{6.9}$$

(a)   (b)
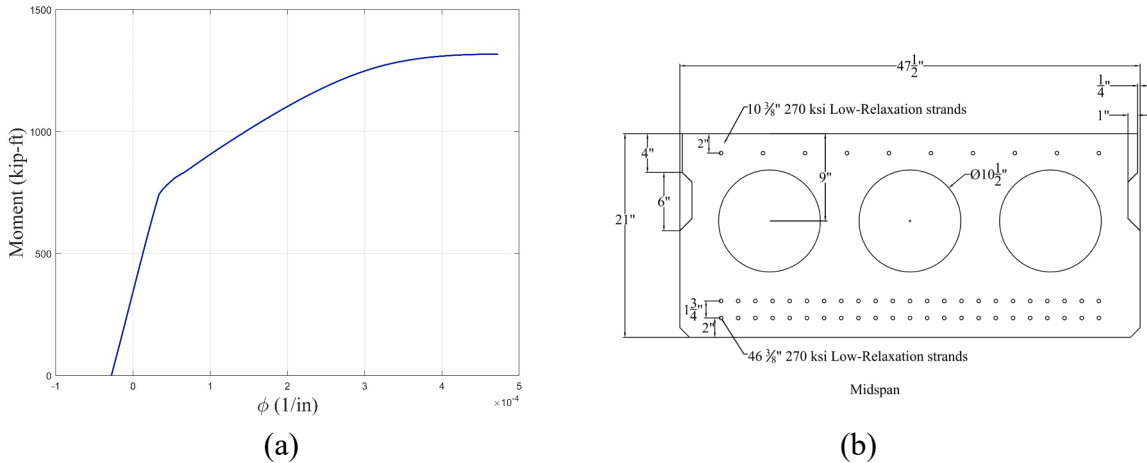
Figure 6.3: (a) Moment-curvature analysis of nominal Rehoboth Bridge beams; (b) cross section

(a)   (b)
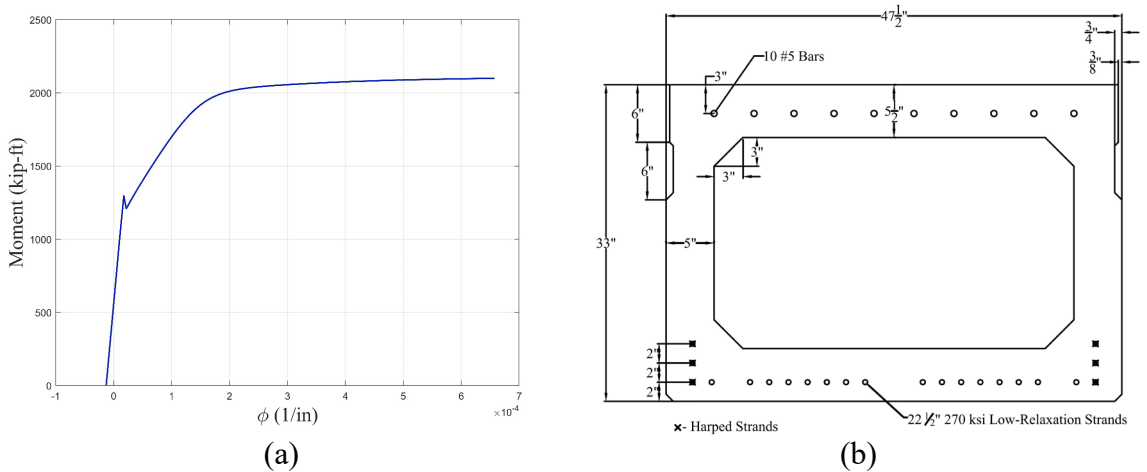
Figure 6.4: (a) Moment-curvature analysis of nominal Essex Bridge beams; (b) cross section

Using specified material properties, the moment strength of the nondeteriorated Essex Bridge beams calculated using a moment-curvature approach was 2,099.4 kip-ft. This value is used as baseline for the following comparisons. When using the AASHTO prestressing stress equation (Eq. 6.9) in combination with the Whitney stress block, the moment strength was determined as 1,972.7 kip-ft (6% lower than moment-curvature analysis). Using the Ramberg–Osgood equation (Eq. 6.7) to estimate strand stress at moment strength, the capacity was estimated equal to 2,088.3 kip-ft (0.5% lower than moment-curvature analysis). When the PCI handbook equation for prestressing strand stress (Eq. 6.6) was used in combination with the Whitney stress block, the moment strength was estimated at 2,123.7 kip-ft (1.2% higher than moment-curvature analysis). The moment strengths for the Essex and Rehoboth Bridge beams computed using the different methods are summarized in Table 6.3.

Table 6.3: Nominal moment capacity of beam sections

Bridge	Moment-curvature (kip-ft)	AASHTO LRFD strand equation (kip-ft)	Ramberg–Osgood (kip-ft)	PCI handbook equation (kip-ft)
Rehoboth	1,318	1,243	1,306	1,318
Essex	2,099	1,973	2,088	2,124

The AASHTO equation to compute stress at moment strength in the prestressing strands produced the lowest estimate of moment capacity among the four methods, but the highest difference was only 6% in comparison with moment-curvature analysis. The moment-curvature analysis is considered as the most accurate method used in this research because it involves realistic stress-strain material relations. Furthermore, its use was also accurate in determining the capacity of the Rehoboth beams. Using either the Ramberg–Osgood or the PCI handbook equation for strand stress at ultimate gave similar results to the moment-curvature analysis, therefore indicating that any of these equations are acceptable to estimate the strength of nondeteriorated sections.

6.2 Strength Comparison between Laboratory and Analysis Results

This section focuses on a comparison of the results discussed in Section 5 with the analysis methods described in Section 6.1 when specimens were governed by moment strength. Because failure of Specimen E4 was governed by shear strength at the south end, comparisons are made using code equations for shear strength of prestressed concrete sections for this particular specimen.

6.2.1 Rehoboth Bridge Beams

A comparison of load-deflection curves of the Rehoboth Bridge beams measured during the tests was made to load-deflection curves determined using the sectional moment-curvature analysis procedure presented in Section 6.1. To determine beam load–midspan deflection from the moment-curvature behavior of the beam section, the following procedure was followed. The moment diagram along the length of the beam was determined for the various loads existing on the beams before and during testing (Figure 6.5). Load was applied at 1-kip increments in the analysis to achieve a smooth curve similar to that achieved in an experiment. To get an accurate estimate of the deflection at midspan, the beam was discretized into 0.5 in. increments. A corresponding curvature diagram was developed for the associated moments at the established nodes of each beam segment, with the curvatures corresponding to the moment from Figure 6.3. Numerical integration was then used to develop rotation diagrams, and with numerical integration again, deflection curves were established. Deflection at midspan for the corresponding load applied was extracted at each load increment for comparison with the measured value in the experiment. The preexisting beam deflection prior to test was calculated by considering self-weight and the weight of the frame applied to the specimen and analysis. The self-weight (beam and spreader beam)

deflection was subtracted from the rest of the analysis to set the initial loading and deflection equal to zero and establish a curve that would be representative of values measured during the experiment.

The three beams from the Rehoboth Bridge (Specimens R2, R3, and R4) exhibited similar load-deflection behavior (Figure 6.6 through Figure 6.8). Curves from analysis were constructed subtracting deflections caused by beam self-weight and the weight of the loading frame. Three key points in the curve obtained from the experiment results are identified in the figures: the cracking load, yield load, and ultimate load. The cracking load was identified when a visible loss in stiffness of the load-deflection curve was observed during testing and verified visually. The yield load was estimated from the results of the moment-curvature analysis (specifically the point at which the strands reached their yield stress of 243 ksi) and plotted in the experimentally determined load-deflection plots as shown in the figures. Since the test data were collected every 3 seconds, yield was identified as the closest load to what was predicted analytically. The values corresponded approximately to changes in slope of the load-deflection diagram of each of the specimens as shown Figure 6.6 through Figure 6.8. A peak load of 195.4 kip was predicted using the moment-curvature analysis, given the testing configuration. All the specimens exceeded the calculated peak load, confirming the ability of the analytical tools used for nondeteriorated beams. The maximum difference in measured to calculated peak load did not exceed 10%.

For the cracking load, a separate analysis determining the moment at which the tensile stress in the bottom fiber of the beam would reach the modulus of rupture was used to determine the moment at which the beam would be expected to crack. The moment applied to the cross section from effective prestressing force was used in determining the required moment needed to reach the cracking moment. The predicted applied load to induce cracking in the specimens, after subtracting moment induced by self-weight of beam and test beams, was 90.3 kip. The load where flexural cracking was observed during the tests exceeded the calculated cracking load. Because all calculations were based on specified material properties, it is not surprising that the measured values moderately exceeded those predicted by calculation.

Although load was predicted accurately by the models used, deflections were not. The difficulty in accurate deflection calculation is not unique to this research. There is larger variability in modulus of elasticity of concrete than any other mechanical property involved in the calculations presented here. The modulus of concrete can be off by as much as 50%, so deflection calculations are hard to match with laboratory results. A reduction in modulus is also observed after concrete creep, so deflection calculations are often below measured values as experienced in Specimens R3 and R4 (Figure 6.7 and Figure 6.8).

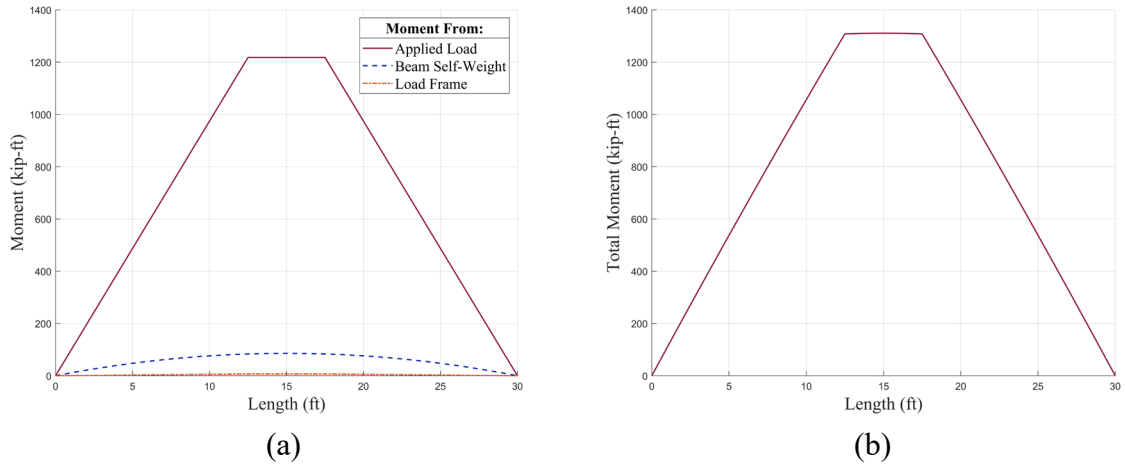Figure 6.5: (a) Moment diagrams for applied loads, self-weight, and load frame for ultimate capacity predicted by moment-curvature analysis and (b) total moment diagram
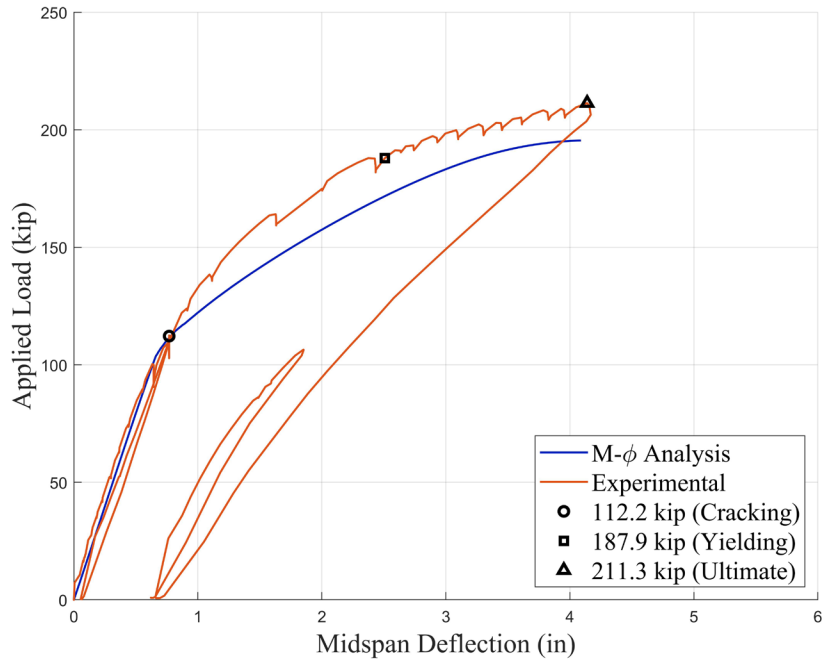

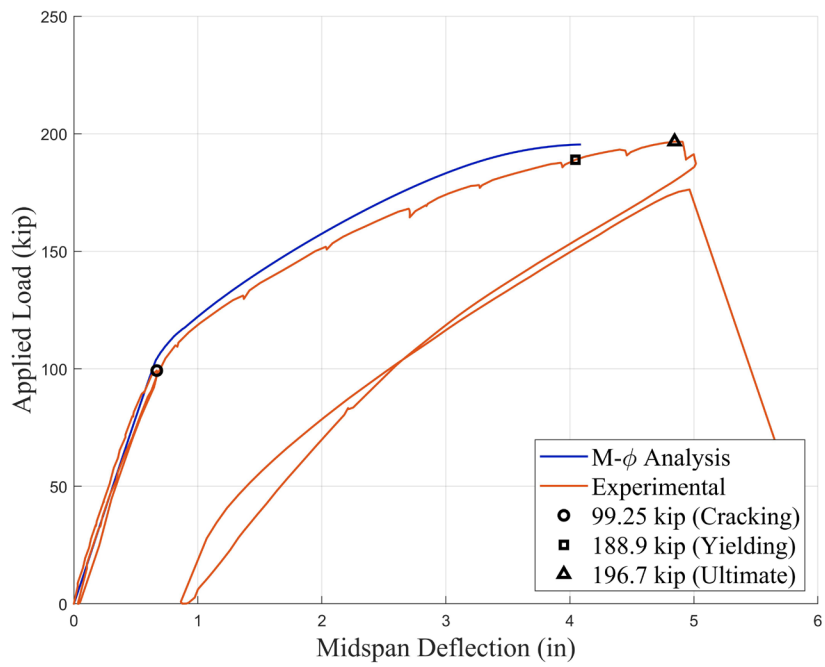Figure 6.6: Specimen R2: measured and calculated load-deflection response

Figure 6.7: Specimen R3: measured and calculated load-deflection response
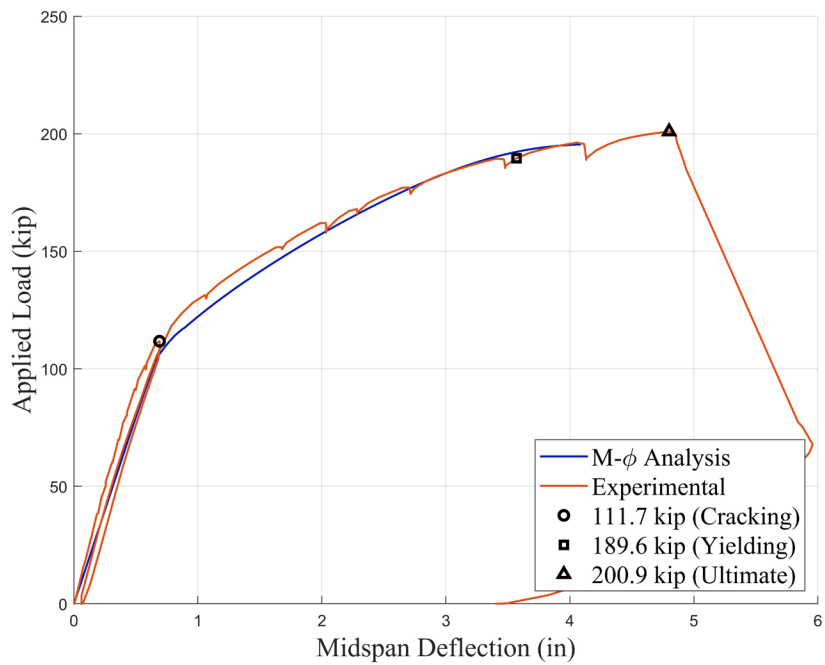
Figure 6.8: Specimen R4: measured and calculated load-deflection response

6.2.2 Essex Bridge Beams

Each of the Essex Bridge specimens experienced a unique failure mode. Specimen E4 failed after the formation of diagonal tension cracks occurred at the south end of the beam, indicative of a shear failure. Specimen E3 experienced a flexural failure as discussed in Section 5. Specimen E9 also showed signs of imminent flexural failure after cracks extended toward the top of the beam. Specimen E3 and Specimen E9 showed flexural cracks forming in the constant moment region and flexure-shear cracks forming right outside of the constant moment region. A summary of the maximum applied loads, maximum midspan moments, and the percentage of applied-to-calculated moment strength are listed in Table 6.4. Because of premature shear failure and variations in strands area remaining in the cross sections along these severely deteriorated beams, none were able to reach the estimated moment strength. Load rating recommendations presented in Section 7 will be based on the measured maximum moments along with the condition of the beams prior to testing.

Table 6.4: Essex Bridge beams applied loads and maximum midspan moments

Load/moment	Specimen E4	Specimen E3	Specimen E9
Maximum applied load (kip)	83.2	127.7	168.5
Maximum midspan moment (kip-ft)	940.7	1,356.3	1,714.8
Calculated moment strength (%)	44.8	64.6	81.7

6.2.3 Specimen E4

Specimen E4 achieved an applied load of 83.2 kip after failing in shear at the south end (Section 5.4.4; Figure 6.10). The maximum load, including the weight of the topping assumed uniformly distributed (2.5-in.-thick asphalt layer with a unit weight of 0.14 kip/ft^3), the weight of the spreader beams, and self-weight of the prestressed beam result in a maximum moment at midspan of 940.7 kip-ft. A summary of the contributors to the total midspan moment are listed in Table 6.5. Figure 6.9 shows the moment diagram for all loads in the test, corresponding to approximately 44.8% of the calculated moment capacity of a nondeteriorated beam. During the test, no flexural cracks were observed to form; only shear cracks formed primarily on the web near the south end of the beam. At this end, one of the webs was noticeably thinner because of shifting of the void-former used during construction, as previously discussed in Section 5 (Figure 5.20). Diagonal cracking occurred mostly in this web limiting the capacity for the beam to resist higher loads (Figure 5.22). Figure 6.10 shows the load-deflection curve, which shows the sudden drop in load experienced during the test as the cracks that formed in web and web-bottom flange connection widened.

Table 6.5: Maximum midspan moment from various loads for Specimen E4

Applied load (kip-ft)	Self-weight (kip-ft)	Topping (kip-ft)	Load frame (kip-ft)	Total (kip-ft)
738.2	159.6	23.2	19.7	940.7

Note: failure occurred at the south end.
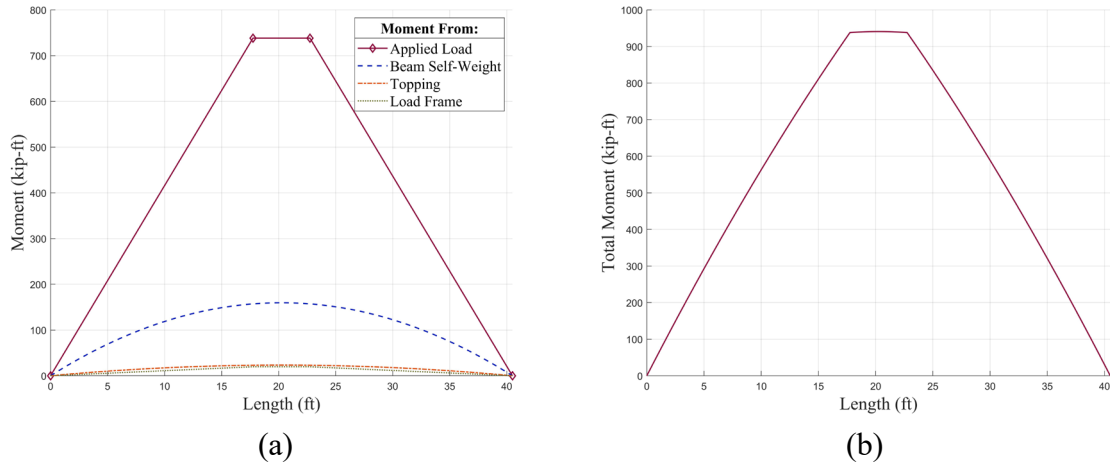
Figure 6.9: Specimen E4 moment diagrams: (a) individually applied/acting loads; (b) total moment
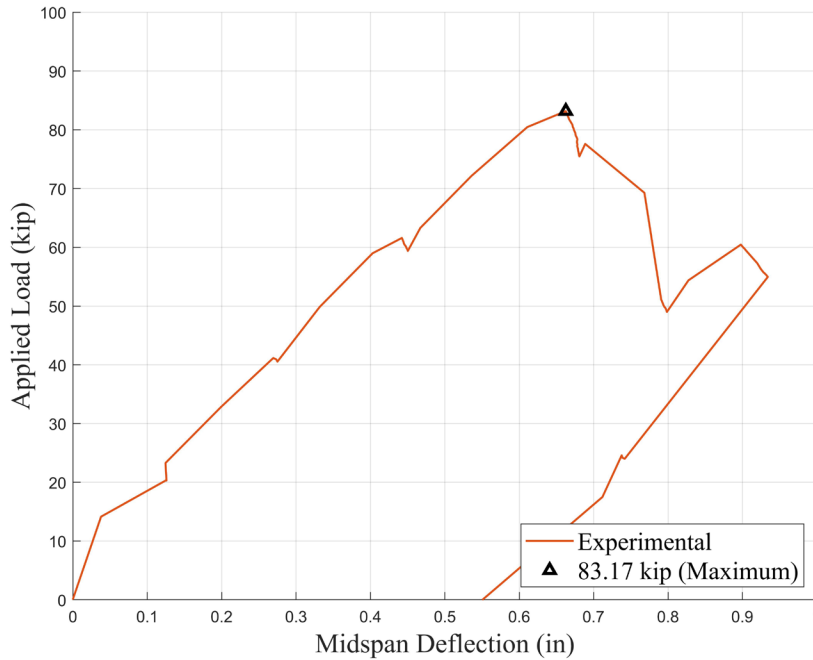
Figure 6.10: Specimen E4 load-deflection curve with critical points

Because failure was caused by shear in the thin web, shear strength was calculated using available equations in the AASHTO *LRFD Bridge Design Specifications (6)*. Results are summarized in Table 6.6. Only web shear strength equations were considered to estimate shear strength near the end of the beam. According to AASHTO specifications, web shear strength, V_{cw}, is determined using Eq. 6.10, where f_{pc} (ksi) is the effective stress in the concrete at the centroid of the section, d_v is the effective shear depth, and V_p is the shear strength contribution by harped strands:

$$V_{cw} = \left(0.06\sqrt{f_c'} + 0.30 f_{pc}\right) b_w d_v + V_p \text{ (kip)} \qquad (6.10)$$

As an initial lower-bound estimate, the contribution of harped strands to V_{cw} was neglected ($V_p = 0$). Furthermore, the following values were used in the calculations (the sum of measured web widths was less than the sum of nominal web widths [10 in.]):

- $d_v = 0.72h = 15.12$ in. (from AASHTO LRFD specifications); and
- $b_w = 8.5$ in. (measured width of both webs),

resulting in a web shear strength of 71.6 kip. The shear force experienced at the end was 61.2 kip (from applied load, weight of frame, and self-weight including topping). If the individual web is considered, the resistance of the thinner web was 25.3 kip, corresponding to less than half of the total web shear strength. Including the stirrups of the section (no. 4 stirrups spaced at 16 in.), the resistance per leg of stirrup is 17.8 kip per Eq. 6.11. The total resistance of the web would be 43.1 kip. The total shear force estimated in the thin web was higher than the calculated shear strength neglecting contribution of stirrups.

$$V_s = \frac{A_v f_y d_v}{s} \text{ (kip)} \tag{6.11}$$

Table 6.6: Shear strength calculations for Specimen E4

Shear force (kip)	Shear force per web (kip)	Shear resistance for thin web (kip)	Shear resistance per stirrup leg (kip)	Total shear resistance (kip)
61.2	30.6	25.3	17.8	43.1

Note: Failure occurred at the south end.

6.2.4 Specimen E3

Specimen E3 reached an applied load of 127.7 kip, estimated from peak in the load-deflection plot (Figure 6.13). An ultimate moment of 1,356.3 kip-ft at midspan was calculated for the test configuration. The entrapped water weight in the middle cell of the beam was estimated by taking an assumed unit weight of water of 62.4 lb/ft³ and multiplying by the distance between the diaphragms, the width between the webs, and an assumed depth of water within the middle cell of 3 in. The moment diagrams from the individual loads and the total moment are shown in Figure 6.11, and the midspan moments are given in Table 6.7. The beam moment determined during the test was approximately equal to 64.6% of the calculated moment strength of nondeteriorated beam using specified material properties.

Table 6.7: Midspan moments from various loads for Specimen E3

Applied load (kip-ft)	Self-weight (kip-ft)	Topping (kip-ft)	Load frame (kip-ft)	Water (kip-ft)	Total (kip-ft)
1,141.2	161.5	23.6	19.8	10.2	1,356.3

Note: Failure occurred at a section just north of the north load points.
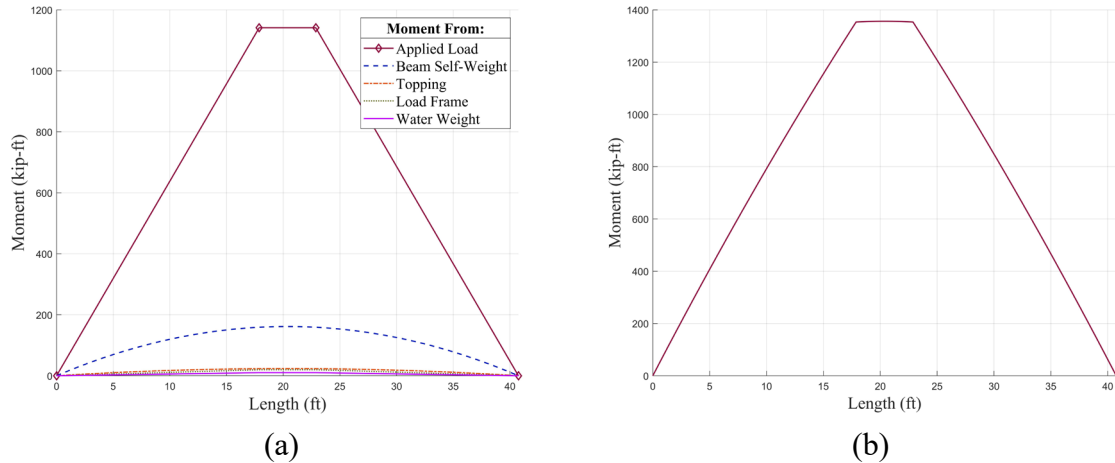
Figure 6.11: Specimen E3 moment diagrams: (a) individually applied loads; (b) total moment

After the test, the beam was examined to determine whether strands had ruptured to estimate their contribution to moment capacity of the beam. During the test, some of the strands were exposed due to spalling of concrete cover (Figure 6.12). These strands were considered ineffective for moment capacity of the beam. Nine visible strands were exposed after the loss of concrete cover, many of which exhibited corrosion, including pitting or fractured wires.

Figure 6.12: Specimen E3: visible deterioration of strands after spalling of concrete cover
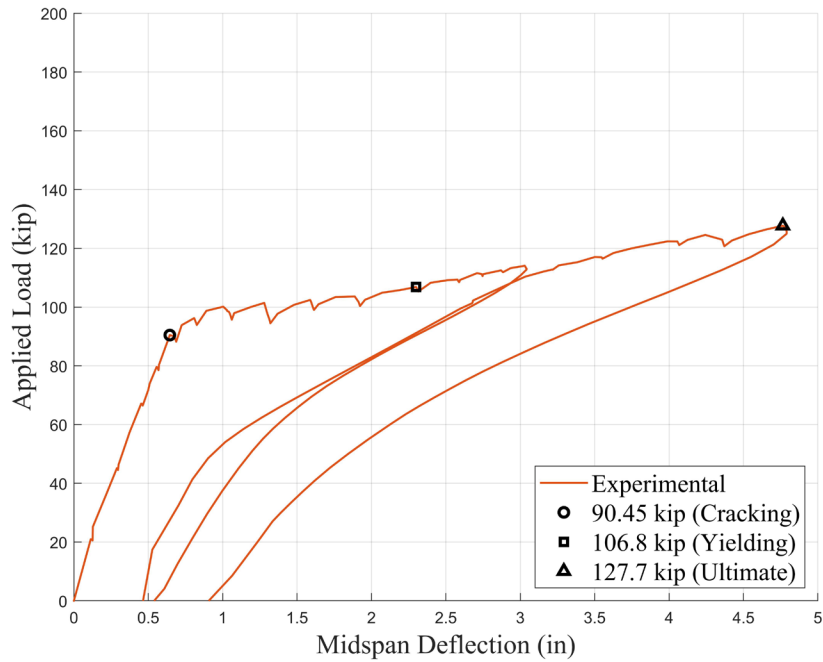
Figure 6.13: Specimen E3 applied load-deflection curve with critical points

6.2.5 Specimen E9

The maximum applied load to Specimen E9 was 168.5 kip, estimated from the peak in the load-deflection plot (Figure 6.16). An ultimate moment at midspan of 1,714.8 kip-ft was calculated using the testing configuration. This moment corresponds to 81.7% of the moment strength of the nondeteriorated beam. A summary of the maximum midspan moments induced by all loads acting at the time of testing are summarized in Table 6.8. The moment diagrams of the different loads (existing and applied loads) and the total moment diagram during the test are shown in Figure 6.14.

Table 6.8: Midspan moments from various loads for Specimen E9

Applied load (kip-ft)	Self-weight (kip-ft)	Topping (kip-ft)	Load frame (kip-ft)	Total (kip-ft)
1,509.1	162.2	23.7	19.9	1,714.8

Note: Failure occurred at a section near the north load points within the shear span.

(a)   (b)
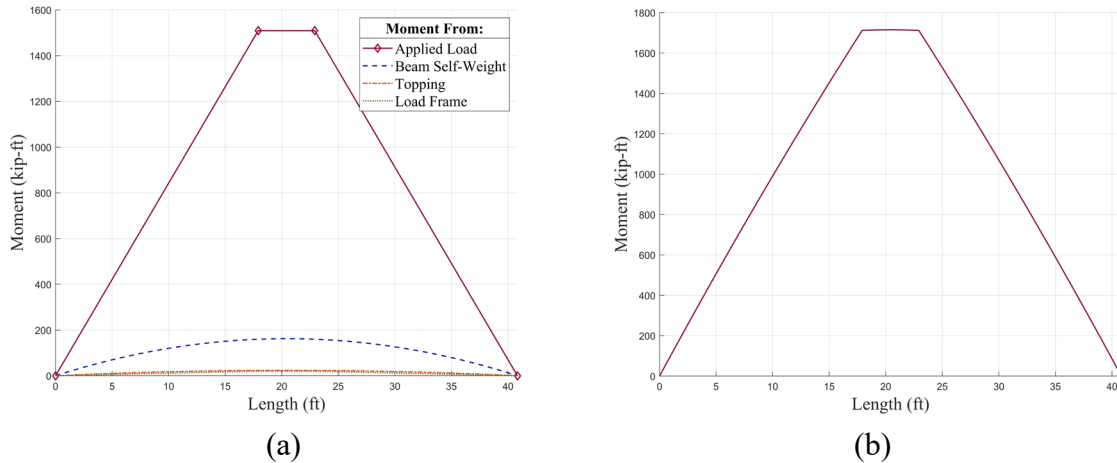
Figure 6.14: Specimen E9 moment diagrams: (a) individually applied loads; (b) total moment

 After the test, Specimen E9 was examined to determine whether strands had fractured locally to estimate the reduction in moment strength from the nondeteriorated condition. Some of the strands were exposed because of spalling of the concrete, and therefore were considered to be ineffective to the moment capacity of the beam. Four strands were exposed after loss of the concrete cover, some of which exhibited corrosion, such as pitting of wires, or strands fully fractured strand (Figure 6.15).

Figure 6.15: Visible strand corrosion and section loss in Specimen E9 after spalling
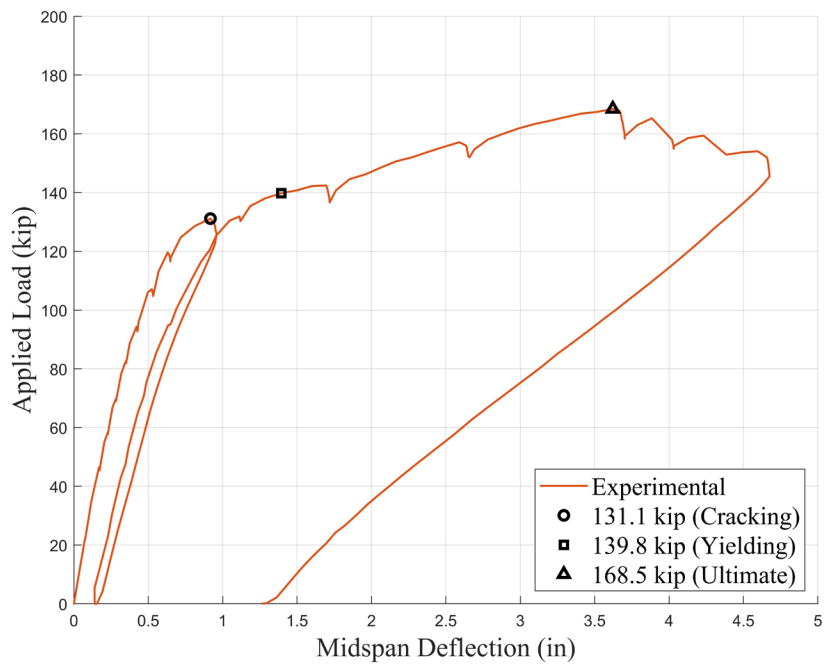
Figure 6.16: Specimen E9 applied load-deflection curve with critical points

In Section 7, the results from testing presented in this section are used to analyze the current load rating procedure described in the MassDOT *LRFD Bridge Manual (1)*. With these results, recommendations are made on improvements to more accurately estimate the capacity of deteriorated prestressed concrete beams.

This page left blank intentionally.

7.0 Prestressed Concrete Bridge Load Rating Procedures

In this section, the current procedure to evaluate the capacity of deteriorated prestressed concrete girders using the MassDOT *LRFD Bridge Manual (1)* is presented and evaluated using the laboratory tests of deteriorated beams presented in Section 6. A proposed rating procedure is described in this section, and recommendations to modify existing load rating procedures in the MassDOT *LRFD Bridge Manual (1)* are presented.

7.1 Evaluation of Current Procedures

According to the MassDOT *LRFD Bridge Manual (1)*, deterioration of existing prestressed concrete bridge girders has occurred if one or more of the following conditions are present: (1) cracking in the longitudinal direction of the beam; (2) concrete spalling; (3) exposed stirrups; and (4) exposed strands, which may include wire rupture. The degree of deterioration experienced by existing beams as evidenced through rust staining of the concrete surface and differential deflection between adjacent precast/prestressed beams is not easily quantified. Because of this, staining and differential deflection are not included as deterioration conditions in the MassDOT *LRFD Bridge Manual*, and their presence is not used to reduce moment strength.

7.1.1 Description of Current Prestressed Concrete Bridge Load Rating Procedures

Section 7.2.10 of the MassDOT *LRFD Bridge Manual (1)* includes guidance for engineers on how to include certain deterioration conditions to compute the moment strength of deteriorated girders to determine the load rating of existing prestressed concrete bridges. For convenience, relevant sections are copied from the MassDOT *LRFD Bridge Manual (1)* as follows:

> *7.2.10.2.   In the vicinity of exposed reinforcing steel stirrups deduct 100% of the strand area located in the bottom row directly above the limits of the exposed stirrups. Deduct 25% of the area of the strands in the next row directly above the limits of the exposed stirrups. Deduct 25% of the area of the strand(s) in the bottom row next to the area of the exposed reinforcing stirrups.*

> *7.2.10.3.   In the vicinity of exposed prestressing strands deduct 100% of the strand area within the limits where they are exposed. Deduct 50% of the area of the strands in the next row directly above the limits of the exposed strands. Deduct 50% of the area of the strand(s) in the bottom row next to the limits of the exposed prestressing strands.*

7.2.10.4.   In areas of concrete delamination without exposed reinforcing stirrups or prestressing strands deduct 50% of the area of the prestressing strands located in the row directly above the limits of the delamination. Deduct 10% of the area of the prestressing strand(s) in the bottom row next to the limits of the delamination.

7.2.10.5.   A longitudinal crack shall be considered to be a delamination that is six inches wide centered on the crack. The length of the delamination shall be the length of the crack plus six inches at each end of the crack. The loss of prestressing force at this theoretical delamination shall be calculated in accordance with Paragraph 7.2.10.4 above.

7.2.10.6.   The reduced prestressing force due to losses as calculated in the paragraphs above shall only apply to the area of the deterioration. Outside of these areas, all prestressed strands shall be assumed to be 100% effective and shall be appropriately re-developed into areas of sound concrete. For example, a strand with 100% loss will require 100% of its development length before it is considered fully effective again. Likewise, a strand with 50% section loss will require 50% of its development length, in sound concrete, before it is fully effective again.

7.1.2 Comparison between Current Procedures and Laboratory Tests

The deterioration condition of two of the specimens that exhibited flexural failure modes (Specimen E3 and E9) tested in this research was used to determine the corresponding strand reduction based on Section 7.2.10 of the MassDOT *LRFD Bridge Manual*. This was then compared with the moment capacity estimated through testing. Each beam had a section that was determined to be the critical section that would control the capacity of the beam, as shown in Figure 7.1 and Figure 7.2 for Specimens E3 and E9, respectively. The critical section was the one that had visibly exhibited the largest amount of deterioration and could lie outside of the region where highest moments were generated in the beam. Specimen E4 was not included in the flexural capacity ratings because its failure mode was governed by shear in the south end of the beam. Each beam had two sections that were identified to apply the MassDOT current procedure to capacity equations. These sections are called Section 1 and Section 2 and can be seen in Figure 7.1 and Figure 7.2.
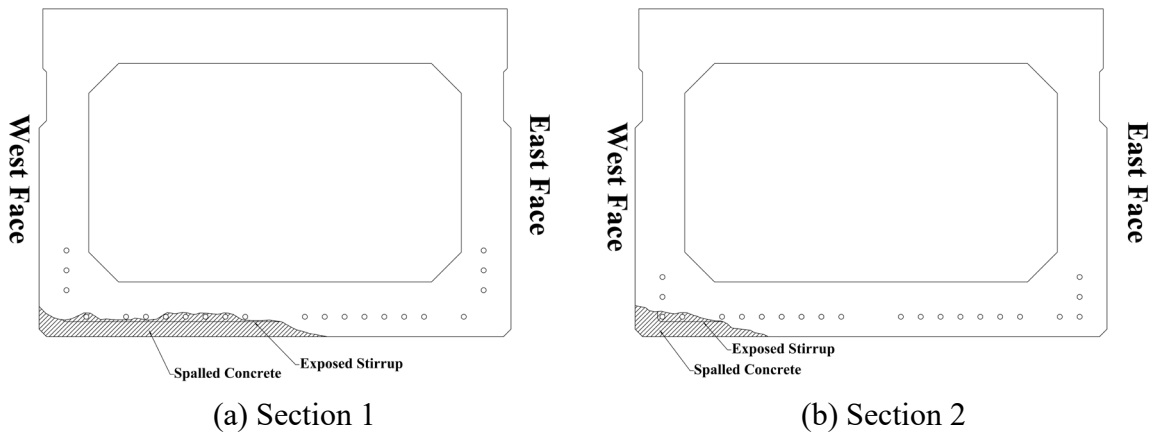
(a) Section 1

(b) Section 2
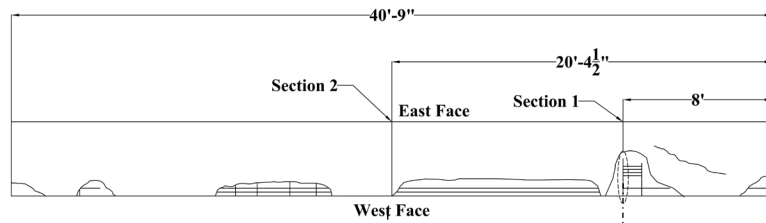
(c) Bottom view of beam
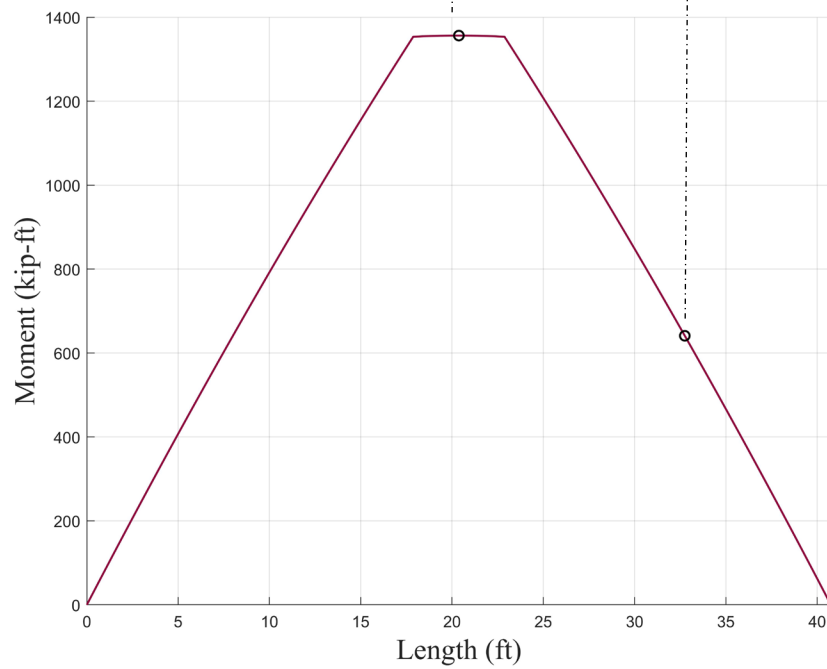
(d) Moment diagram from total loads

Figure 7.1: Deterioration condition of Specimen E3 at Section 1 and Section 2

(a) Section 1   (b) Section 2

(c) Bottom view of beam
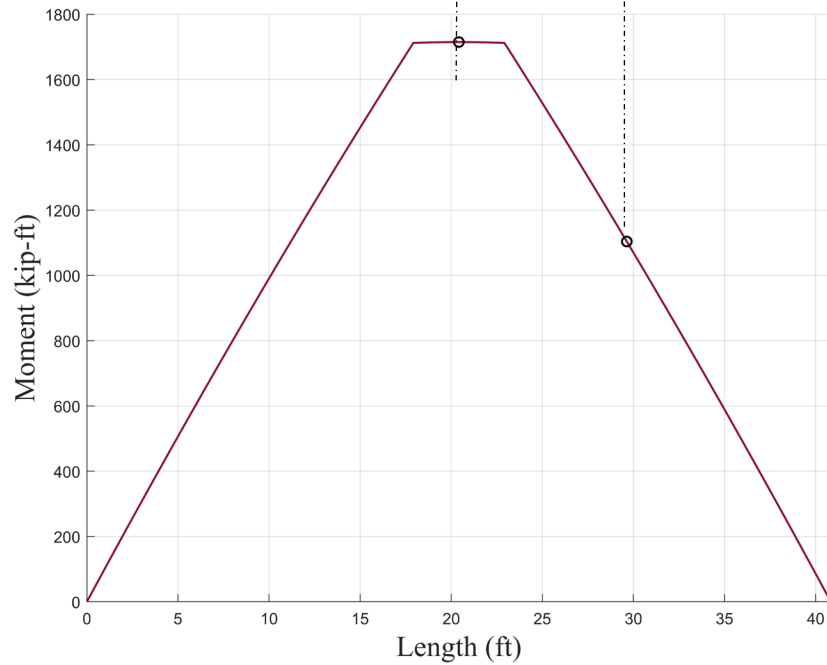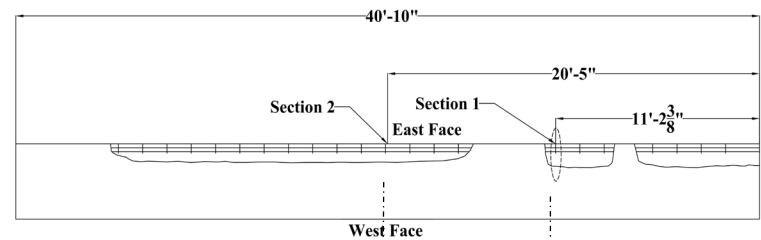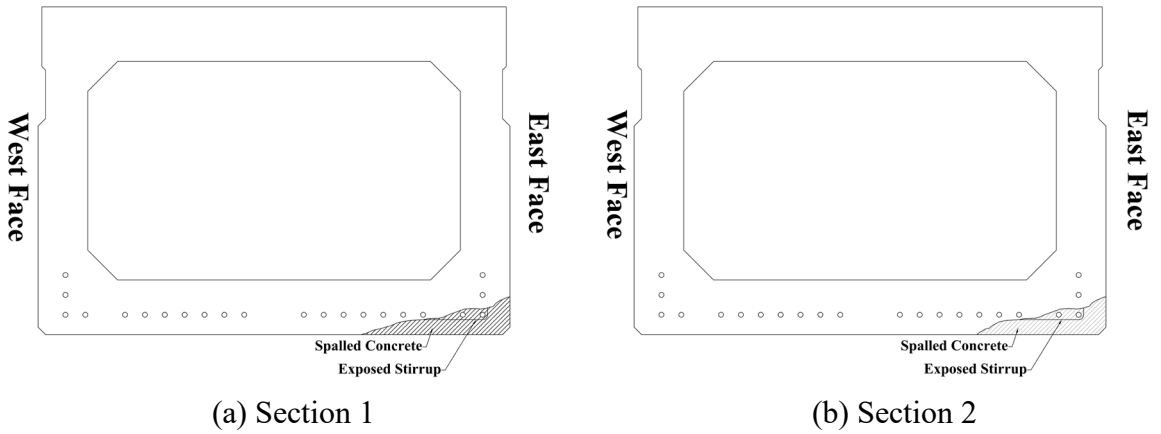
(d) Moment diagram from total loads

Figure 7.2: Deterioration condition of Specimen E9 at Section 1 and Section 2

The moment strength of deteriorated beams was estimated by using the moment-curvature analysis presented in Section 6 (Hognestad concrete model and Ramberg–Osgood model for prestressing steel). In the analysis, the reduced areas of prestressing strand shown in Figure 7.3 and Figure 7.4 were used. The moment strengths of these deteriorated sections were compared with the total moment (applied plus existing) to evaluate the procedure in the MassDOT bridge manual.

(a) Section 1   (b) Section 2
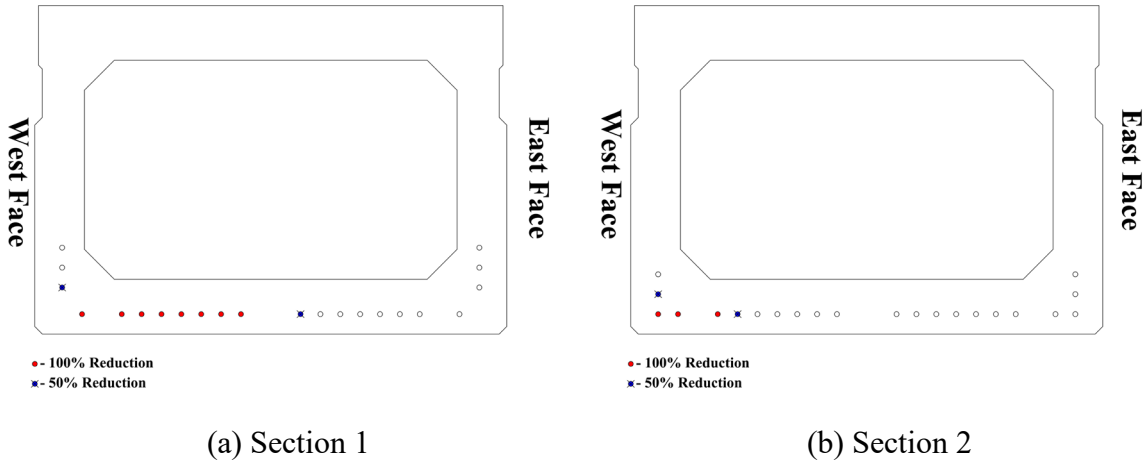
Figure 7.3: Specimen E3: Reduced areas of prestressing strand per MassDOT procedure

(a) Section 1   (b) Section 2
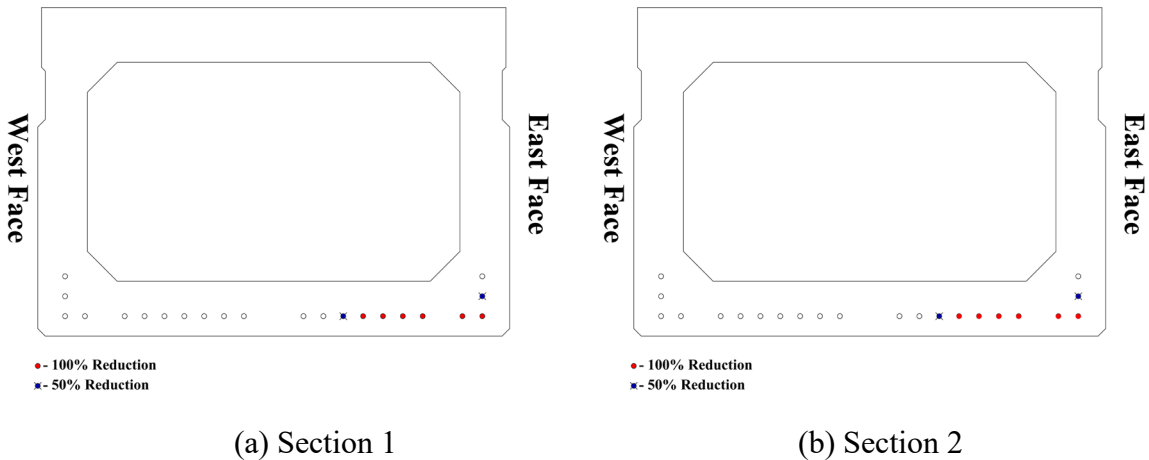
Figure 7.4: Specimen E9: Reduced areas of prestressing strand per MassDOT procedure

The strength of each specimen was evaluated at the two sections indicated in Figure 7.1 and Figure 7.2. The sections corresponded to the section with the highest amount of deterioration and the section where the total moment was highest. Specimen E3 reached a total moment of 641.0 kip-ft at the section with the highest amount of deterioration and 1,356.3 kip-ft at the section with highest total moment. Specimen E9 reached total moments of 1,103.8 kip-ft and 1,714.8 kip-ft at the section with the highest amount of deterioration and the section with highest total moment, respectively.

The calculated strength outside the described sections had to account for development length of strand outside of the deteriorated region. Moment strength of sections with partially developed strand was reduced in proportion to distance from sections located at or beyond the full development length. Equations in Section 5 of the AASHTO *LRFD Bridge Design Specifications (6)* were used to determine the development length of strand for the box beams in this study. Eq. 7.1 applies to the development length for all pretensioned concrete beams, where f_{ps} is the stress in the prestressing strand at ultimate moment strength (determined in this study from moment-curvature analysis), and f_{pe} as given in Section 6. The value of κ was taken as 1.6 for all Essex beam specimens, because they have a depth exceeding 24 in. Table 7.1 lists the development length values calculated for the strand used in the Essex beams.

$$l_d = \kappa \left(f_{ps} - \frac{2}{3} f_{pe} \right) d_b, \text{ where } \kappa = 1.6 \qquad (7.1)$$

Table 7.1: Development lengths for different sections of each specimen

Specimen	Section 1 (in.)	Section 2 (in.)
Specimen E3	125.8	124.5
Specimen E9	125.4	125.4

Because Section 1 of Specimen E3 is located less than the development length away from the support, the moment strength at that section was reduced accordingly. All other sections were located at distances greater than the development length from the support, so the estimated moment strength at these sections only considered reductions associated with strand deterioration but not reductions associated with development length. Table 7.2 summarizes the moment capacity calculations for each section of each beam in comparison with the total moment at the corresponding section. Clearly, the MassDOT procedure results in an overestimation of the capacity of Specimens E3 and E9 in all but one case (Section 2, Specimen E9).

Table 7.2: Moment capacity: moment-curvature analysis and MassDOT strand area reduction

Specimen	Total moment at Section 1 (kip-ft)	Moment capacity at Section 1 (kip-ft)	Total moment at Section 2 (kip-ft)	Moment capacity at Section 2 (kip-ft)
Specimen E3	641.0	931.5	1,356.3	1,740.1
Specimen E9	1,103.8	1,463.1	1,714.8	1,463.1

7.2 Recommended Procedure to Determine Moment Strength of Deteriorated Prestressed Concrete Beams

As discussed in Section 7.1, except for Specimen E4 that failed prematurely in shear, the two other specimens were unable to withstand higher moments than estimated using procedures in Section 7.10.2 of the MassDOT *LRFD Bridge Manual (1)*. Because of the overestimation of the current procedures, modifications to the existing procedure were proposed based on the observed deterioration of the beams both before and after the experiments, to more accurately account for the effect that deterioration has on strand areas.

Longitudinal cracking, spalling, exposed stirrups, and exposed strands were considered satisfactory indicators of strand deterioration leading to loss of strand area. The adjustments were primarily based on the percentage of reductions and strands affected by observed deterioration indicators in the beams.

The proposed modifications to the current MassDOT procedure to identify strand deterioration and consequent area reduction are based on observations made during laboratory tests, particularly results from testing of Specimen E3. The proposed modifications are presented in Section 8 as changes to relevant sections of the MassDOT bridge manual for ease in their incorporation. Their justification is as follows:

- Strand deterioration could be present under concrete that has not yet spalled. It is recommended that during inspection, the area of concrete exhibiting significant cracking or surrounding a spalled area be assessed by tapping to determine its soundness. If areas of concrete are not sound, 100% of the strand under this area should be deducted from the section at 100% throughout the unsound region. If the area of concrete surrounding a spall is sound, then the area of strand adjacent to the spall should be decreased by 50% of the area of strands.

During testing of Specimen E3, areas of concrete spalled adjacent to previously identified deteriorated regions (Sections 3 and 4, see Figure 7.5). These two additional spalled regions are shown as dark hatched areas in Figure 7.5. Section 4 is close to the northwest load-point application. Sections 3 and 4 experienced very similar spalling patterns to Section 1 (Figure 7.6; only the first three corner strands were exposed prior to testing). Although these areas were adjacent to previously spalled areas, they did not show significant evidence of potential for strand corrosion; however, after concrete spalling during the tests, the exposed strand showed a significant amount of corrosion and, because of concrete spalling, experienced loss of bond to the surrounding concrete. These sections, therefore, could not develop the moment capacity estimated following the MassDOT bridge manual procedures. The proposed modifications to the MassDOT bridge manual particularly apply to areas adjacent to spalled regions of concrete or other areas where loose concrete may be present covering strands that might be severely deteriorated.
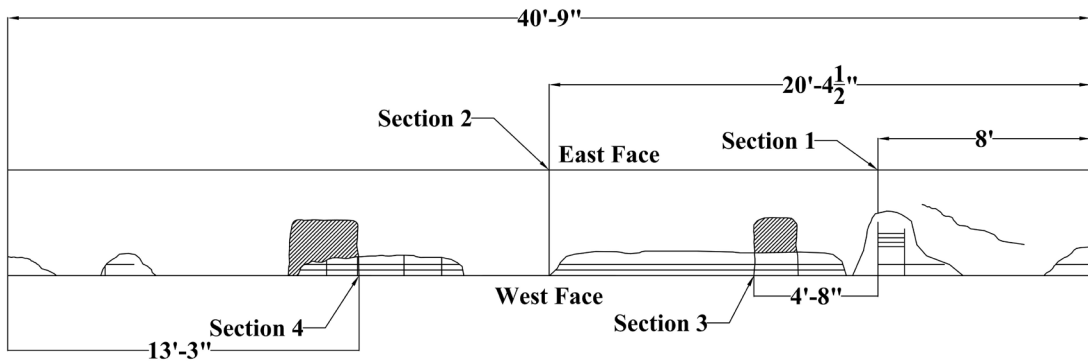
(a) Deterioration mapping on bottom surface (hatched area spalled after test)

(b) Section 3 after the test

(c) Section 4 before and after test
Figure 7.5: Deterioration of Specimen E3
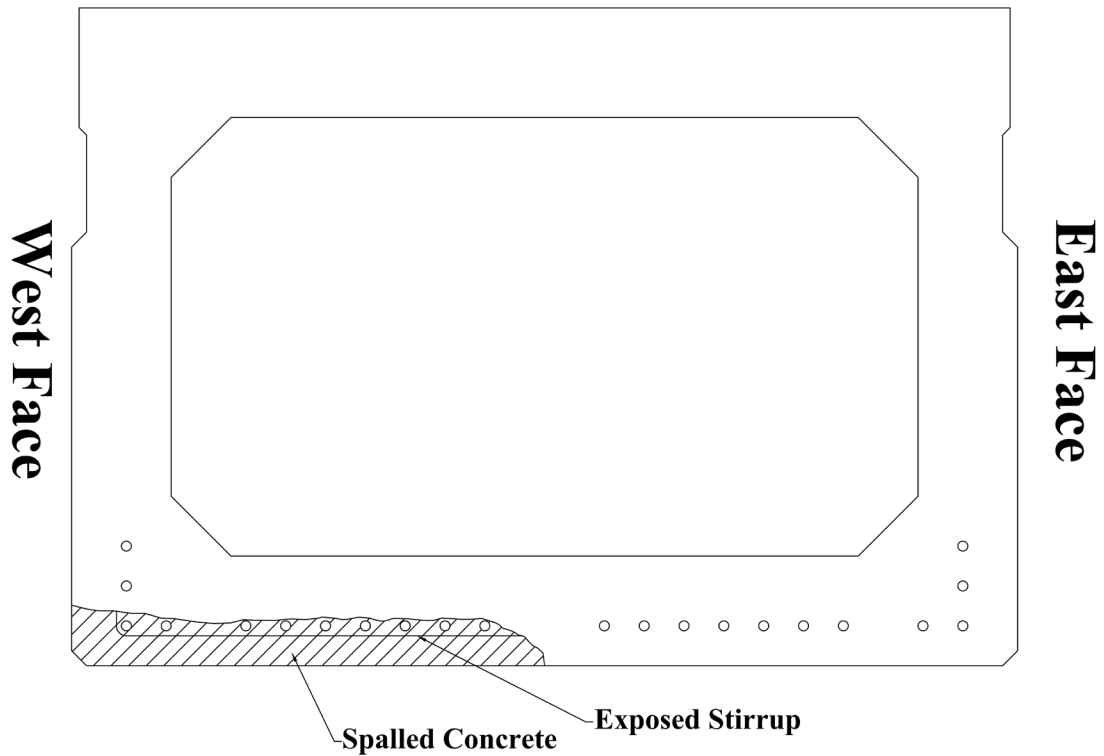
Figure 7.6: Cross section of Sections 3 and 4 of Specimen E3 after testing

The section with the highest amount of visible deterioration occurred outside the constant moment region for Specimen E3 and along the length of the beam for Specimen E9. Because of changes in total moment and deterioration along the beams, the section controlling moment capacity could lie outside the regions of maximum moment. It is recommended to determine moment strength along the beam to capture strength of sections affected by deterioration. Sectional moment strength should be compared with moment demand using appropriate load factors for each relevant combination to determine the value that will control rating.

7.3 Determination of Moment Strength using Proposed Recommendations to Account for Deterioration

The proposed procedure was compared to the current MassDOT bridge manual procedure described in Section 7.1 and to the moment capacity determined through testing to assess the proposed procedure. The proposed recommendations do not change current percentages in area reductions in the bridge manual, but recommendations are provided on where to begin accounting for development length and how to identify regions of concrete that may be

covering severely deteriorated strands. Therefore, magnitudes in reductions applied to strands that are exposed stay the same, but the number of strands that are affected by a reduction may increase if the concrete cover spalled and ended up revealing corroded strands.

In Specimen E3, additional strands than those that were initially exposed were considered for reduction based on areas of spalled concrete. Furthermore, development of exposed strand was considered to initiate outside of the spalled region in sections that had sound concrete after testing (determined by light tapping). Concrete surrounding the spalled region near Section 3 (Figure 7.5) was identified as being sound, so development of strand was considered to initiate outside of the spalled region. For the spalled region in the proximity of Section 4, sound concrete was identified at a distance of 2 ft away from the spalled region toward the center of the beam (Figure 7.5c, for reference). A moment capacity diagram for Specimen E3 is shown in Figure 7.7, superimposed on the total moment diagram. Moment strength was determined at each section using the moment-curvature approach, accounting for partial development of strand based on deterioration including spalling. The values used for the analysis at different locations along the span are listed in Table 7.3. As shown, the calculated capacity diagram crosses the total moment diagram at a section approximately located at 15 ft from the north end of the beam. The calculations with the proposed modifications predict a slightly lower capacity than what the beam experienced during the test. However, a slight northward modification to the point where strands were considered to start developing (just to the left of 15 ft), would produce a moment strength diagram that ends up crossing the total moment diagram at almost the total load applied during the test. This example illustrates the sensitivity of moment strength (and eventual beam rating) on the section where strand starts developing adjacent to deteriorated beam regions with spalled concrete, so being conservative in this respect seems warranted.
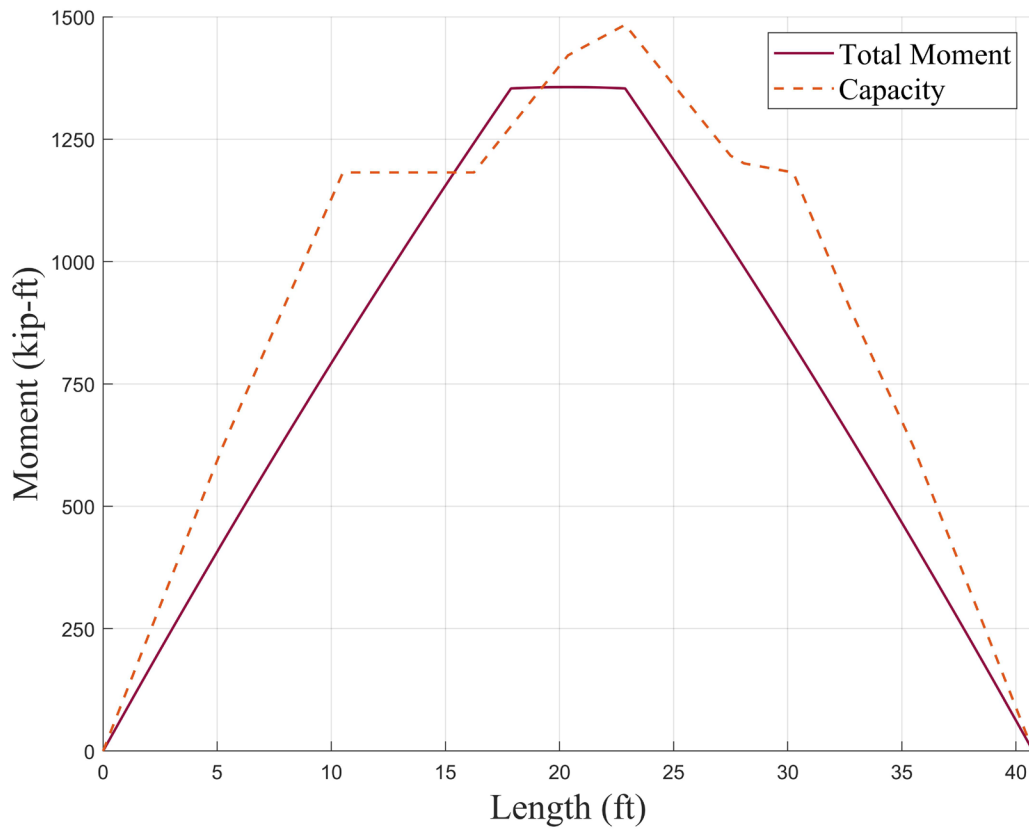
Figure 7.7: Specimen E3: Total moment (solid line) and moment strength (dotted line)

Table 7.3: Specimen E3: Calculated moment strength and area of strand

Beam section from north end (ft)	Moment Strength (kip-ft)	Estimated area of strand (in^2)
0	0	0
5.25	623.5	1.00
10.51	1,182.0	1.87
11.25	1,182.0	1.87
16.25	1,182.0	1.87
17.875	1,276.6	1.99
20.375	1,421.3	2.23
22.875	1,483.7	2.33
27.50	1,216.3	1.89
28.08	1,200.6	1.84
30.25	1,182.0	1.63
32.75	902.1	1.43
35.50	623.5	1.00
40.75	0	0

For Specimen E9, Sections 1 and 2 had the same numbers of deteriorated strands (Figure 7.4), leading to the same moment strength without considering effects of strand developments. Because Section 2 lies within the maximum moment region, this section represents the critical section that controls the capacity of the beam. Two calculations were conducted to estimate capacity at Section 2: one assuming that only exposed strands prior to the test were deteriorated and therefore their area had to be reduced, and the second assuming that the region adjacent to this spalled region prior to the test contained loose concrete although there was no visual evidence of it (three additional strands were deducted for the second assumed condition). As shown in Table 7.4, the calculated moment capacity assuming reductions only on strands exposed prior to the test resulted in a better predictor of total moment than the one where additional strands were deducted for the potential of further spalling after loading. These calculations demonstrate that the current method for strand area reduction works as long as areas that are likely to spall with loading (i.e., those that already contain loose concrete) are identified adequately.

Table 7.4: Specimen E9 (Section 2): Calculated moment strength

Total Moment (kip-ft)	Moment Strength: Deduction of exposed strand only (kip-ft)	Moment Strength: Deduction of exposed strand and 3 adjacent strands (kip-ft)
1,714.8	1,602.0	1,463.1

8.0 Summary and Conclusions

The primary objective of this research was to develop reliable load rating procedures for deteriorated precast/prestressed concrete box beams or voided slabs. The objective was accomplished by first examining factors that contributed to the observed deterioration of these types of bridges and subsequently testing beams obtained from two bridges scheduled for replacement. Existing load rating provisions in the MassDOT *LRFD Bridge Manual (1)* were assessed using results of the laboratory tests. This section presents a summary and key conclusions from the different activities of the research project. Proposed changes to existing load rating provisions in the MassDOT *LRFD Bridge Manual* for precast/prestressed box beams and voided slabs are presented.

8.1 Summary and Conclusions from Database and Inspection Report Investigation

The initial part of the research concentrated on identifying any trends on deterioration for prestressed voided slab or prestressed adjacent box-beam bridges. Parameters that may have contributed to deterioration of these two types of bridges were studied by mining data from the NBI Database. Using the condition rating in the database, only bridges with a condition rating of 5 or below were considered as severely deteriorated. The parameters considered as potential contributors to corrosion deterioration were studied; these included bridge proximity to water body (river or coastline), construction era by decade, Massachusetts highway district, road type (interstate, state, rural), vehicular traffic count, and so forth. Year of construction by decade showed the highest correlation with condition rating. Bridges built in the 1970s and 1980s had a lower condition rating than in other decades studied (from the 1950s through 2010s). Bridge location, particularly in proximity to areas of higher population density, also showed some correlation with condition rating.

The inspection reports were collected for precast/prestressed adjacent box-beam bridges and adjacent voided slab bridges with a condition rating of 5 or below as listed in the NBI Database. The study of inspection reports was conducted to identify the characteristics of physical deterioration (cracking, spalling, rusting, etc.) and their relationship with condition rating included in the inspection report. Great variability was found in different inspection reports between the physical deterioration observed and the assigned condition rating.

Deterioration conditions were classified into seven categories (indicators of potential deterioration), including concrete rust staining, hairline cracking, deflection differences between adjacent beams, wide cracking, concrete spalling, strand corrosion, and strand severing. These conditions were found by individual study of pictures in the inspection reports. The less severe indicators of deterioration (concrete staining, hairline cracking) showed few clear trends with overall condition rating value assigned to each bridge. For the

more severe deterioration conditions (deflection differences between adjacent beams, wide cracking, concrete spalling, and strand corrosion or rupture), stronger trends emerged with condition rating, but there was still some variability and inconsistency among the different values of condition rating. For example, some of the bridges with a condition rating of 5 had more frequent apparent severe deterioration than some that were assigned a condition rating of 3.

8.2 Summary and Conclusions from Selected Bridge Candidates and Laboratory Tests

To accomplish the main goal of the research project, testing of prestressed concrete beams obtained from bridges scheduled for replacement was conducted. The two bridges were identified as candidates for this research because they were scheduled for replacement within the duration of the project and had a superstructure consisting of either prestressed voided beam slabs or adjacent prestressed concrete box beams. Prestressed beams were obtained from a voided slab bridge located in Rehoboth, Massachusetts (Rehoboth Bridge) and an adjacent box-beam bridge located in Essex, Massachusetts (Essex Bridge).

Three beams were recovered from each bridge and delivered to the Brack Structural Testing Laboratory at the University of Massachusetts Amherst. The beams from the Rehoboth Bridge had no visible deterioration that could potentially impair the load-carrying capacity of the element. Beams from this bridge had minor cracking and small concrete spalling that likely occurred during bridge demolition. Beams from the Essex Bridge had significant deterioration at several sections along the span of the beam, including concrete spalling, surface rust staining, exposed corroded strands, exposed corroded stirrups, and fractured strands. All the beam specimens were tested in the laboratory under a 4-point load arrangement to determine the moment strength of the beams and assess the effect that deterioration had on strength.

The Rehoboth Bridge beam specimens, having no significant deterioration, exhibited a flexural failure. The main findings from this group of specimens are summarized as follows:

1. During testing, the specimens sequentially went through flexural cracking, strand yielding, and concrete crushing as would be expected from a prestressed concrete beam designed under current specifications.

2. The maximum load obtained during the tests was reliably calculated using advanced techniques (moment-curvature analysis) or design equations using common assumptions on strand stresses at ultimate and an equivalent stress block for concrete. This demonstrated that design equations provide reliable estimates of strength, although the predictions were slightly more conservative than those obtained from moment-curvature analysis.

3. The Rehoboth Bridge had a skewed geometry, so beams were tested at the same skew angle in the field. Beams twisted during the tests, which generated larger

displacements along one side of the beam than the other. Twisting did not affect moment strength significantly, although load cell readings indicated loads were not applied evenly on both sides of the beams.

4. Despite beam twisting, failure of beams consisting of concrete in compression spread through the entire beam width.

5. No shear failures were observed.

The Essex Bridge beam specimens had significant deterioration and exhibited a variety of failure modes. Two of the specimens (Specimens E3 and E9) reached a flexural failure at an applied load that was lower than anticipated assuming a nondeteriorated condition of the beams. One specimen that had a very narrow web (Specimen E4) and showed indications of concrete splitting in the end region along the harped strands within the web of the box exhibited a premature shear/splitting failure at loads significantly lower than the estimated moment strength of the beam. The key findings from this group of specimens are summarized as follows:

1. Specimens E3 and E9 reached a peak load that was well below estimated, assuming the beams had no deterioration. Concrete crushing was not observed, but instead indications of strand slip and wire rupture limited the load-carrying capacity of these specimens. The section that governed capacity in each specimen was located within the beam shear span (between load point and support) or was in the proximity of the load point.

2. Delaminated areas of concrete located adjacent to exposed stirrups and strands were not detected prior to testing. Concrete in these areas spalled during testing, subsequently exposing severely deteriorated strands and stirrups that extended across beam half-width that were not identified as possibly deteriorated prior to testing.

3. One of the specimens (Specimen E3) contained trapped water within the center portion that leaked after the formation of flexural cracks during testing. This finding highlights the importance of considering the possibility of strands in upper layers being corroded, especially if drains are clogged or nonexistent under the boxes.

4. Specimen E4 failed prematurely in shear at one end of the specimen. Shear failure initiated in one of the webs that was significantly thinner than the other web of the box. It was clear that the form used to create the void in the box shifted during fabrication, leading to an inadequately thin web. Diagonal cracks that formed along strands located within the web depth eventually caused strands to slip because of loss of bond.

The results from the Essex Bridge beams (Specimens E3, E9, and E4) were used to evaluate the MassDOT *LRFD Bridge Manual* rating provisions and to propose recommendations as needed to achieve better estimates of moment strength. The current procedure to estimate strand loss as a consequence of deterioration was found to give nonconservative (higher)

moment strengths than measured in the laboratory. A new approach to estimate the reductions in strand cross section, especially in the region adjacent to exposed strand and stirrups was developed as presented in the following section.

8.3 Modifications to the Load Rating Provisions for Prestressed Concrete Beams in the MassDOT *LRFD Bridge Manual*

Although a limited number of laboratory tests was conducted for this research, the test results provided an opportunity to evaluate the rating procedures for severely deteriorated prestressed adjacent box girders that had severely deteriorated strands and stirrups from corrosion. These recommendations are considered also applicable to prestressed voided slab beams even though the tests that were conducted on this type of element consisted of nondeteriorated beams.

The proposed modifications to the current MassDOT Load Rating provisions for prestressed concrete beams *(1)*, particularly applicable to adjacent box beams and deck slabs are presented within the relevant sections of the bridge manual. Material proposed to be removed is written in strikethrough and material proposed for addition is written using underlining. For ease of incorporation into the bridge manual, all current sections that pertain to procedures to estimate reductions for deteriorated strands and reinforcement are presented below with the corresponding section numbers, even if a section is proposed to remain without modification.

> *7.2.10.2 In the vicinity of exposed reinforcing steel stirrups deduct 100% of the strand area located in the bottom row directly above the limits of the exposed stirrups. Deduct 25% of the area of the strands in the next row directly above the limits of the exposed stirrups. Deduct 25% of the area of the strand(s) in the bottom row next to the area of the exposed reinforcing stirrups.*
>
> *7.2.10.3 In the vicinity of exposed prestressing strands deduct 100% of the strand area within the limits where they are exposed. Deduct 50% of the area of the strands in the next row directly above the limits of the exposed strands. Deduct 50% of the area of the strand(s) in the bottom row next to the limits of the exposed prestressing strands, <u>unless strands are located in an area of concrete delamination (see 7.2.10.4)</u>.*
>
> *7.2.10.4 In areas of concrete delamination without exposed reinforcing stirrups or prestressing strands deduct ~~50%~~ <u>100%</u> of the area of the prestressing strands located in the row directly above the limits of the delamination. Deduct 10% of the area of the prestressing strand(s) in the bottom row next to the limits of the delamination.*

110

7.2.10.5 Longitudinal and/or transverse cracks shall be considered <u>as evidence of a potentially delaminated area</u> ~~to be a delamination that is six inches wide centered on the crack~~. The <u>length of the delamination</u> ~~delaminated area~~ shall be <u>estimated by lightly tapping the concrete using a masonry hammer</u> ~~the length of the crack plus six inches at each end of the crack~~. The loss of prestressing force ~~at this theoretical delamination~~ <u>within this area</u> shall be calculated in accordance with Paragraph 7.2.10.4 ~~above~~.

7.2.10.6 The reduced prestressing force due to <u>area</u> losses as calculated in the paragraphs above shall only apply to the ~~area~~ <u>region</u> of the deterioration. <u>Strands shall be considered partially developed until they reach a distance equal to their development length outside the deteriorated regions. Development of strands shall only be considered to occur within sound concrete.</u> ~~Outside of these areas, all prestressed strands shall be assumed to be 100% effective and shall be appropriately re-developed into areas of sound concrete~~. For example, a strand with 100% <u>section</u> loss <u>from deterioration</u> will require 100% of its development length before it is considered fully effective again. Likewise, a strand with 50% section loss will require 50% of its development length~~,~~ in sound concrete, before it is <u>considered</u> fully effective again.

The tests conducted in this research also revealed the large variation of web thicknesses in box girders of the era that was studied (mid-1970s to mid-1980s decades). Variation in web thickness was apparently caused by movement of the void form that was used during construction (polystyrene or cardboard). As-built web thicknesses are nearly impossible to determine in adjacent box girder bridges because of lack of accessibility. Therefore, a conservative approach is proposed to alert engineers to also consider checking the capacity of the beams for shear in determining the load rating for these types of bridges, as follows:

7.2.10.7 The shear strength of adjacent box girders shall consider the possibility of shifting of the void form during construction. Unless an accurate estimate of web thickness can be determined, the shear strength of adjacent box beams shall be calculated using a web thickness equal to the design web thickness minus 1.5 in.
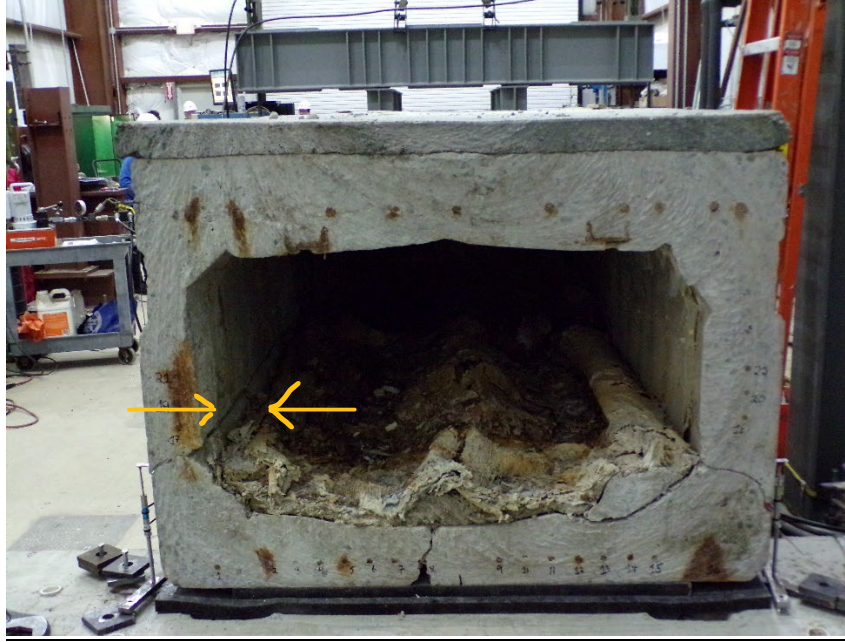
Figure 7.2.10-3: Example of web thickness variation

8.4 Recommendations on Inspection and Condition Rating

The primary goal of this research was to develop recommendations on load rating of prestressed concrete bridges to include effects of corrosion deterioration. Within prestressed concrete bridges, the types of bridges that have been subjected to significant deterioration from strand corrosion are slab deck bridges and adjacent box girder bridges. To reliably determine the degree that corrosion of strands is affecting moment and shear strength of existing girders, thorough and consistent inspection methods need to be implemented.

Through a detailed study of inspection reports during the conduct of this research (Section 3), it was found that different reports had highly variable levels of detail related to the condition of bridges. Even if two bridges were given the same condition rating, the condition of individual elements of the superstructure varied significantly as determined from written and photographic details provided in the inspection reports. This led the research team to suggest, as an initial set of recommendations, that MassDOT develop more detailed and consistent guidance that inspectors could use to base their condition assessment of deteriorated bridges. An example of the guidance that might be provided is reproduced as Table 8.1 (copied from Section 3 for convenience).

It would be useful to include representative photographs of the condition that is noted in the Tables shown in Attachment 4-1 of the MassDOT *Bridge Inspection Handbook (30)*, for example, the degree of efflorescence and/or rust staining that might constitute different condition states of 2 through 4. Providing detailed recommendations on inspection

procedures to adopt for deteriorated prestressed concrete bridges is beyond the scope of this research, but it should be noted that consistent inspection reports constitute a critical step in the ability to produce accurate estimates of load rating of deteriorated bridges.

A first natural step in the development of detailed inspection procedures would be to collect and conduct a detailed study of the inspection methods that are being used in other states. For example, Table 2.1 provides, as an example, the inspection guidance used by PennDOT that could be modified for potential adoption by MassDOT for condition rating of deteriorated prestressed concrete bridges *(2)*. More detailed guidance as included in this table could serve as a starting point to provide consistency among inspector reports. Finally, to facilitate consistency and promote automation, development of electronic tools that can be used for data collection in the field, if not already available, would ensure all needed information is in the inspection forms and can be readily uploaded for review.

Table 8.1: Condition rating guide (from MassDOT inspection reports)

Code		Condition	Defects
N	—	Not Applicable	—
G	9	Excellent	Excellent condition.
G	8	Very Good	No problems noted.
G	7	Good	Some minor problems.
F	6	Satisfactory	Structural elements show some minor deterioration.
F	5	Fair	All primary structural elements are sound but may have minor section loss, cracking, spalling or scour.
P	4	Poor	Advanced section loss, deterioration, spalling or scour.
P	3	Serious	Loss of section, deterioration, spalling or scour have seriously affected primary structural components. Local failures are possible. Fatigue cracks in steel or shear cracks in concrete may be present.
C	2	Critical	Advanced deterioration of primary structural elements. Fatigue cracks in steel or shear cracks in concrete may be present or scour may have removed substructure support. Unless closely monitored it may be necessary to close the bridge until corrective action is taken.
C	1	"Imminent" Failure	Major deterioration or section loss present in critical structural components or obvious vertical or horizontal movement affecting structure stability. Bridge is closed to traffic but corrective action may put it back in light service.
—	0	Failed	Out of service: beyond corrective action.

This page left blank intentionally.

9.0 References

1. MassDOT. *LRFD Bridge Manual Part I.* Boston, MA: Department of Transportation, Highway Division, Bridge Section, 2020.

2. Naito, C., Sause, R., Hodgson, I., Pessiki, S., & Macioce, T. Forensic Examination of a Noncomposite Adjacent Precast Prestressed Concrete Box Beams. 2010, Vol. 15, 4, pp. 408-418.

3. Alfailakawi, A., Roberts-Wollmann, C., Matthew, H., & Koutromanos, I. *Experimental and Analytical Evaluation of Residual Capacity of Corrosion-Damaged.* Richmond, VA: Virginia Transportation Research, 2020.

4. ASTM. *Standard Test Method for Compressive Strength of Cylindrical Concrete Specimens.* West Conshohocken, PA: ASTM, 2020.

5. ASTM. *Standard Test Methods for Testing Multi-Wire Steel Prestressing Strand.* West Conshohocken, PA: ASTM, 2020.

6. American Association of State Highway and Transportation Officials (AASHTO). *AASHTO LRFD Bridge Design Specifications* (9th ed.)*.* Washington, DC: AASHTO, 2020.

7. Yuan, J., & Graybeal, B. Full-Scale Testing of Shear Key Details for Precast. 2016, Vol. 21, 9.

8. American Association of State Highway and Transportation Officials (AASHTO). *Manual for Bridge Inspection.* Washington, DC: AASHTO, 2019.

9. Fernandes, B., Titus, M., Nims, D. K., Ghorbanpoor, A., & Devabhaktuni, V. Field Test of Magnetic Methods for Corrosion Detection in Prestressing Strands in Adjacent Box-Beam Bridges. *Journal of Bridge Engineering.* 2012, Vol. 17, 6, pp. 984-988.

10. Setty, C. J. Truck Testing and Load Rating of a Full-Scale 43-Year-Old Prestressed Concrete Adjacent Box Beam Bridge. *MS Thesis.* 2012.

11. Huffman, J.M. Destructive Testing of a Full-Scale 43 Year Old Adjacent Prestressed Concrete Box Beam Beam Bridge: Middle and West Spans. *MS Thesis.* 2012.

12. Steinberg, E., Sargand, S., Miller, R., & Nims, D. *Structural Evaluation of LIC-310-0396 and FAY-35-17-6.82.* s.l.: ODOT Innovation, Research & Implementation Section, 2011.

13. *Evolution and Performance of Box Beam Bridges in Indiana.* Molley, R. T., Whelchel, R. T., Williams, C. S., & Frosch, R. J. s.l.: PCI, 2019. 2019 PCI Conference and National Bridge Conference.

14. Attanayake, U., Berke, N., Amunugama, H., & Basnayake, K. *Concrete Deterioration of Prestressed Bridge Beams.* Lansing, MI: Michigan Department of Transportation Research Administration, 2022.

15. Gunasekaran, D., Mirdad, A. H., & Andrawes, B. Capacity and Load Rating of In-Service Precast Prestressed Concrete Bridge Deck Girders with Transverse Cracks. *Journal of Performance of Constructed Facilities.* 2022, Vol. 37, 2.

16. Campione, G., & Zizzo, M. Influence of strands corrosion on the flexural behavior of prestressed concrete beams. *Structures.* 2022, pp. 1366-1375.

17. Hognestad, E. *An Experimental Study of Combined Bending and Axial Load in Reinforced Concrete Members.* Urbana, IL: University of Illinois Engineering Experiment Station, 1951. Bulletin No. 399.

18. Mander, J. B., Priestly, M. J., & Park, R. Theoretical Stress-Strain Model for Confined Concrete. *Journal of Structural Engineering.* 1989, Vol. 114, 8, pp. 1804-1826.

19. American Concrete Insitute: Committee 318. *Building code requirements for structural concrete: (ACI 318-19) and commentary (ACI 318R-19).* Farmington Hills, MI: ACI, 2019.

20. International Federation for Structural Concrete (fib). *CEB-fib Model Code 2010.* Lausanne, Switzerland: s.n., 2012. Vols.1 & 2. fib Bulletins No. 65 & 66.

21. Murcia-Delso, J., & Shing, P. Bond-Slip Model for Detailed Finite-Element Analysis of Reinforced Concrete Structures. *Journal of Structural Engineering.* 2014, Vol. 141, 4.

22. Precast/Prestressed Concrete Institute. *PCI Design Handbook* (8th ed.). Chicago, IL: PCi, 2017. MNL 120-17.

23. Lu, Z.-H., Li, F., & Zhao, Y.-G. *An Investigation of Degradation of Mechanical Behaviour of Prestressing Strands Subjected to Chloride Attacking.* 2016. 5th International Conference on Durability of Concrete Structures.

24. Deng, N., Xu, J., Zhu, G., & Han, Z. Study on the Mechanical Properties of Corroded Steel Strands at Deflection Angles. *Buildings.* 2023.

25. Federal Highway Administration (FHWA). *Recording and Coding Gude for the Structure Inventory and Appraisal of the Nation's Bridges.* Washington, DC: s.n., 1995. FHWA-PD-96-001.

26. Federal Highway Administration (FHWA). *Bridge Inspector's Reference Manual.* s.l.: FHWA, 2012. FHWA NHI 12-050.

27. Attanayake, U., Berke, N., Amunugama, H., & Basnayake, K. *Concrete Deterioration of Prestressed Bridge Beams.* Lansing, MI: Michigan Department of Transportation Research Administration, 2022.

28. Campione, G., & Zizzo, M. Influence of strands corrosion on the flexural behavior of prestressed concrete beams. *Structures.* 2022, pp. 1366–1375.

29. Wang, Z.H., Li, L., Zhang, Y.-X., & Wang, W.-T. Bond-slip model considering freeze-thaw damage effect of concrete and its application, *Engineering Structures*, Vol. 201, 2019, 109831.

30. MassDOT. *Bridge Inspection Handbook.* Boston, MA: Department of Transportation, Highway Division, Bridge Section, 2015.

10.0 Appendix A: Inspection Report Data Collection

Appendices are found at https://doi.org/10.7275/jtg8-5v06.

11.0 Appendix B: Instrumentation Readings